Upper ocean variability and Tropical cyclones in the South West Indian Ocean

Daneeja Mawren

Department of Oceanography
University of Cape Town

This dissertation is submitted for the degree of
Doctor of Philosophy

University Cape Town September 2018

I would like to dedicate this thesis to my loving parents ...

Declaration

I hereby declare that except where specific reference is made to the work of others, the contents of this dissertation are original and have not been submitted in whole or in part for consideration for any other degree or qualification in this, or any other university. This dissertation is my own work and contains nothing which is the outcome of work done in collaboration with others, except as specified in the text and Acknowledgements. This dissertation contains fewer than 80,000 words including appendices, bibliography, footnotes, tables and equations and has fewer than 150 figures.

Daneeja Mawren
September 2018

This work has been supervised by the following :

***Supervisor** :
Prof. Chris Reason
Department of Oceanography, University of Cape Town, 7700 Rondebosch, Cape Town, South Africa

* Signatures are on file in the Science Faculty

I confirm that I have been granted permission by the University of Cape Town's Doctoral Degrees Board to include the following publication in my PhD thesis, and where co-authorships are involved, my co-authors have agreed that I may include the publication:

Chapter 4 : Mawren, D. and Reason, C.J.C., 2017. Variability of upper-ocean characteristics and tropical cyclones in the South West Indian Ocean. Journal of Geophysical Research: Oceans, 122(3), pp.2012−2028.

STUDENT NAME : **DANEEJA MAWREN**

STUDENT NUMBER : **MWRDAN001**

SIGNATURE : Signed by candidate

DATE : 24^{th} **May 2018**

Acknowledgements

This thesis would not have been possible without the financial assistance provided by the Faculty of Science fellowship and the UCT Postgrad Funding Office. I would also like to thank the AGU Ocean Sciences Meeting travel grant and Aegean Conferences student award for providing funding to attend international conferences during my studies, which helped broaden my horizon.

To my friends in the Oceanography department, Majambo, Fehmi, Katherine, Luca Jeremy, Jerome and Obadias thank you for all the animated discussions we shared in the office and for playing an integral part in keeping me motivated. Also a big thank you to my bestie, Elodie who has always been there to preserve my sanity throughout this PhD.

To Nico, thank you for your unerring encouragement, sublime omelettes and for putting up with me and my seemingly endless soliloquies about work. Thanks for everything, Nakas. My sincere thanks goes to my family and wonderful sister, for propelling me forward with their unconditional support and for bearing with me during all these years that I have been engaged in this project. A special mention goes to my Dad who has always been fascinated about tropical cyclones and who transfered this passion onto me since I was a child. To my mum who worked almost just as hard on this thesis as I have with all the prayers and offerings she made to all temples around Mauritius.

Finally, I would like to thank my supervisor, Prof. Chris Reason for giving me the opportunity to pursue this PhD. His critical eye has improved this work no end, and his continuous guidance, constructive and honest feedback were invaluable. I am also grateful that he was always available and for making it possible for me to attend numerous conferences and workshops during the course of my PhD. I was very fortunate to have you guiding me through it. Thank you Chris!

Abstract

Tropical cyclones (TCs) are the most devastating weather phenomenon in nature with the powerful storm surge events occurring when severe and large TCs make landfall along coastlines. Although there have been significant strides in the TC track forecasts over the last 30 years, skills in TC intensity prediction still lag behind. Intensity may be impacted by the mixing length temperature (known as Tdy) and barrier layer thickness (BLT). Similar to cyclones in other tropical ocean basins, tropical cyclones in the South West Indian Ocean also cause significant social and economic damage in southeastern Africa and Madagascar. To forecast TC intensity more accurately, monitoring upper ocean conditions in the South Indian Ocean is of top priority. Two areas in the relatively poorly studied South Indian Ocean where such upper ocean characteristics of relevance to tropical cyclones need to be better understood are the Seychelles Chagos Thermocline Ridge (SCTR) and the Mozambique Channel.

In the first part of the study, the variability of Tdy and BLT in the South West Indian Ocean, focused on the SCTR region and their relationships with tropical cyclones are investigated. It is shown that rapid cyclone intensification is influenced by large Tdy values, thick barrier layers and the presence of anticyclonic eddies. Both BLT and Tdy fields are modulated by the westward propagation of Rossby waves, which are often associated with ENSO. For example, the 1997-1998 El Niño shows a strong signal in Tdy, SST and BLT over the South West Indian Ocean. After this event, an increasing trend in Tdy occurred over most of the basin which may be associated with changes in atmospheric circulation. A rise in SST, Power Dissipation Index and frequency of Category-5 tropical cyclones also occurred post-1998. A case study of TC Bansi in the South West Indian Ocean and its relation to upper ocean heat content was presented. This tropical cyclone is of interest due to its unusual track and also because of all the damage it caused. Anomalously deep thermocline and high Tdy values were observed around December 2014-January 2015 in the South West Indian Ocean and analysis of the upper ocean structure during Bansi showed that its rapid intensification to

Category 4 was related to its passage over a high Tdy (warm core) eddy region and a deep barrier layer.

The second area focussed on, the Mozambique Channel, is not only a region of relatively high TC activity with highly vulnerable coastal populations, but also very energetic in terms of mesoscale ocean eddies and tidal forcing. Changes in upper ocean characteristics in the Mozambique Channel due to tidal forcing are examined as they may have significant impacts on the upper ocean structure and thus influence tropical cyclones which often occur in this region. Two experiments were conducted using the Regional Ocean Modelling System (ROMS); one forced with tides (***Tide***) and the other experiment without tidal forcing (***NoTide***). On seasonal time scales, the tidal forcing simulation shows warmer temperatures in the upper layer particularly near strong ocean currents (North East Madagascar Current and South East Madagascar Current). In ***Tide***, warming near these currents is intensified during winter due to the southeast trade winds, while in summer, poleward advection of warmer waters south of 16-17 ^{o}S seemed more prominent. On weather time scales, these changes in the upper ocean structure, especially near the coast or in shallow regions can alter the intensity of passing tropical cyclones. When a storm encounters a warm anticyclonic eddy, as the case of TC Japhet studied in the thesis, the SST cooling by the cyclone is substantially reduced, the mixing length temperature is increased and the mixed layer is deepened. These changes can be important for TC evolution.

SST variability over the South West Indian Ocean influences southern African summer rainfall and the regional atmospheric circulation either through regional modes as well as influences the landfall frequency of tropical cyclones on Mozambique (Vitart et al., 2003). Besides SST, a link has recently been found between the regional precipitation over southern Africa and tropical cyclone heat potential (a measure of upper ocean heat content) in the South West Indian Ocean (Malan et al., 2013). In this study, the relationships between an index of southern African summer rainfall (SARI) and Tdy in the South Indian Ocean at zero (January-March) and one season (October-December) lag were analyzed. A region in the southern Mozambique Channel, termed as Tdy_{smc}, showed the strongest positive correlation with SARI at zero lag. Another strong but negative correlation with SARI at one season lag is found in the core of the Seychelles Chagos Thermocline Ridge region, termed as Tdy_{csctr}. Composite analysis (neutral with respect to ENSO) indicated that when Tdy_{smc} is enhanced

over the South Mozambique Channel during JFM, positive rainfall anomalies prevail over large parts of subtropical southern Africa and the Congo Basin with reduced rainfall occuring over most of Madagascar and northern Mozambique. The rainfall differences are associated with enhanced easterly flow towards Madagascar transporting more moisture towards Mozambique and Tanzania, consistent with the increased rainfall. During positive Tdy_{smc} JFM seasons, more tropical cyclones (TCs) were formed in the SWIO and more of them crossed the Mozambique Channel compared to negative Tdy_{smc} seasons. Furthermore, during positive Tdy_{smc} seasons, the landfalling TC was generated in the Mozambique Channel while during the negative Tdy_{smc} ones, it was formed in the central South Indian Ocean. Positive Tdy_{smc} seasons also have increased number of Category-5 TCs in the Mozambique Channel. These results suggest that changes in the mixing length temperature, Tdy_{smc} index which can be estimated from satellite data can be useful to monitor and potentially predict regional precipitation as well as the frequency and intensity of tropical cyclones that impact the southeastern coast of Africa.

Table of contents

List of figures

List of tables

Chapter 1

Introduction

Tropical cyclones (TCs) are low-pressure disturbances that develop over warm tropical oceans. They can extend more than 1000 km in diameter and are considered to be the most devastating disasters in nature with the powerful storm surge events occurring when strong TCs make landfall along coastlines. These systems are known as Hurricanes in the North Atlantic and Northeastern Pacific, Typhoons in the Northwestern Pacific or Tropical cyclones in the Indian and Pacific oceans. In the South West Indian Ocean (0 – 40 ^{o}S; 30 – 90 ^{o}E), tropical storms (including tropical cyclones) are generated mainly from late November to April, with on average 12-13 per season (Mavume et al., 2009) and typically peak during the months of January and February. There have been marked cases in the South West Indian Ocean where sudden intensification of storms has caused major infrastructural damage and loss of life in Mozambique and Madagascar. A few studies conducted in other basins have found that such intensification can be initiated when cyclones pass over regions of positive upper-ocean thermal anomalies. Since TCs interact not only with the surface layer of the ocean but with the subsurface layers (i.e. from the surface, down to a depth of 100 m; (Price, 1981; Lin et al., 2003; Sanford et al., 2011; Lin, 2012)), it is also of importance to understand the ocean-atmosphere interaction during the passage of a tropical cyclone, not only in terms of the sea surface temperature, but also of the upper-ocean thermal structure. The variability of the upper-ocean temperature modulates TC intensity (Emanuel et al., 2004) as the latent heat available in the upper layers of the ocean provides the source of energy necessary for the cyclone to sustain its system.

The passage of TCs creates a wake at the surface of the ocean, bounding water that is reduced by a few degrees Celsius (Bender et al., 1993; Cione and Uhlhorn, 2003). This

cooling is mostly due to entrainment of cooler water upwelled by intense winds, rather than heat loss through air-sea exchanges (Price, 1981; D'Asaro, 2003). Strong wind stress gives rise to large velocity shear in the upper layers of the ocean which in turn deepens the mixed layer. This as a result generates sea surface cooling and subsurface warming (Emanuel, 2001). Subsequently, the SST is re-established to normal values by oceanic processes, leading to a net positive heat flux into the ocean. In this thesis, the possible implications of upper ocean thermal anomalies on subsequent tropical cyclone events are investigated. Some studies (D'Asaro, 2003; Goni and Trinanes, 2003; Lin et al., 2005; Shay et al., 2000) showed evidence that when a tropical cyclone encounters a warm eddy with a thick mixed layer depth and an increased upper ocean heat content, it undergoes a rapid intensification. A positive feedback between intense TCs and positive thermal anomalies at the bottom of the mixed layer is likely to be at play. Usually the heat anomaly is not shown at the surface which indicates the important role of subsurface temperature in predicting tropical cyclone intensity (Goni and Trinanes, 2003). In recent years, the increase in computing power and improved modelling and observation capabilities have improved tropical cyclone trajectory forecasts but methods in predicting TC intensity are behind. The variability of upper ocean characteristics such as temperature, mixed layer depth, heat content and barrier layer thickness that are important for TC evolution needs to be better understood.

Two areas in the relatively poorly studied tropical South Indian Ocean where such upper ocean characteristics of relevance to tropical cyclones need to be better understood are the Seychelles Chagos Thermocline Ridge and the Mozambique Channel. These two areas are focussed in this thesis. **Figure 1** illustrates these two areas together with some of the main circulation features in the western Indian Ocean region. The Seychelles-Chagos Thermocline Ridge is labelled as A and the Mozambique Channel as B on the schematic diagram below. The Seychelles-Chagos Thermocline Ridge (hereafter SCTR, (Hermes and Reason, 2008)) is a region of upwelling sustained by wind stress curl between the southeasterly trades in the south and equatorial westerlies in the north (Xie et al., 2002; McCreary Jr et al., 1993; Vialard et al., 2009). The 5-10 ^{o}S band in the Indian Ocean is a region where the occurence of significant climatic influences take place. The coupling between the surface, subsurface temperature layer and the sensitivity of the atmosphere to the sea surface temperature contributes to strong air-sea interactions on different time scales (Vialard et al., 2009) in the SCTR region which can affect areas remotely through atmospheric connections. Also, this region is where the Madden-Julian Oscillation (MJO) is associated with strong SST variability. Duvel et al.

(2004) proposed that a shallow thermocline in the SCTR region inhibits the deepening of the mixed layer during strong wind bursts,leading to an enhancement in the SST signal related to MJO. Interestingly, the SCTR region is a cyclogenesis area for tropical cyclones striking inhabited islands of the South West Indian Ocean and the eastern coast of Africa. A few studies have found that changes in the heat content in the SCTR region can influence tropical cyclone activity in the neighbouring area (Jury et al., 1999; Xie et al., 2002; Chowdary et al., 2009). The variability of the subsurface thermal structure in the SCTR region is correlated with the duration of tropical cyclone days in the region, where a reduction in the upwelling will result in an increase in the heat content, enhancing intensification of storms (Jury et al., 1999; Xie et al., 2002; Reason and Keibel, 2004; Washington and Preston, 2006). This link was emphasized during the 2006/2007 austral summer, when areas of Madagascar and central Mozambique encountered devastating floods following a series of strong cyclones with longer tropical cyclone days (Hermes and Reason, 2008; Malan et al., 2013). This, therefore, provides a strong incentive to better understand the variability of upper ocean characteristics and their relationships with tropical cyclones across the SCTR region.

The second area focussed on, the Mozambique Channel, is not only a region of relatively high TC activity with highly vulnerable coastal populations, but also very energetic in terms of mesoscale ocean eddies and tidal forcing. According to Mavume et al. (2009), Mozambique and Madagascar have coastlines of approximately 2700 and 4800 km respectively where more than half of their population live in coastal areas, relying on farming and fishing. Several prominent TCs that crossed the Channel intensified just before they make landfall over Mozambique and therefore led to substantial loss of life and damage (e.g. TC Eline in 2000, (Dyson and Van Heerden, 2001; Reason and Keibel, 2004); TC Favio in 2007, (Klinman and Reason, 2008)). Since the Mozambique Channel is a region of strong tidal activity, it is worth investigating the role that tides may play in influencing the upper ocean characteristics that are important for TC evolution and potential intensification. Several studies related to tides and fisheries (Gammelsrød, 1992; de Boer et al., 2000; de Sousa et al., 2006; Fennessy and Isaksen, 2007) have been conducted in the Mozambique Channel but effects of tides on the upper ocean heat content remain poorly understood. Recently, Chevane et al. (2016) compared model simulations with and without tides to illustrate the effects of tides on the mean vertical stratification on Sofala bank. To the best of our knowledge, tidal effects on TC ocean characteristics have not been previously studied, so including this parameter in ocean models can be important for forecasting TC intensification and in turn,

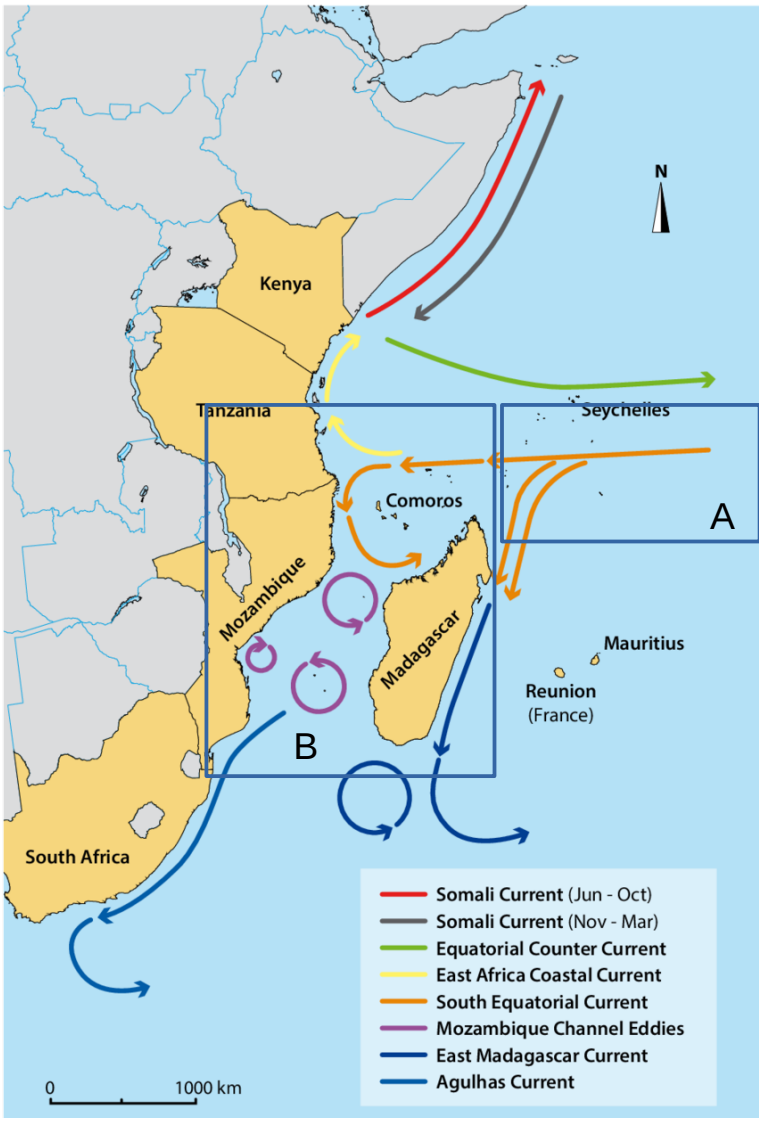

Fig. 1.1 Some of the major ocean currents in the Western Indian Ocean basin, indicated schematically showing source regions of mesoscale eddies from the Mozambique Channel and East Madagascar Current. Labeled countries on the map are developing countries (some are the poorest in the world) in the South West Indian Ocean. (**A**) Part of the Seychelles-Chagos Thermocline Ridge and (**B**) the Mozambique Channel are the main areas of study. *Adapted from Lutjeharms 2006*

improving predictions of rainfall over TC affected regions.

Strong winds associated with a tropical cyclone inflict damage directly upon human infrastructure, causing economic deficits and loss of human life (Sheets, 1990; Elsberry, 2002; Rappaport, 2000; Blake et al., 2007) but heavy rainfall accumulated from TCs can also be a destructive factor. On average, the precipitation linked with TCs contributes to less than 10 % of the total precipitation over the global tropics and about 50 % of the total precipitation over a large part of ocean basins (Lin and Chan, 2015). Each year in the South West Indian Ocean, about 12-13 TCs are formed, accounting for about 14 % of the global total (Jury et al., 1993; Ho et al., 2006; Mavume et al., 2009). About 5% of the TCs make landfall over the southern African mainland (Vitart et al., 2003; Reason and Keibel, 2004) often carrying floods to the coastal lowlands (Crimp and Mason, 1999; Dyson and Van Heerden, 2002; Klinman and Reason, 2008; Malherbe et al., 2012). However, individual TC events can have massive impacts when they make landfall e.g. Hurricanes Irma (2017) in the US and TC Dineo (2017) in Mozambique. Tropical cyclone Dineo brought widespread damage to Mozambique after making landfall, killing a total of 7 people, 130,000 people were displaced and 20,000 houses were destroyed. In addition to ENSO-driven variability, SST over the South West Indian Ocean can also influence the regional atmospheric circulation (e.g. (Mason, 1995; Reason and Mulenga, 1999; Behera and Yamagata, 2001; Reason, 2001)) and hence have an impact on the frequency and intensity of tropical cyclones hitting the southeastern coast of Africa (Vitart et al., 2003). The aim will be to also investigate the relationship between the upper-ocean heat content in the Mozambique Channel and southern African summer rainfall with a focus on the frequency of TCs in the region.

Given the importance of tropical cyclones for the climate of the South West Indian Ocean region and their frequent devastating impacts on Madagascar and Mozambique, the first objective is to assess the interannual variability and trends in upper ocean characteristics that are important for their generation and evolution, with a focus on the Seychelles Chagos Thermocline Ridge. In achieving this objective, reanalysis data were used due to its larger spatial and temporal coverage in the area. The goal of this research is also to find a significant link between the variability of tropical cyclone frequency and intensity in the South West Indian Ocean to the oceanic-atmospheric circulation (or Climate modes). The second objective of this study is to investigate the effects of tides on the upper-ocean characteristics and their

impact on tropical cyclones in the Mozambique Channel, one of the most turbulent ocean areas in the world. To realise this goal, two experiments were conducted using a Regional Ocean Modelling System (ROMS), namely one configuration forced with tides and the other without tides. The third objective is to use satellite and reanalysis data to find a link between the upper-ocean temperature, tropical cyclones in the Mozambique Channel and their impact on summer rainfall over the Southern African mainland.

This thesis will proceed as follows: **Chapter 2** describes in details the dynamic and climatic role of the South West Indian Ocean and presents an overview of Tropical Cyclones. **Chapter 3** is a detailed description of the Regional Ocean modelling system (ROMS), an assessment of its performance with respect to observations and also other data and methodology used. **Chapter 4** investigates the variability of the upper ocean characteristics and tropical cyclones in the South West Indian Ocean. **Chapter 5** discusses the effects of tides on the upper-ocean structure and potential impact on tropical cyclones in the Mozambique Channel. **Chapter 6** focusses on the link between the upper-ocean temperature and southern African summer rainfall variability. Finally, **Chapter 7** summarises the conclusions of this work and presents avenues that warrant further investigation.

Chapter 2

An overview of the dynamics and climatic role of the South West Indian Ocean

2.1 Indian Ocean Overview

Despite its smaller size in relation to other basins, the Indian Ocean is considered to be the most complex (Heirtzler, 1977). It is the only tropical basin to be bounded by a continental landmass to the north, due to the Asian continent.The western Indian Ocean is bounded by Africa to a latitude of 34S, where the Agulhas Current flows along the east and south coast of South Africa. The current retroflects south of South Africa and transports heat and salt from the South Indian Ocean into the South East Atlantic. The eastern Indian Ocean is bounded by Australia but is open to the Pacific both in the midlatitudes south of this continent and in the tropics via the flow through the Indonesian archipelago. The semi-enclosed nature of the South Indian Ocean basin results in a circulation strongly dependent on the regional wind field but with significant influences from the Indonesian throughflow and interactions with the Southern Ocean (Figure. 2.1).

The Indian Ocean is less explored due to the lack of both oceanographic and meteorological data particularly in the Southern basin. On the other hand, the northern part received special attention due to the reversal of wind (detailed description of the monsoonal winds in section 2.2) and surface current patterns (see section 2.3) associated with the monsoon climate; the South West Monsoon (SWM) blowing from June to September and the North

East Monsoon (NEM) blowing from November to February. Prior to the identification of dipoles (Saji et al., 1999; Behera and Yamagata, 2001), the Indian Ocean was regarded by climate scientists to be somewhat passive, as compared to the Pacific (and Atlantic Oceans) which clearly had identified modes of variability. After the strong 1997 Indian Ocean Dipole (IOD) (Webster et al., 1999; Saji et al., 1999; Murtugudde et al., 2000), the Indian Ocean received the attention it deserves.

2.2 Winds and the Indian Ocean Monsoon

The main forces that generates ocean currents are the wind exerting a stress on the sea surface (known as the wind-driven circulation) and buoyancy fluxes between the ocean and the atmosphere (known as the thermohaline circulation), which changes the density of the water. The wind-driven circulation is the most energetic and is confined to the upper kilometre of the ocean while the thermohaline circulation, associated with the overturning circulation is linked with major water masses of the global ocean. The South Indian Ocean , south of 10 ^{o}S, is dominated by Southeast trade winds that persists throughout the year (Lutjeharms, 2006) (Figure. 2.2). These winds strengthen during austral winter, north of 10 ^{o}S and are determined by the monsoon circulation (Annamalai and Murtugudde, 2004). As observed by (Woodberry et al., 1989), the monsoon influence is extended until 15 ^{o}S in the Mozambique Channel.

A seasonal reversal in the direction of the winds is considered to be a contrasting feature of the monsoonal regions across the globe (Cadet, 1979; Gadgil, 2003) extending over large parts of the tropics (25 ^{o}S-35 ^{o}N; 30 ^{o}W-170 ^{o}E; (Ramage, 1971)), including a large part of the Indian Ocean. The monsoon climate occurs as part of a larger phenomenon with the formation of low and high pressure systems over the Asian continent. There are two mechanisms that drive the monsoon : differential (land-ocean) sensible heating and tropospheric latent heating (Clemens et al., 1991). Three climatic situations are apparent in regions affected by the monsoon, the Northeast monsoon, the Southwest monsoon and the inter-monsoon. The Northeast monsoon (austral summer monsoon), occurs from December to March and prevailing winds during this period are northeasterlies over the North Indian Ocean (Figure. 2.2a). However, upon crossing the equator, the winds reverse to northwesterlies and converge with the southeast trade winds, winds south of about 10 ^{o}S of the South Indian Ocean (Hastenrath and Greischar, 1991). The Southwest monsoon (austral winter monsoon) dominates the annual cycle of the Indian Ocean (Yamagata et al., 2004) and is prevalent

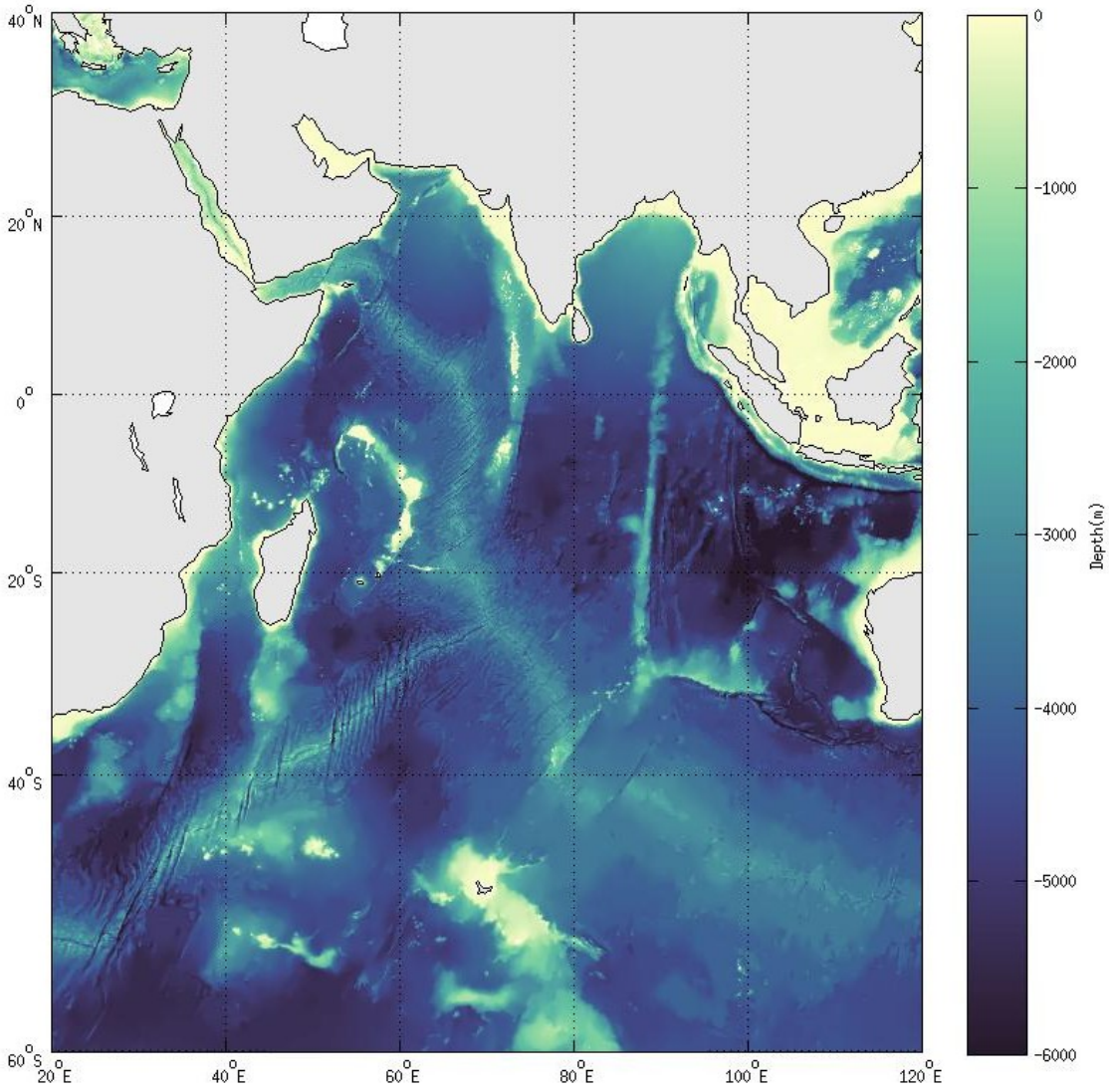

Fig. 2.1 Bathymetry of the Indian Ocean. (Data source : ETOPO2)

between June and September (Tomczak and Godfrey, 2003). This causes a complete reversal of the winds over the North Indian Ocean (Rao and Ram, 2005). The southeast trade winds in the Southern Hemisphere extends north to about 5 ^{o}S and recurve while crossing the equator, becoming southwesterlies (Figure. 2.2b). During this season, a low-level atmospheric jet of strong southwesterlies, known as the Somali Jet is formed along the Somali coast and leads to strong upwelling.

The inter-monsoon periods occur between April-May and October-November and are characterized by a strong westerly flow that dominates in the equatorial regions (Payet et al., 2004). During this period, the winds along the Somalian coast weaken and lead to a decrease in the upwelling, giving rise to warmer water. The latter is carried eastward by strong equatorial currents known as Yoshida-Wyrtki jet, generated by equatorial westerlies (Yamagata et al., 2004).

2.3 Inter-tropical Convergence Zone and Rainfall over the Southern African mainland

In addition to the seasonal reversal of the winds, the monsoon is also characterized by a distinct contrast in precipitation (Pfeiffer et al., 2006) which controls the annual cycle of the sea surface temperatures (SSTs) in the Indian Ocean. The monsoon climate is dominated by the Intertropical Convergence Zone (ITCZ) (Figure. 2.3), which divides the wind circulation between the northern and southern hemispheres (Sikka and Gadgil, 1980). The ITCZ is a transition belt where the global northeast and southeast trades converge, inducing upward motion and rainfall (Wallace and Hobbs, 1977). Strong uplift and heavy precipitation is the result of intense heating by solar radiation. The heating also drives a meridional atmospheric circulation known as the Hadley Cell. This cell consists of rising air at the equator and descending air at about 30 ^{o}N and 30 ^{o}S. The largest range is in the Indian Ocean, reaching 10-15 ^{o}S in January and 25-30 ^{o}N in July. During the southwest monsoon, the Southeast trade winds form a steady flow of air expanding into south Asia, transporting huge amount of water vapour from the Indian Ocean towards the Asian subcontinent and results in heavy precipitation over land. River runoff into the Bay of Bengal and rainfall over the NE Indian Ocean during the Southwest monsoon creates a large pool of fresher water (Figure. 2.4) in that part of the ocean. In the western equatorial Indian Ocean and in the Arabian sea, evaporation and upwelling associated with the Southwest monsoon results in a large summer

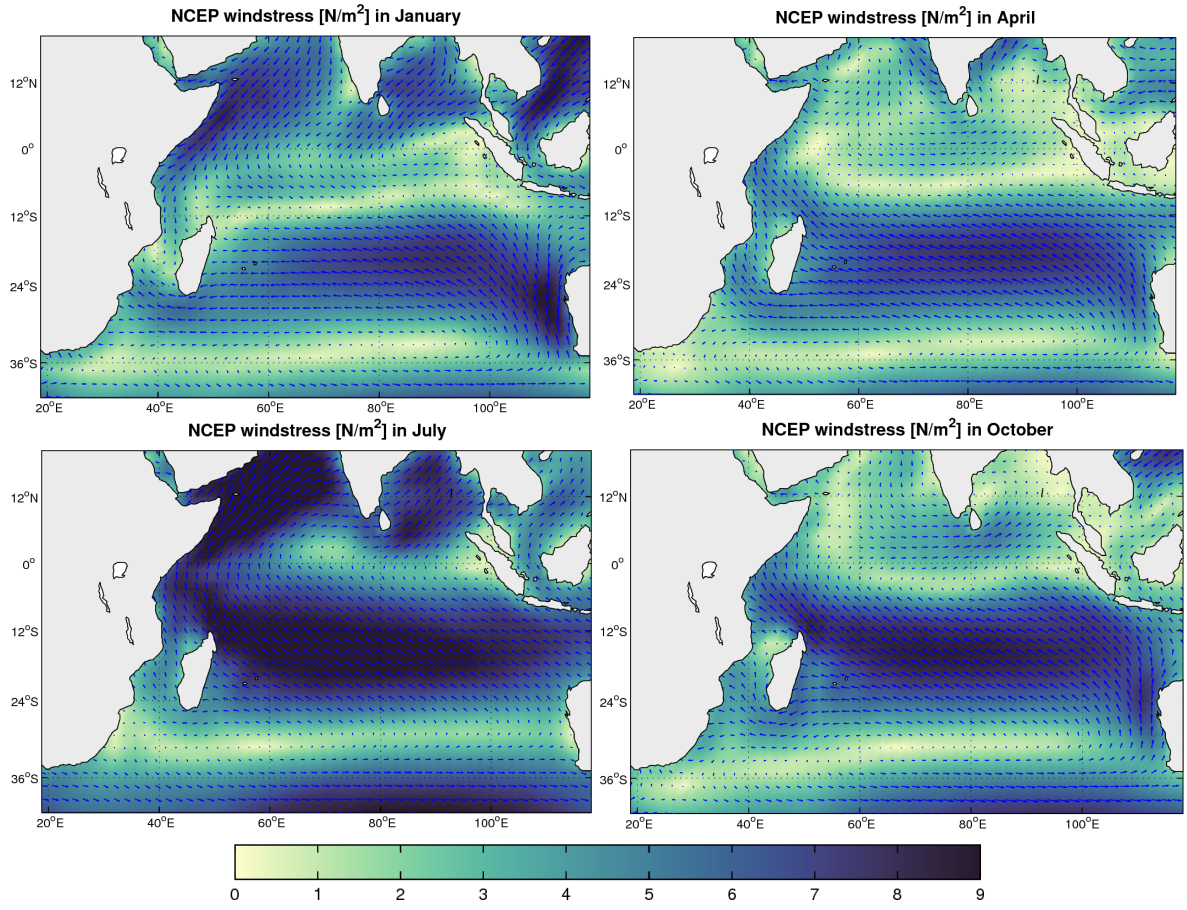

Fig. 2.2 Monsoon wind stress fields from NCEP climatology for (a) January, (b) April, (c) July and (d) October

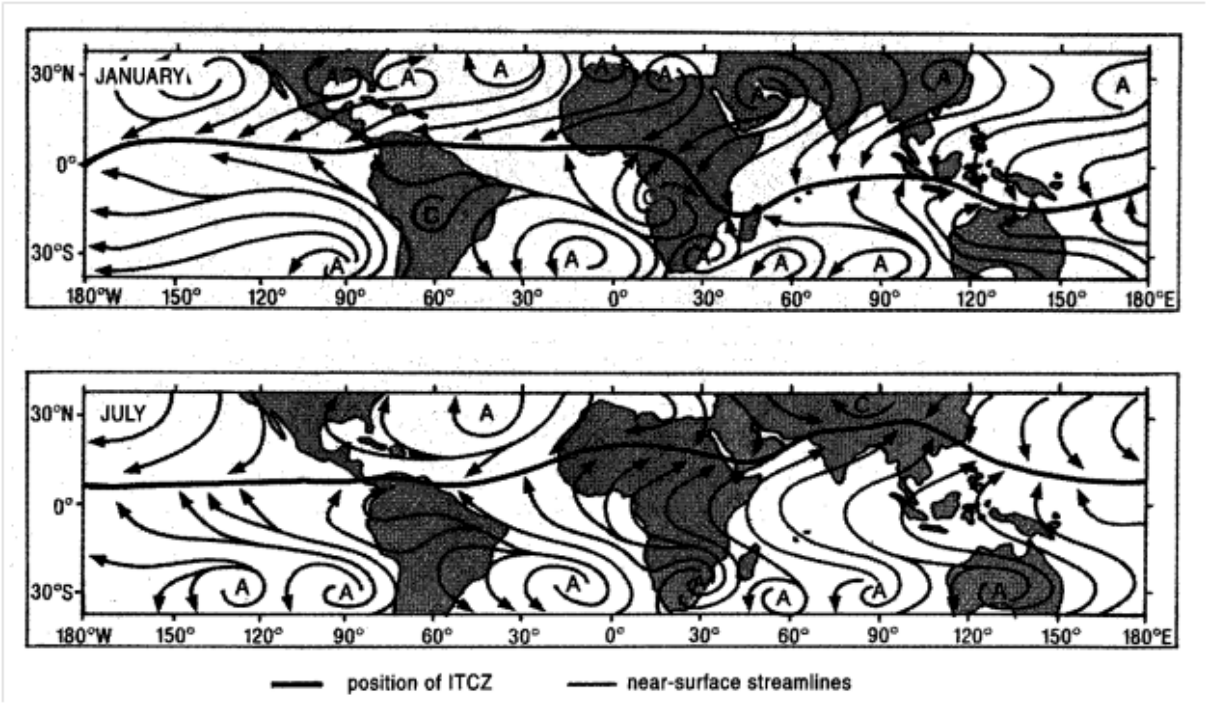

Fig. 2.3 Positions of the Intertropical Convergence Zone (ITCZ) including schematic streamlines of near surface flow for summer (January) and winter (July), where 'A' and 'B'represent the anticylonic centres and cyclonic centres respectively (from Tyson and Preston-Whyte, modified after Hastenrath, 1985)

cooling (Rao and Sivakumar, 2000; Vinayachandran et al., 2004). On the other hand, the dry northearterly winds of the northeast monsoon flow from the Asian continent toward the warm tropical Indian Ocean, where the excessive precipitation takes place along the ITCZ, located at about 5-10 ^{o}S (Rao and Ram, 2005).

During the Northeast monsoon (austral summer monsoon), when the atmospheric pressure gets very low, cyclones may form in the areas of atmospheric depression and instability (Payet et al., 2004). The active cyclonic season in the South Indian Ocean occurs from November to April with a peak in cyclogenesis during January and February. Cyclones formed in the South Indian Ocean tend to have a westward trajectory towards the east coast of Madagascar and recurve southeast into open waters in the central South Indian Ocean. From July-August, the ITCZ is over land and therefore cyclones are rare. According to Reason and Keibel (2004), only 5% of tropical cyclones make landfall on the Southern African mainland. These synoptic-scale systems may have an impact on the underlying ocean by increasing

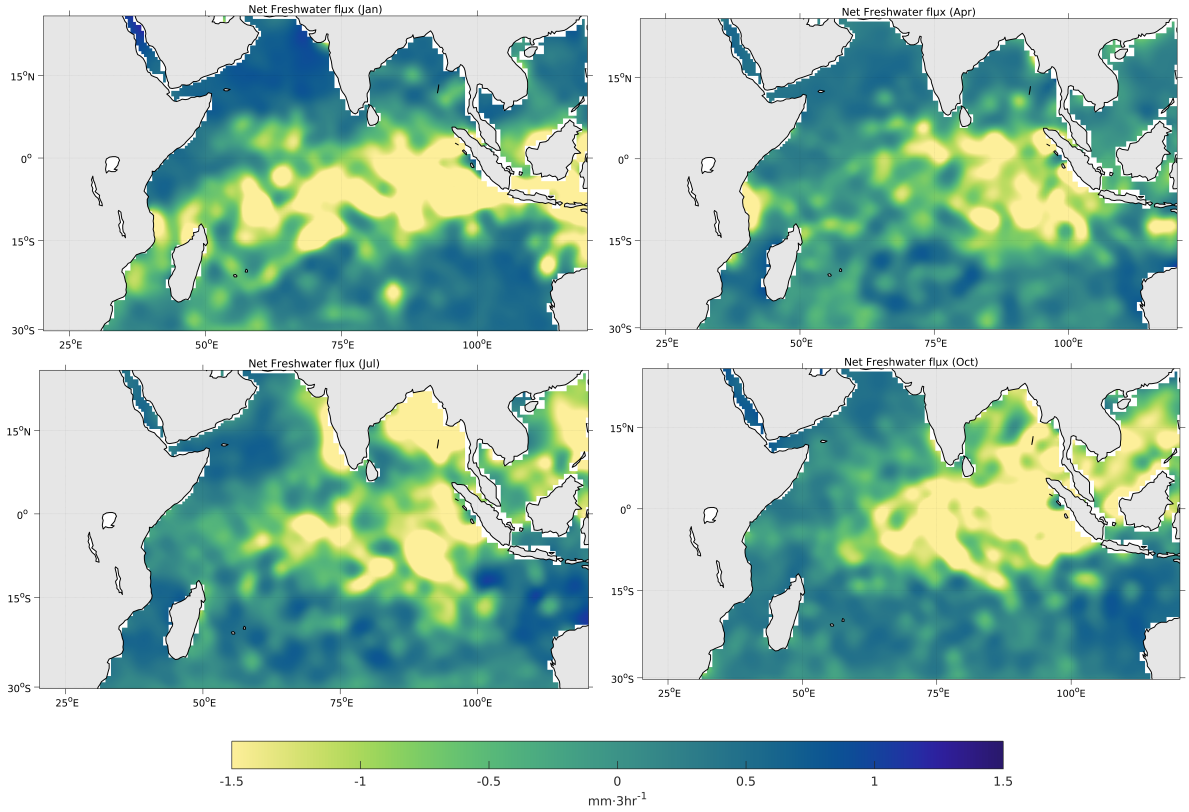

Fig. 2.4 Seasonal net freshwater flux,i.e. Evaporation - Precipitation (E-P; Data source: Comprehensive Ocean-Atmosphere Data Set). The freshwater flux indicates the development of the ITCZ, in which precipitation is dominating. The Arabian sea and the Southeast Indian feature excess evaporation due to all year round high pressure system.

the mixed layer depth (Dickey et al., 1998) and decreasing the SST due to upwelling (Price, 1981).

2.4 South West Indian Ocean circulation

The oceanic wind-driven circulation in the South Indian Ocean, south of 10 °, is mainly dominated by the incoming waters from the broad westward flowing South Equatorial Current (Wyrtki, 1971; Tomczak and Godfrey, 2003; Stramma and Lutjeharms, 1997). The South Equatorial Current (SEC) is linked with the Subtropical gyre of the South Indian Ocean and

the Indonesian throughflow (Quadfasel et al., 1996; Gordon and McClean, 1999; Schott et al., 2009) (Figure. 2.5). East of 105 ^{o}E, the SEC ranges between 7 ^{o}S and 15 ^{o}S (Quadfazel and Swallow, 1996). A few studies (New et al., 2007; Swallow et al., 1988; Schott and McCreary Jr, 2001) using hydrographic measurements have found that the volume transport of the SEC between 10 ^{o}S – 16 ^{o}S in the west Indian Ocean vary between 50 Sv – 55 Sv. When the SEC reaches the east coast of Madagascar, between 17 ^{o}S and 20 ^{o}S, it bifurcates to the north and south of Madagascar, as the Northern (NEMC) and Southern East Madagascar current (SEMC).

The two branches were estimated to carry about 30 Sv and 20 Sv respectively (Swallow et al., 1988; Schott et al., 1988). The NEMC follows the northeast coast of Madagascar at Cape Amber and meanders to the west toward the African continent at a propagation speed of about 0.5 m/s, a width of 200 km and a depth of about 1100 m deep (Schott et al., 1988). As the NEMC reaches the African coast at 11 ^{o}S, the flow is splitted into two branches, a northward branch forms the East African Coastal Current (EACC) along the Tanzanian coast zone (Schott et al., 1988) and the southward branch flows through the Mozambique Channel (Sætre, 1985; Tomczak and Godfrey, 2003; Schott and McCreary Jr, 2001). A few studies (Gründlingh, 1995; DiMarco et al., 2002; Biastoch and Krauss, 1999) have shown that the flow in the Mozambique Channel is more complicated than a simple western boundary current but were in fact of a series of cyclonic and anticyclonic eddies (Harris, 1972; de Ruijter et al., 2002; Ridderinkhof and De Ruijter, 2003). The SEMC, south of the east coast of Madagascar is characterized as the small western boundary current (Schott et al., 1988) with a width of 120 km, a length of about 650 km (Nauw et al., 2008), 1100 m deep (Siedler et al., 2009) and a propagation speed of about 1.10 m/s. It flows southward along the east coast of Madagascar trailing the continental shelf break to the southern tip of Madagascar (Schott et al., 2009; DiMarco et al., 2000). (Lutjeharms, 1981) was among the first one to propose that the SEMC retroflects at the southern tip of Madagascar to flow eastwards as an East Madagascar Return Current. However other studies refuted this hypothesis and suggested that the current curves northwest into the southern Mozambique Channel and flows anticyclonically soutwestward towards Africa (Tomczak and Godfrey, 2003; DiMarco et al., 2002). Based on a high resolution nested model and satellite remote sensed data, (Siedler et al., 2009) came up with a more robust conclusion suggesting that the SEMC holds two different regimes which switches from one mode to the other, based on how intense the SEMC is. In one regime, the connection between the Agulhas current and the SEMC follows a straight path when the flow of the SEMC is mostly westwards while on the second mode,

the SEMC retroflects and moves eastwards when the flow is mainly southeastwards.

The greater Agulhas Current (AC) System in the Southwest Indian Ocean plays a key role in the global ocean circulation (Ruijter et al., 1999; Lutjeharms, 2006). The dominant sources of the AC are not only from the outflow of the Mozambique Channel nor the East Madagascar Current but mostly from the recirculation of the South West Indian Ocean subgyre (Harris, 1972; Stramma and Lutjeharms, 1997). A greater part of the flow, about 40 Sv of the total volume flux of the upper 1000m of the Agulhas Current (65Sv) is derived from the subgyre (Biastoch and Krauss, 1999). When the current reaches the southwesternmost limits of the southwestern tip the Agulhas Bank, South Africa, it retroflects and feeds back into the South Indian Ocean as the eastward flowing Agulhas Return Current (Figure. 2.6; (Beal et al., 2011)). The retroflection known as the Agulhas retroflection transport warm, saline Indian Ocean water into the South Atlantic Ocean (Biastoch et al., 2008) through eddies, rings and filaments. The migration of these mesoscale features have shown to play an important role on the strength of the meridional overturning circulation, which in turn has implications on the global climate (Weijer et al., 1999; de Ruijter et al., 2002; Peeters et al., 2004; Biastoch et al., 2008, 2009; Beal et al., 2011).

2.5 Water masses in the South West Indian Ocean

There are three basic kinds of water masses that dominates in the Indian Ocean: incoming waters from other basins, those generated through subduction within the Indian Ocean and those generated by mixing with other water masses (Schott and McCreary Jr, 2001). In the Northwest Indian Ocean, evaporation exceeds precipitation, leading to high salinity waters in the Arabian Sea, Red Sea and Persian Gulf (Morales et al., 1996). These water masses get subducted and can be traced as they propagate from their source regions (Quadfasel et al., 1996; Swallow et al., 1983). Low-salinity waters coming from the eastern Indian Ocean are transported into the western Indian Ocean through the South Equatorial Current and also from the Southern Ocean through subduction at the Subtropical Convergence (Warren et al., 1976; Wyrtki, 1971).

The northern and southern water masses are separated by a front between 5-12 ^{o}S and characterises the influence of the subtropical gyre and the monsoon system (Wyrtki, 1973). During the northeast monsoon, in the northern Arabian Sea, Arabian Sea High Salinity Water

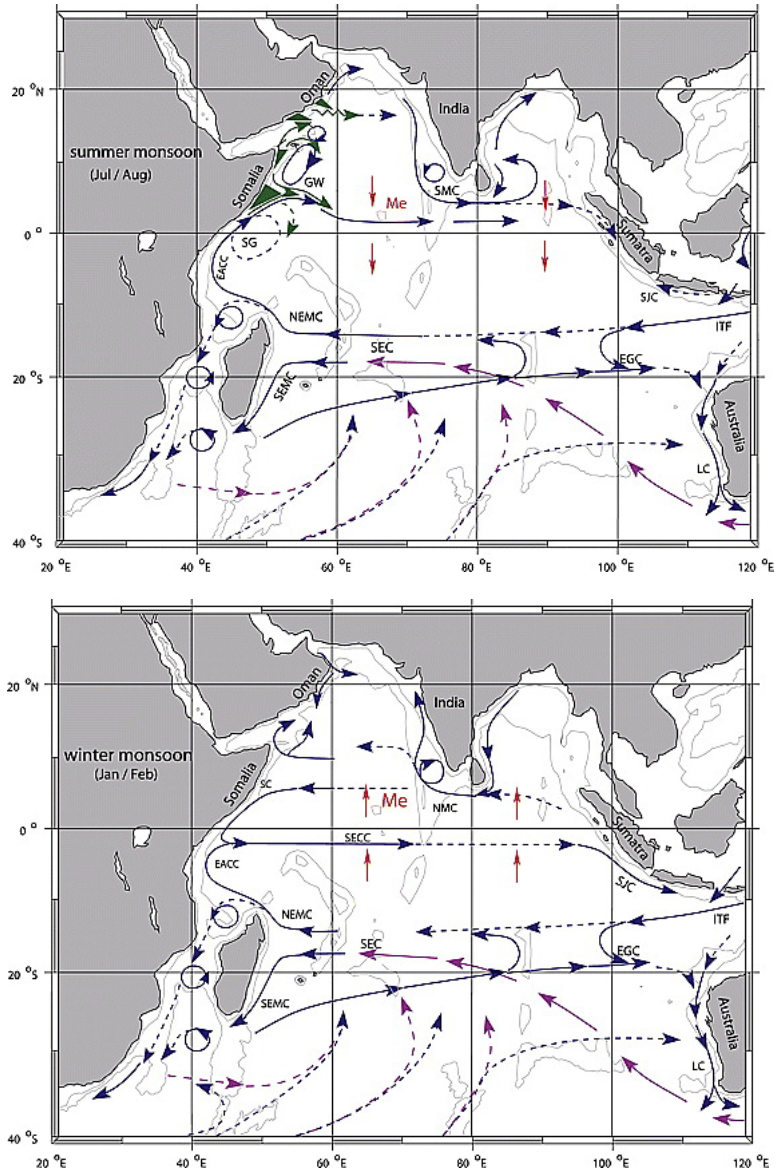

Fig. 2.5 Schematic diagram of the large surface circulation of the Indian Ocean during (a) the peak Southwest Monsoon (Jul/Aug) and (b) the peak Northeast Monsoon (Jan/Feb) showing the following features : the South Equatorial Current (SEC), South Equatorial Countercurrent (SECC), Northeast and Southeast Madagascar current (NEMC and SEMC), East African Coastal Current (EACC), Somali Current (SC), Southwest and Northeast Monsoon Currents (SMC and NMC), South Java Current (SJC), East Gyral Current (EGC), Leeuwin Current, Indonesian Throughflow (ITF), the Southern Gyre (SG) and Great Whirl (GW) with associated upwelling wedges (green arrows). The magenta lines indicate the subsurface return flow of the super gyre. The red vectors represent the direction of meridional Ekman transports. [After: Schott and McCreary, 2001]

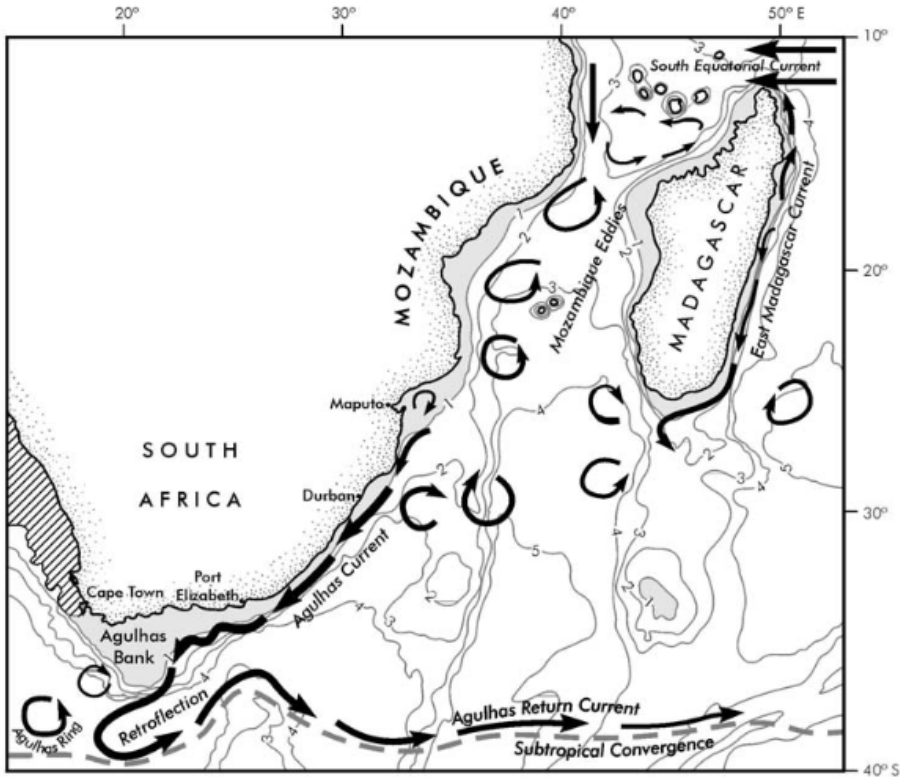

Fig. 2.6 Schematic diagram of the ocean dynamics in the greater Agulhas Current System. The arrows represent the ocean currents and the curvilinear features portrays mesocale eddies. The bathymetric contours are expressed in km [After : Lutjeharms (2006)]

(ASHSW), with specific temperature and salinity values of 26.8 ^{o}C and 36 psu respectively (Figure. 2.7) spreads underneath the mixed layer as a salinity maximum (Morrison, 1997; Schott and Fischer, 2000). However, the strong northwestward coastal current along the west coast of India restricts the spreading of this water mass to the west of 67 ^{o}E while the equatorial currents prevents the southward spreading of ASHSW (Kumar and Prasad, 1999).

The warm and saline Red Sea Intermediate Water (RSIW), formed in that lateral sea, spreads from the north through the strait of Bab el Manded into the Gulf of Aden where it is modified though mixing (Beal et al., 2000). This water mass is characterized by temperatures of around 22 ^{o}C, a salinity maximum of around 39 psu (Figure. 2.7) and the preferred spreading route of RSIW after emerging from the Gulf of Aden into the Arabian Sea is southwestward along the African continental shelf with enhanced flow during the Northeast Monsoon (Beal et al., 2000; Schott and Fischer, 2000). This water mass often occur as patches over the large parts of the Indian Ocean (Shapiro and Meschanov, 1991), it crosses the equator and spread southward into the Agulhas current though the Mozambique Channel (Roman and Lutjeharms, 2009) and within the East madagascar Current (Donohue and Toole, 2003).

The Indian Equatorial Water (IEW) is characterized by small vertical salinity differences, a combination of Indian Ocean waters coming from the north, south and Indonesian Through-flow Water (ITW) (You and Tomczak, 1993). The IEW extends from 150 m to 200m deep and has a temperature and salinity range of 8.0 – 25 ^{o}C and 34.6 – 35.2 psu, respectively (Rao and Ram, 2005). The ITW derived from Pacific Ocean central waters is altered when entering the Indonesian Seas (Song et al., 2004) and flows into the Indian Ocean with more intense flow in the upper layers than in the lower subsurface layers (You and Tomczak, 1993). As this water mass is transported westward by the South Equatorial Current, it slowly dilutes (Song et al., 2004). During the Southwest Monsoon, the ITW tend to spread into the tropical Indian Ocean along the east coast of Africa.

In the tropics, the formation of warm fresh Tropical Surface Water (TSW; (New et al., 2007)) is contributed by excess precipitation over evaporation in the northeastern part of the Indian Ocean, surface warming and the influx of fresh ITW. This water mass located between 0 – 20 ^{o}S, within the north of the SEC, is characterized by temperatures warmer than 24 ^{o}C and salinities in the range 34.4 – 34.6 psu (figure 2.8), where it bifurcates along the east coast of Madagascar. The formation of salinity maximum-water, the Subtropical Surface Water

(STSW; (Morales et al., 1996; Schott and McCreary Jr, 2001)), is attributed due to excess evaporation over precipitation between 25 – 35 ^{o}S in the subtropical, anticylonic gyre of the Southern Hemisphere and subducts below the fresher TSW in the north (Wyrtki, 1973; Karstensen and Quadfasel, 2002). The water mass is characterized by salinity values greater than 35.5 and a neutral density range of 25.5 – 26.4 kgm^3 (Beal et al., 2006). The STSW spreads towards the western boundary at a core depth of 200-250 m within the SEC and shallows as it spreads to a depth of about 100 m (Swallow et al., 1988) and enters the Agulhas Current System by the flow of the southern extension of the East Madagascar Current (Beal et al., 2006).

Similar to the SAMW, the Indian Central Water (ICW) originates at the Subtropical Convergence of the Southern Hemisphere (Tomczak and Godfrey, 2003). This water mass is usually below the thermocline, 200m deep and is characterized by values of temperature ranging between 8 ^{o}C and 25 ^{o}C and salinity between 34.6 and 35.8 (Emery, 2001). The Antartic Internediate Water (AAIW) formed at the Antartic Convergence enters the basin at intermediate depths from the southeast (Fine, 1993). This water mass is formed in the subfrontal zone through subduction and is characterized by an oxygen minimum and a salinity minimum. The low salinity minimum is a result of excess precipitation over evaporation in the area of formation (Schott and McCreary Jr, 2001). In the Indian Ocean, AAIW has the same properties as in the Pacific or Atlantic oceans,i.e. temperatures in the range 2 - 2.5 ^{o}C and salinity of 33.8 psu (Figure. 2.7). However the salinity and temperature increases 34.3 psu and 3 - 4 ^{o}C respectively when the the AAIW enters the subtropical gyre (Tomczak and Godfrey, 2003). AAIW is located in the range 800 – 1200 m deep (Donohue and Toole, 2003) and the distribution of the AAIW is restricted to south of 10 ^{o}S (Tomczak and Godfrey, 2003).

The buoyancy gain and net heat experienced by the North Indian Ocean due to the Asian continent preventing the generation of bottom and deep waters through convection. These waters are formed by mixing or imported into the Indian Ocean through other basins and as such the thermocline circulation of the Indian Ocean represents a conversion of cold, dense, imported waters to warmer waters (Toole and Warren, 1993). Below 3800m, the Indian Ocean is dominated by the Antarctic Bottom Water (AABW) also called the Circumpolar Deep Water (CDW). This water mass is characterized by a temperature of 0.3 ^{o}C and a salinity value of 34.7 psu (Emery, 2001). It is formed in the Southern Ocean and enters into the South West Indian Ocean via the Mozambique Channel and Madagascar basins, through the fractures of the South West Indian Ocean Ridge, near 30 ^{o}S and 56 ^{o}E- 59 ^{o}E (Tomczak

and Godfrey (1994)). It occurs at a depth of more than 4000 m and is characterized by high salinity and oxygen concentrations (Toole and Warren, 1993).

The North Indian Deep Water (NIDW; (Schott and McCreary Jr, 2001)), ranging between 1500m – 3800m (Tomczak and Godfrey, 2003) is limited in oxygen and has a higher salinity due to mixing with older intermediate waters. In the Southwest Indian Ocean, the increased oxygen and salinity gives NIDW the characteristics of diluted North Atlantc Deep Water (NADW). NADW is confined to the extreme southwest of the Indian Ocean, particularly the Natal Valley and the Mozambique Basin by the presence of the Madagascar and Davie ridges (Toole and Warren, 1993). The cold and saline NADW is formed in the North Atlantic Ocean through convection and is spread into the Indian and Pacific Oceans via the Southern Ocean (van Aken et al., 2004). This water mass is then converted to fresher Lower Circumpolar Deep Water (LCDW) in the Southern Ocean through upwelling and mixing with other water masses (Callahan, 1972; Park et al., 1993). Due to large-scale upwelling (Stommel, 1958), NADW and LCDW are believed to rise to shallower depths in the Pacific and Indian Oceans and in the process are warmed by diapycnal mixing with the overlaying less dense water (Munk, 1966). The NIDW has a lower oxygen and higher nutrient content than NADW (Park et al., 1993; You, 2000) while the Upper Circumpolar Deep Water (UCDW) is distingushed from LCDW by its lower oxygen and higher nutrient concentrations.

2.6 Climatology of the upper ocean temperatures and salinities in the South West Indian Ocean

Sea surface temperature plays a major role in the distribution of moisture, heat and gases across the ocean-atmosphere. A few factors, namely, solar radiation, sensible heat flux and release of latent heat of evaporation all play a major role on the influence of the ocean on the atmosphere. The momentum exchange at the air-ocean interface is associated with the surface wind stress. Strong winds can deepen the ocean mixed layer depth (MLD) thereby modulating the efficiency of surface heat fluxes in controlling the upper ocean heat content. This therefore preconditions the subsequent upper ocean variation (Kako and Kubota, 2007; Cronin et al., 2013; Tozuka and Cronin, 2014) which is essential for the development of atmospheric cyclones (Yu and McPhaden, 2011; Seo and Xie, 2013; Jullien et al., 2014). Fluctuations in the air-sea interaction affects the intensity of monsoon and associated rate of

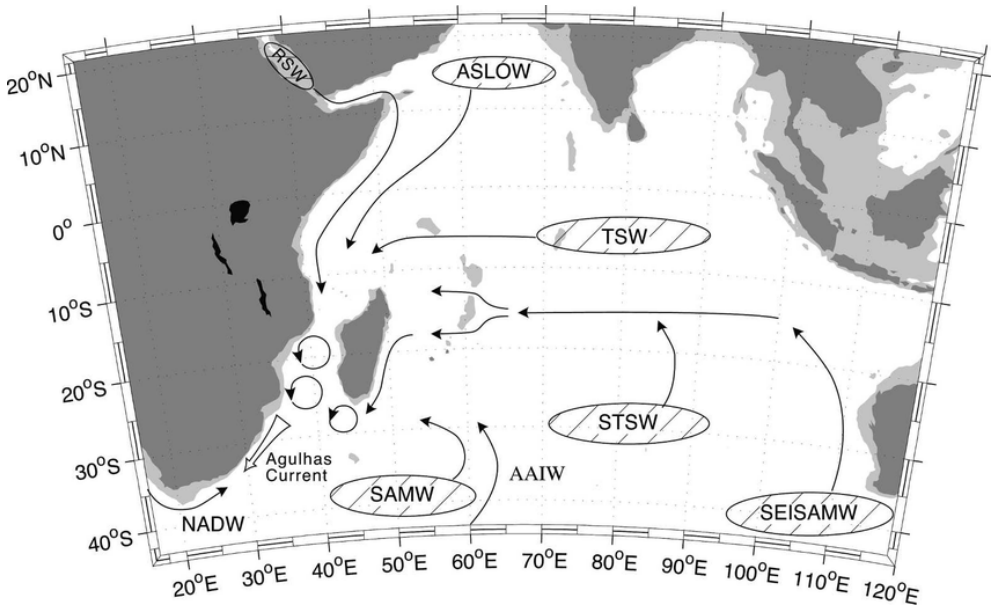

Fig. 2.7 Schematic representation of the main water masses of the Indian Ocean and their path of propagation towards the Greater Agulhas Current System. The encycled water masses indicates their local fomation, while the others, are imported from the other oceanic basins. [After : Beal et al., (2006)].

precipitation over regional areas.The tropical Indian Ocean and its link with the atmosphere influences both the regional and global climate.

Figure 2.8 shows the seasonal climatology of SST in the South West Indian Ocean. During December-February (Northeast Indian Ocean Monsooon), tropical Indian Ocean is warm with values reaching 28 ^{o}C around northeastern part of the domain and are stretched zonally across the central Indian Ocean. This equatorial feature is comparable to that of the western Pacific warm pool. The summer SSTs in the Mozambique Channel range from 28 ^{o}C to 31 ^{o}C with cooler SSTs (28 - 29 ^{o}C) south of 20 ^{o}S. During autumn (March - May) and spring (September - November), the pattern of SST in the channel is similar to summer but with slightly lower temperatures (25 - 29 ^{o}C). Coldest SSTs (25 ^{o}C) are visible east of Madagascar while during spring the waters extend more equatorward as compared to autumn. However, during the Southwest monsoon (austral winter), the western sector experiences cooling (Behera et al., 2000) with temperatures dropping by about 5 ^{o}C (reaching 24-26 ^{o}C) in the Mozambique Channel and (23-25 ^{o}C) east of Madagascar. The influence of the monsoon winds on SST in the equatorial Indian Ocean is so dramatic that the seasonal cycle in the SSTs are larger than in any other tropical ocean (Slingo et al., 2005). The strong southwesterlies of the Southwest monsoon cause a cooling of the sea surface through evaporation and entrainment (Behera et al., 2000). Other key areas of upwelling occur in the

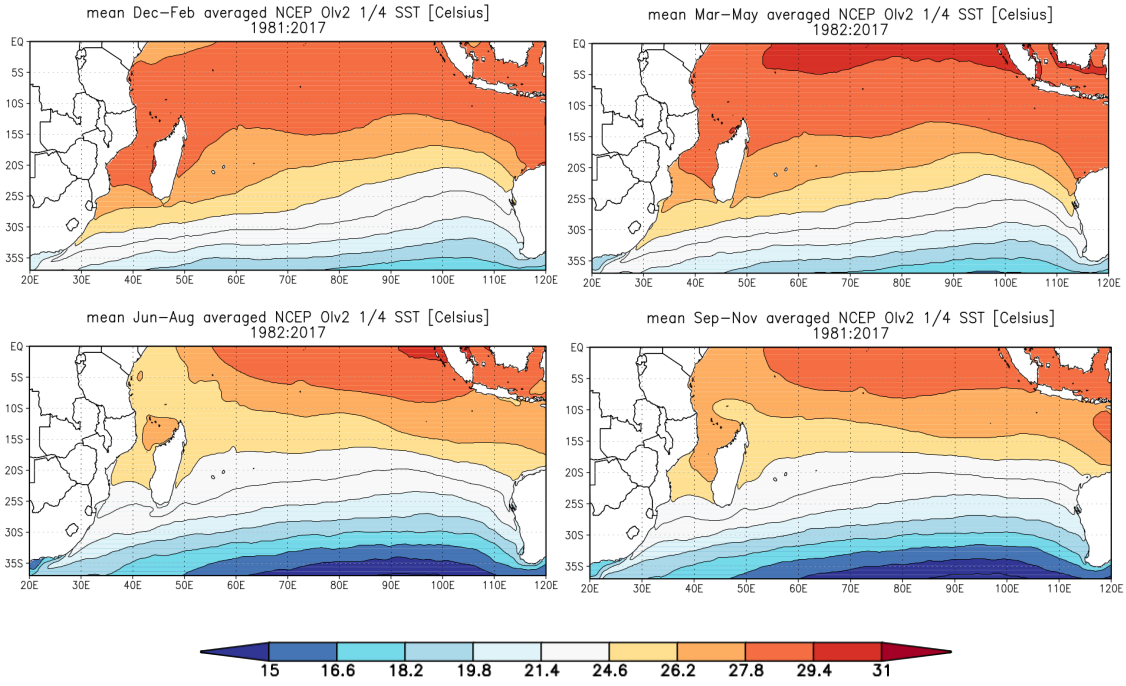

Fig. 2.8 Seasonal Climatology of Sea Surface Temperature (^{o}C) in the South Indian Ocean. [Source: NOAA Optimum Interpolation (OI) Sea Surface Temperature (SST) V2 (https://www.esrl.noaa.gov/psd/data/gridded/data.noaa.oisst.v2.html)]

band 5-10 ^{o}S (Schott et al., 2009; Hermes and Reason, 2008, 2009) is the Seychelles-Chagos thermocline ridge (SCTR), a region where the occurence of significant climatic influence take place. The SCTR is sustained by wind stress curl between the southeasterly trades in the south and equatorial westerlies in the north (Xie et al., 2002; McCreary Jr et al., 1993; Vialard et al., 2009).The relation between the surface, subsurface temperature layer and the sensitivity of the atmosphere to SST contributes to strong air-sea exchanges on different time scales (Vialard et al., 2009) in the SCTR region which can affect areas remotely through atmospheric connections. A few studies have found that changes in the heat content in the SCTR region can influence tropical cyclone activity in the neighbouring area (Jury et al., 1999; Xie et al., 2002; Chowdary et al., 2009).

Salinity together with temperature are determinants of density and thus play an important role in ocean dynamics. Changes in salinity in the open ocean mainly depend on the difference between precipitation and evaporation. However, sea surface salinity (SSS) values are also

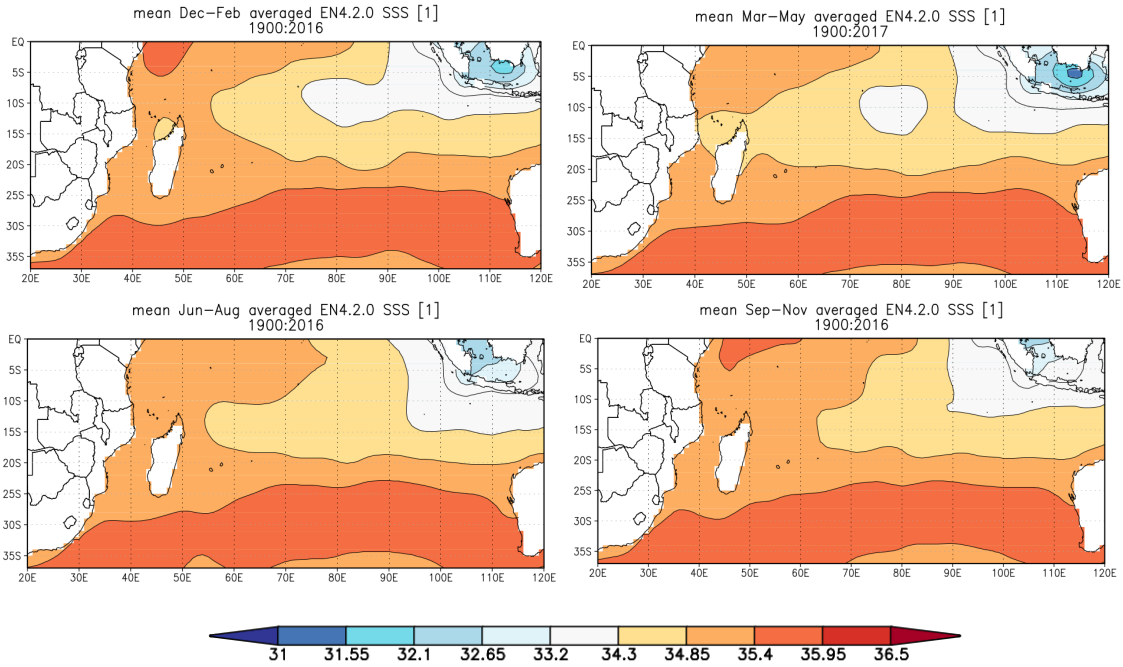

Fig. 2.9 Seasonal Climatology of Sea Surface Salinity (psu) in the South Indian Ocean. [Source : Salinity EN4 (version 4.2.0) supplied by the Met Office]

affected by advection and mixing processes (Rao and Ram, 2005). In the Indian Ocean, additional factors influencing the salinity are river inflow, the influx of more saline water from the Red Sea and Persian Gulf, and the influx of less saline water from the Indonesian Throughflow (Han and McCreary, 2001). In the Indian Ocean, as in the other oceans, SSS (Figure 2.9) closely follows the precipitation-evaporation (P-E) distribution (Figure 2.4).The precipitation in the east exceeds the precipitation in the west (Figure 2.9). A SSS maximum occurs near 30 ^{o}S, corresponding with the P-E minimum. SSS decreases south of 30 ^{o}S and into the Southern Ocean reflecting the influx of freshwater from the melting of Antarctic sea ice. The eastern tropical Indian Ocean display surface salinities near and below 34.5 psu. During summer and spring, there is an increase in SSS towards the coast of Africa in the northwestern part of the domain (Figure 2.9) due to the great excess in evaporation over precipitation experienced by the Red Sea and Persian Gulf resulting in very saline water (Tomczak and Godfrey, 2003).

2.7 Tropical cyclones

2.7.1 Definition of a Tropical Cyclone

A Tropical cyclone (hereafter TC) is a warm-core, low-pressure system which is generated over warm tropical waters with deep convection and a closed cyclonic surface circulation with a well-structured centre (Holland and Lander, 1993) (Figure. 2.10). Tropical cyclones in the Indian or South Pacific Oceans, hurricanes in the north Atlantic and northeastern Pacific or typhoons in the northwestern Pacific are all common names used to describe the same powerful phenomena.

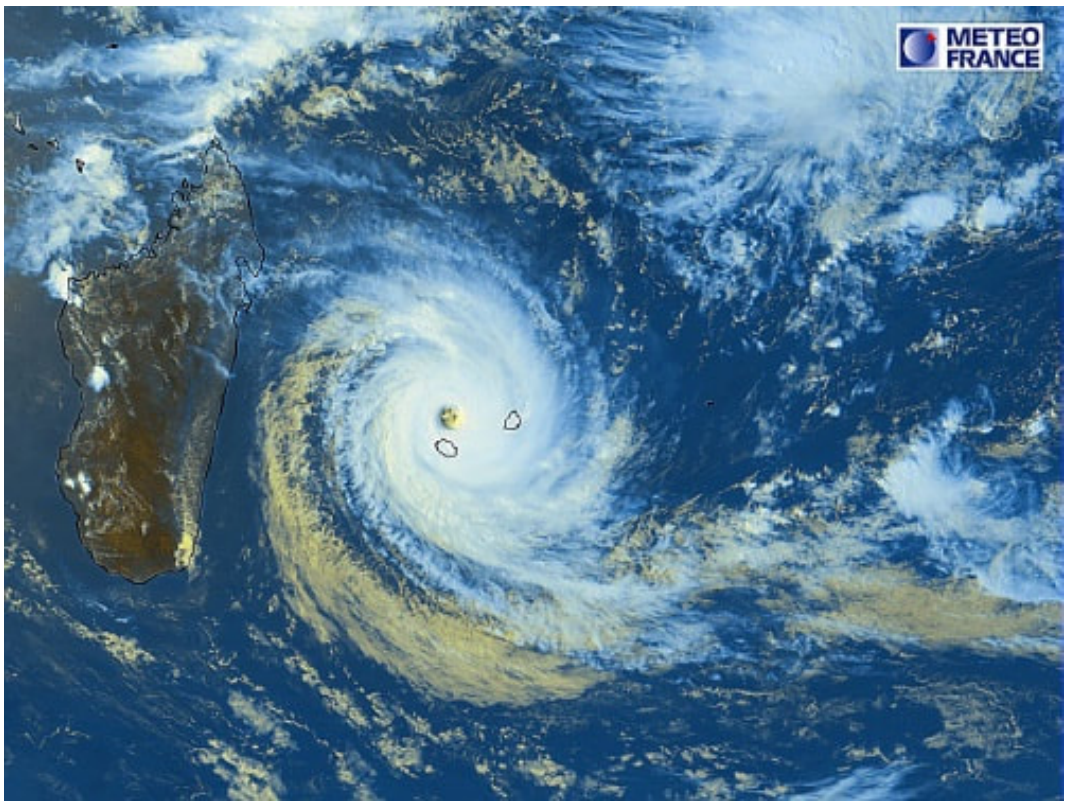

Fig. 2.10 Satellite picture of Tropical Cyclone Bansi (with a well-defined centre) developed over the South West Indian Ocean reaching a Category 5 tropical cyclone on the 13th Feb 2015.

TCs are categorized according to their maximum sustained wind speed (known as MSW) at the surface as either 1-min or 10-min averages being the most typical measure of TC intensity. Cyclones with a MSW of less than 17 m/s are called tropical depressions and once their MSW exceed 17 m/s, they are assigned a name and become tropical storms. Should the

Category	Sustained Wind speeds
Tropical Disturbance	< 50 km/h < 13 m/s
Tropical Depression	51 – 62 km/h ~ 14 – 17 m/s
Moderate Tropical Storm	63 – 88 km/h ~ 18 – 24 m/s
Severe Tropical Storm	89 – 117 km/h ~ 25 – 33 m/s
Tropical Cyclone	118 – 165 km/h ~ 33 – 45 m/s
Intense Tropical Cyclone	166 – 212 km/h ~ 46 – 58 m/s
Very Intense Tropical Cyclone	> 212 km/h > 59 m/s

Table 2.1 The South West Indian Ocean Tropical Cyclone Intensity Scale based on the maximum sustained wind speeds of tropical cyclones, adopted from Meteo-France La Reunion.

named storm intensify further and exceed 33 m/s, it is then classified as a tropical cyclone. Over the South West Indian Ocean, TCs are monitored by the Meteo-France meteorological station in La Reunion island (MFR, RSMC La Reunion), located east of Madagascar. Meteo-France uses seven categories, denoted as the Meteo-France TC intensity scale (shown in Table. 2.1 below), to classify storms in the South West Indian Ocean based on a 10-min average.

Tropical cyclones require the following specific environmental conditions to form and maintain their systems (Gray, 1968; (Pielke, 1990)):

* Oceanic temperature above 26 ^{o}C in the surface layer to provide enough energy to fuel its engine

* High relative humidity at mid troposphere to sustain deep convection
* Pre-existing low-level and/or upper-level disturbance
* Weak vertical wind shear
* a location poleward about 4^o to 5^o of latitude
* an atmosphere that enables the temperature to cool with height

2.7.2 The structure and life cycle of a Tropical Cyclone

A tropical cyclone is composed of three main parts, namely the rainbands, the eye and the deep eyewall clouds. Towards the centre of the cyclone, air spirals are clockwise in the Southern Hemisphere (counter-clockwise in the Northern Hemisphere) and circulate in the opposite direction out at the top (National Weather Service (2010)) as depicted in Figure. 2.11. The eyewall of a storm can increase or decrease in size and secondary eyewalls can be formed. These may lead to fluctuation in wind speeds which regulate the intensity of the storm. The formation of a secondary eyewall is associated with a rise in the potential intensity, a decrease in the vertical wind shear, a thick thermocline, reduced upper tropospheric zonal winds and middle to upper relative humidity (Kossin and Sitkowski, 2009).

The different stages of a tropical cyclone include formation, development, mature stage and dissipation. In the intensification phase, the momentum from the outer to the inner core strengthens the wind field and the formation of the eye wall cloud (Weatherford, 1989). During the second stage, the eye becomes larger and the filling of the inner core is carried on through the movement of air towards the centre of the cyclone. The longer the storm stays in this stage and as long as the eye exists, the larger will be the radius of the damaging winds. During the last stage, the outer wind starts to weaken with the disappearing of the eye (Weatherford, 1989).

2.7.3 Tropical cyclones in the South West Indian Ocean

Seasonal occurrence and Impact of Tropical cyclones

Tropical cyclones are recurring phenomenon in the South West Indian Ocean (SWIO), with about 12-13 tropical cyclones are generated west of 100^oE (Fink and Speth, 1998; Mavume

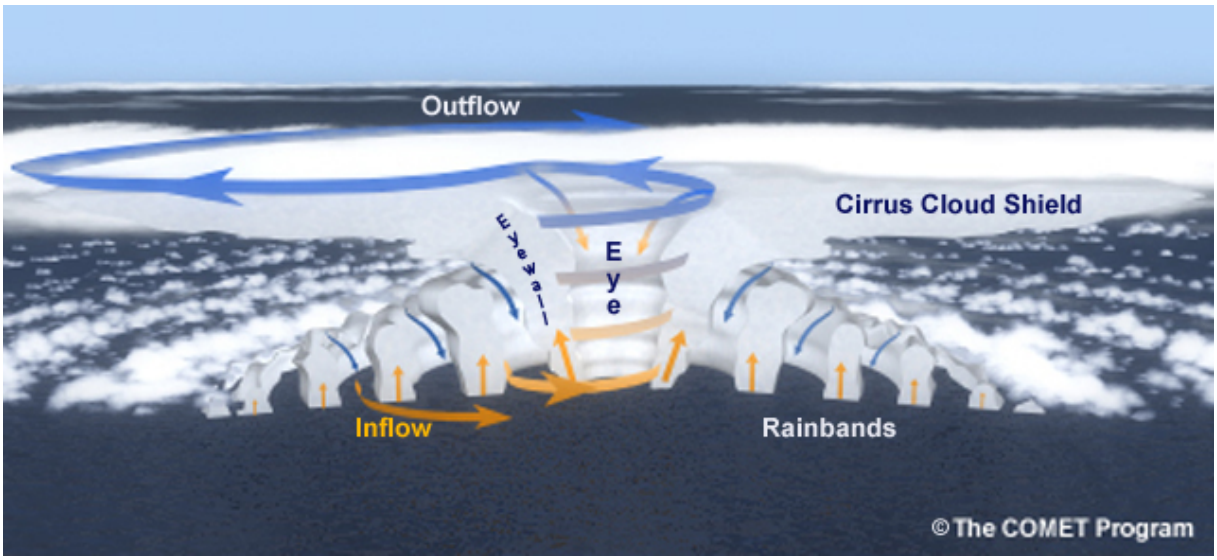

Fig. 2.11 A vertical cross section diagram of a tropical cyclone in the Northern hemisphere, with arrows indicating air flow in and around the eye. [Source : https://serc.carleton.edu/eslabs/hurricanes/2c.html]

et al., 2009). In the SWIO, cyclones occur from November-April with a peak in January-February and the inhabitants of the western part of the basin are at risk to recurring TC impacts. TCs pass near Mauritius and Reunion quite frequently and can cause material damage and societal disruption, though loss of human life is under control by a well-structured TC warning system implemented on these islands (Parker and Jury, 1999; Roux et al., 2004). Tropical cyclones cause severe damage when they make landfall over underdeveloped countries. According to Mavume et al. (2009), over the period 1952- 2007, 152 TCs out of 633 in the southwestern Indian Ocean made landfall in Madagascar and Mozambique.

Madagascar and Mozambique have also endured many devastating impacts from tropical cyclones (Jury et al., 1993; Naeraa and Jury, 1998; Chang-Seng and Jury, 2010b) and the population's vulnerability is increasing due to the increased number of inhabitants residing along the coast. In late February 2000, flooding associated with TC Eline claimed 600 lives and approximately 2 million people had to be displaced (Mavume, 2008). On 22nd February 2007, after being formed one week prior in the South Indian Ocean, TC Favio made landfall on the southern coast of Mozambique as a category 3 cyclone (Klinman and Reason, 2008). Favio aggravated an already occurring flood which led to 4 fatalities and 70 injuries. Businesses, hospitals and schools were damaged as well as a prison from which 600 prisoners escaped. In addition, 120,000 people were displaced in Mozambique due to flooding. The

islands National Disaster Risk Management Office announced that more than 17,000 people were impacted by the tropical cyclones with 13 reported deaths and the destruction of approximately 1500 homes (IRIN - https://www.irinnews.org/africa/southern-africa/mozambique, 2015b).

Landfalling tropical cyclones and associated rainfall

In this SWIO, about three landfalling tropical cyclones occur over Madagascar and/or Mozambique each year (Mavume et al., 2009). Over than damages caused by storm surges over these coastal areas during landfall, TC rainfall can also trigger widespread flooding over some parts of the southern African mainland (Reason and Keibel, 2004; Crimp and Mason, 1999), like Mozambique, Zimbabwe, eastern part of South Africa and Botswana. Between 1948 and 2008, after making landfall over the southern African subcontinent, about 45 tropical cyclones brought rainfall over the Limpopo River Basin (Malherbe et al., 2012). Vitart et al. (2003) analysed the risk of landfalling systems over Mozambique using both observations and numerical models by pointing out predictors and potential physical mechanisms that are accountable for changes in the risk of landfall over Mozambique on a day to day basis. Results suggest that ENSO and SWIO SSTs have a large impact on the risk of landfalls over Mozambique (Vitart et al., 2003).

Impact of Large-scale climate modes on tropical cyclones

Large scale circulation patterns related to TC activity in the southern Indian Ocean have been previously analysed and are relatively well understood. The El Nino Southern Oscillation (ENSO), the Madden-Julian Oscillation, and the Indian Ocean Dipole, or Zonal Mode, are the main large-scale climate modes that modulate the spatial distribution and frequency of cyclogenesis in the southern Indian Ocean (Kuleshov and de Hoedt, 2003; Bessafi and Wheeler, 2006; Ho et al., 2006; Camargo et al., 2007; Kuleshov et al., 2008; Leroy and Wheeler, 2008; Chan, 2009; Kuleshov et al., 2009; Vitart et al., 2010).Zonal steering flow (850–200 hPa) computed across the tropical and subtropical parts of the basin is more westerly (easterly) during El Niño (La Niña). Consequently, during La Niña, Mozambique experiences more TC making landfall, while during El Niño, westerly steering flows increase the probability TCs recurving just east of Madagascar (Jury et al., 1999; Vitart et al., 2003; Reason and Keibel, 2004; Ho et al., 2006; Camargo et al., 2007; Kuleshov et al., 2009), therefore reducing

the number of TCs making landfall over the southern african mainland. Chang-Seng and Jury (2010a) agree that La Niña is associated with a rise in the frequency and duration of intense TCs in the southwestern Indian basin. However, although ENSO plays a significant role in climate variability in the global tropics and subtropics, it does not describe fully the variability in the global tropical and subtropical air-sea interaction, nor does it explain in totality the variability of TC trajectories in the southwestern Indian ocean (Fauchereau et al., 2003; Vitart et al., 2003; Huang and Shukla, 2007; Klinman and Reason, 2008). Reason and Keibel (2004) have studied the evolution of TC Eline and its impacts over the southern Africa mainland. This cyclone was the longest lived TC observed (29 days) and the precursor for the synoptic conditions was a La Nina event which produced favourable conditions for this event.

The Subtropical Indian Ocean Dipole (SIOD) also plays a main role in ocean-atmosphere variability in the southern Indian Ocean, impacting TC trajectories on interseasonal to seasonal time scales (Ash and Matyas, 2012). The SIOD is denoted by the second empirical orthogonal function of southern Indian Ocean tropical and subtropical SSTA (Behera et al., 2000; Behera and Yamagata, 2001; Qian et al., 2002; Suzuki et al., 2004; Huang and Shukla, 2007). During autral summer season, this pattern is more prominent and in the positive (negative) mode, it is characterised by cool (warm) SSTA in the southeastern Indian Ocean and warm (cool) temperatures in the southwestern Indian Ocean. Cooling mechanisms in the eastern pole during a positive phase are enhanced by southeasterly trade winds,giving rise to an increase in ocean surface evaporation and mixing, while simultaneously, the western warm pole develops with increased poleward Ekman transport of warm SSTs from tropical latitudes, with a reduction in the flow of equatorward cold air and ocean surface evaporation (Reason and Mulenga, 1999; Venzke et al., 2000; Behera and Yamagata, 2001; Qian et al., 2002; Hermes and Reason, 2005; Chiodi and Harrison, 2007; Huang and Shukla, 2007). In positive phase, the SSTA poles are generally the opposite with the flow of cold air and equatorward Ekman pumping located over the southeastern Indian Ocean with persistent cold frontal passages, while warm air advection are more frequent over the southwestern part of the basin, enhancing the formation of tropical cyclones in the area.

Since TCs forming in the central and southeastern Indian Ocean may cross thousands of kilometres to the west to impact southeastern African countries, it is therefore of importance to understand the variability of TC trajectory and the ocean-atmosphere interaction at

intraseasonal to seasonal time scales.

2.7.4 Upper ocean parameters necessary for tropical cyclones genesis and intensification

Environmental interaction which is the interplay between the ocean and the cyclone, is the most important source necessary to influence TC intensity. The energy available for uptake is obtained from warm tropical waters delivered via surface heat flux. Emanuel (1999), showed that the intensity of a cyclone is dependent on three main factors, namely the initial storm intensity, thermodynamic state of the atmosphere necessary for the cyclone to evolve and the upper ocean heat exchange beneath the cyclone. A few studies have found that when a cyclone passes over a thick upper ocean mixed layer, it intensifies rapidly, implying that the upper ocean thermal structure plays an important role in its intensification process (Subrahmanyam et al., 2005; Vissa et al., 2013). (Sutyrin and Khain, 1979) carried out simulations using a coupled model (oceanic and atmospheric boundary layers) and found out that the interaction is strong enough to alter moisture and heat exchanges from the ocean to the atmosphere within a few hours of the formation of the storm and as a result, influences its intensity. Balaguru et al. (2014) showed that the intensity of a tropical cyclone is increased with a rise in SST and upper ocean heat content, leading to a positive feedback during cyclogenesis and intensification. During this process, the evaporation from the ocean's surface stimulates the winds at the surface and increases the moisture supply which in turn increases the latent heat used to drive the circulation.

The most notable effect of TCs on the ocean is the sea surface cooling perceived from satellites, denoted as the TC cold wake. The intense winds of tropical cyclones cause tremendous vertical mixing of the upper ocean and sea surface cooling which acts as a negative feedback on the storm's intensity (Price, 1981; Bender and Ginis, 2000; Lin et al., 2005; D'Asaro et al., 2007; Lloyd and Vecchi, 2011; Balaguru et al., 2012). The translational speed of the storm has an impact on the intensity of the SST cooling, which implies that if the storm has a fast translational speed, the SST cooling is reduced and less energy is necessary to sustain it.

Although SSTs are not the dominant factor that determine TC intensity (Evans, 1993; Mavume et al., 2009), they play an important role in their formation (Palmen, 1948) but the

sub surface ocean thermal structure is considered an important predictor for TC intensification (Goni and Trinanes, 2003; Lin et al., 2009a; Wada et al., 2012). A warm enough mixed layer, is needed for at least two reasons; i) to prevent cool deeper water to reach the surface because of wind-mixing, ii) to support strong turbulent heat fluxes into the atmosphere. Leipper and Volgenau (1972) introduced a metric, known as the Tropical Cyclone Heat Potential (TCHP) to predict the potential for TC formation. The TCHP is the integral of the surface temperature to the depth of 26 ^{o}C isotherm, where the minimum energy needed to sustain or initiate a TC is about 40 kJcm^{-2} (Malan et al., 2013). The conditions prior to the formation of a cyclone is very important in controlling its development; a deeper mixed layer depth with a warmer heat content will withstand longer. While both SST and TCHP serve as useful measures of the upper ocean heat content, they do not represent accurately the ocean stratification effects. Not every storm stirs the ocean to a depth of 26 ^{o}C isotherm but the depth to which it mixes the ocean varies dynamically and depends on the prevailing ocean states. A new metric known as Tdy, uses a varying mixing length to compute the upper ocean heat content and gives a better representation of the ocean stratification. A few studies have shown that replacing the SST or TCHP by Tdy, improves the prediction of TC intensity (Balaguru et al., 2015, 2016; Foltz et al., 2018). The Tdy is calculated as follows:

$$T_{dy} = \frac{1}{L}\int_0^L T(z)dz \tag{2.1}$$

where L is the vertical ocean mixing length of the storm which is estimated as :

$$L = h + (\frac{2\rho_o u_*^3 t}{\kappa g \alpha})^{\frac{1}{3}} \tag{2.2}$$

where h is the initial mixed layer depth, u_* is the friction velocity, t is the time of mixing, κ is the von Kármán constant, g is the acceleration due to gravity, and α is the rate of change of density beneath the mixed layer.

In several TC regions, salinity is almost as important as the temperature of the water. It is the stability of the mixed layer, rather than the temperature alone that prevents the surface water from cooling. Another important parameter for cyclogenesis and TC intensification is the Barrier Layer Thickness (BLT). The BLT depends on the mixed layer depth and acts as an interface for air-sea interactions. During fresh water input (by rainfall or river discharge), a uniform density mixed layer depth becomes shallower than the uniform temperature layer

due to the influence of salinity (Balaguru et al., 2012). The layer between the base of the mixed layer and the base of the isothermal layer is defined as the BLT :

$$BLT = ILD - MLD \tag{2.3}$$

where ILD is the isothermal layer depth and MLD is the mixed layer depth.

2.7.5 Effects of ocean eddies on tropical cyclones

There have been doubts about whether the flow in the Mozambique Channel was continuous (Lutjeharms, 2006) or not. A few studies (Gründlingh, 1995; DiMarco et al., 2002; Biastoch and Krauss, 1999) have shown that the flow is more complex than a simple western boundary current but were in fact of a series of cyclonic and anticyclonic eddies (Harris, 1972; de Ruijter et al., 2002; Ridderinkhof and De Ruijter, 2003). At the tip of northern Madagascar, the NEMC generates large anticyclonic eddies (LaCasce et al., 2008; Collins et al., 2016) which propagate southward into the Channel (de Ruijter et al., 2002; Ridderinkhof and De Ruijter, 2003; Backeberg and Reason, 2010). Around 15-16 ^{o}S, where the channel is narrow, additional anticyclonic eddies are formed and are found to be the most intense (de Ruijter et al., 2002). The western and eastern side of the channel varies differently, the flow on the western side is highly variable with high eddy kinetic energy while that on the eastern side is low (Lutjeharms, 2006). The southward movement of eddies along the shelf edge of the channel may merge with the SEMC in the southern part of the channel and move into the Agulhas Current (Van der Werf et al., 2009).

Previous studies have reported that the presence of warm ocean areas such as ocean currents and warm eddies could influence passing tropical cyclones, causing sudden and unexpected intensification (Shay et al., 2000; Goni and Trinanes, 2003; Lin et al., 2005; Scharroo et al., 2005). According to Mavume et al. (2009), presence of energetic eddies in the western corridor of the Mozambique Channel is a strong indication of a potentially important source of energy for tropical cyclones. Warm ocean eddies are distinguished by a deep and thick 26 ^{o}C isothermal layer, which act as a thermal insulator between TCs and deeper cooler ocean water (Lin et al., 2005; DeMaria et al., 2005). When a tropical cyclone interacts with a warm anticyclonic eddy, the upper ocean mixed layers tend to prevent the entrainment of cold and deep water, leading to a reduced sea surface cooling compared to areas where there are no warm eddies (Shay et al., 2000; Hong et al., 2000; Jaimes and Shay,

2009; Lin et al., 2005; Wu et al., 2007; Lin et al., 2009a,b; Ali et al., 2007; Bender and Ginis, 2000; Vianna et al., 2010).

2.8 Research Questions

- Is the frequency and intensity of tropical cyclones increasing in the South West Indian Ocean? (**Chapter 4**)

- Is there any link between upper ocean characteristics and large-scale climate modes? (**Chapter 4**)

- What are the mechanisms of barrier layer thickness formation in the South West Indian Ocean? (**Chapter 4**)

- What are the upper ocean conditions necessary for tropical cyclone genesis and intensification? (**Chapter 4**)

- Are there any trends in the upper ocean characteristics in the South West Indian Ocean over the period 1980-2010? (**Chapter 4**)

- On the weather scale, how does the upper ocean characteristics influence the evolution of a tropical cyclone? (**Chapter 4**)

- How does tidal forcing influence the upper ocean characteristics? (**Chapter 5**)

- What impact does the tidal forcing have on the upper ocean characteristics on a seasonal and daily time scale? (**Chapter 5**)

- How does the upper ocean structure change when a cyclone encounters an eddy and how including tidal forcing can be important for TC evolution and intensification?

(**Chapter 5**)

- Does the upper ocean heat content (Tdy) in the South Indian Ocean influence summer rainfall over southern Africa? (**Chapter 6**)

- Are there any links between atmospheric circulations and southern African rainfall?(**Chapter 6**)

- How does anomalous Tdy in the Mozambique Channel or over the SCTR region influence the formation, tracks and intensification of tropical cyclones in the SWIO? (**Chapter 6**)

Chapter 3

Data and Methods

3.1 Numerical Modelling

Part of this study is based on a Regional Ocean Modeling System (ROMS) in the AGRIF version used and developed at IRD ("Institut de Recherche pour le Developpement") to simulate the eddy general circulation and the principal lunar, semidiurnal M_2 barotropic and baroclinic tides in the Mozambique Channel. The main objective is to investigate the effect of tidal forcing on the upper ocean structure, which can potentially influence the intensity of passing tropical cyclones in the region. The methodological objective is to construct a robust and reliable high resolution hydrodynamic numerical model for the Mozambique Channel. The model is evaluated against available data from tidal gauges and satellite data (See Appendix A).

3.1.1 The Regional Ocean Modelling System (ROMS)

ROMS is a split-explicit, free surface, ocean-only model discretised in coastline and terrain-following curvilinear coordinates (Shchepetkin and McWilliams, 2003, 2005, 2009). In seperating the solutions to the barotropic and baroclinic modes of the momentum equations, the split-explicit approach reduces the number of time-stepping operations required (Shchepetkin and McWilliams, 2005). The associated gain in computational efficiency allows for simulations to be perfomed at higher resolution, advantageous for studies that focus on the mesoscale.

Governing Equations

ROMS solves the incompressible primitive equations under the Boussinesq and hydrostatic approximations. The boussinesq specifies that density variations that do not pertain to buoyancy forcing are neglected. The latter negates vertical acceleration and the effect of Coriolis on vertical velocity; the vertical pressure gradient is balanced solely by buoyancy forcing in this case. Under these approximations, the horizontal (Eq. 3.1 and (Eq. 3.2) and hydrostatic balance (Eq. 3.5) equations take the following form in cartesian coordinates:

$$\frac{\partial u}{\partial t} + \vec{v}.\nabla u - fv = -\frac{\partial \phi}{\partial x} + F_u + D_u \tag{3.1}$$

$$\frac{\partial v}{\partial t} + \vec{v}.\nabla v + fu = -\frac{\partial \phi}{\partial x} + F_v + D_v \tag{3.2}$$

In addition, three further equations govern the advective-diffusive evolution of tracer properties (Eq. 3.3 and (Eq. 3.4) and the conservation of mass in an incompressible fluid (Eq. 3.6)

$$\frac{\partial T}{\partial t} + \vec{v}.\nabla T = F_T + D_T \tag{3.3}$$

$$\frac{\partial S}{\partial t} + \vec{v}.\nabla S = F_S + D_S \tag{3.4}$$

$$\frac{\partial \phi}{\partial z} = \frac{\rho g}{\rho_o} \tag{3.5}$$

$$\frac{\partial u}{\partial x} + \frac{\partial v}{\partial y} = \frac{\partial w}{\partial z} \tag{3.6}$$

These equations are coupled with a non-linear equation of state (Eq. 3.7) (Jackett and Mcdougall, 1995).

$$\rho = \rho(T, S, P) \tag{3.7}$$

where :

- x, y, z are the zonal, meridional and vertical directions coordinate in a cartesian reference frame (m)
- u, v are the horizontal and w the vertical velocity components in x,y and z, respectively (ms^{-1})

- t is the time (s)
- $\vec{v}$ is a velocity vector
- f is the Coriolis parameter (s^{-1})
- g is the acceleration due to gravity (ms^{-2})
- ρ is the sea water density and ρ_o is the reference density of sea water (1025 kgm^{-3})
- P is pressure (Nm^{-2})
- T is the potential temperature (^oC)
- S is the salinity
- F_u,F_v,F_T,F_S are the forcing terms
- D_u,D_v,D_T,D_S are the dissipative terms
- ϕ is the dynamic pressure

A full description of the ROMS numerical implementation of the above equations can be found in (Shchepetkin and McWilliams, 2003, 2005).

3.1.2 Boundary condition Schemes

As a regional model, ROMS requires boundary information at each of its external faces; the free-surface, bottom and, four lateral boundaries, where it may connect to an external solution. The effects of external forcing at the surface and ocean floor are achieved by the modification of vertical viscosity and diffusivity in the free-surface and bottom boundary layers.

Vertical Boundary Conditions

- At the sea surface : $z = \zeta(x,y,t)$

$$K_v \frac{\partial u}{\partial z} = \frac{\tau_s^x}{\rho_o}(x,y,t) \tag{3.8}$$

$$K_v \frac{\partial v}{\partial z} = \frac{\tau_s^y}{\rho_o}(x,y,t) \tag{3.9}$$

$$K_T \frac{\partial T}{\partial z} = \frac{Q_T}{\rho_o C_p} \tag{3.10}$$

$$K_S \frac{\partial S}{\partial z} = \frac{(E_v - P_\tau)S}{\rho_o} \tag{3.11}$$

$$w = \frac{\partial \zeta}{\partial t} \tag{3.12}$$

- At the seafloor : $z = -H(x,y)$

$$K_v \frac{\partial u}{\partial z} = \frac{\tau_b^x}{\rho_o}(x,y,t) \tag{3.13}$$

$$K_v \frac{\partial v}{\partial z} = \frac{\tau_b^y}{\rho_o}(x,y,t) \tag{3.14}$$

$$K_T \frac{\partial T}{\partial z} = 0 \tag{3.15}$$

$$K_S \frac{\partial S}{\partial z} = 0 \tag{3.16}$$

$$-w + \vec{v}.\nabla H = 0 \tag{3.17}$$

where, in addition to the previous,

- ζ is the sea surface height (m)
- H is the depth of the bottom boundary (m)
- τ_s^x / τ_s^y are the zonal and meridional surface wind stress (Nm^{-2})
- τ_b^x / τ_b^y are the zonal and meridional bottom stresses (Nm^{-2})
- K_v is the vertical diffusivity ($m^2 s^{-1}$)
- K_T and K_S are the horizontal tracer diffusion terms ($m^2 s^{-1}$)
- Q_T is the surface heat flux (Wm^{-2})
- $E_v - P_\tau$ is the surface fresh water balance (evaporation rate (cm/day) minus precipitation rate (cm/day))

- C_p is the specific heat capacity ($Jkg^{-1}K^{-1}$)

The equations. 3.8 and 3.9 are the horizontal momentum transfered into the ocean by atmospheric wind stress at the sea surface, in the x and y directions respectively. The equations. 3.10 and 3.11 are the thermal and freswater fluxes at the sea surface and the equation 3.12 represents the vertical velocities associated with the variation of the sea surface. For the bottom, the equations 3.13 and 3.14 express the momentum transfered into the ocean by friction at the seafloor. The equations 3.15 and 3.16 give the vertical thermal and salt fluxes at the seafloor. The equation 3.17 denote the non-crossing of the topography by the flow at the seafloor.

The components of the surface wind stress τ_s are given by :

$$\tau_s^x = \rho_{air} C_D \sqrt{u_{10}^2 + v_{10}^2}.u_{10} \tag{3.18}$$

$$\tau_s^y = \rho_{air} C_D \sqrt{u_{10}^2 + v_{10}^2}.v_{10} \tag{3.19}$$

For a variable topography, at the seafloor $z = -H(x,y)$, the horizontal bottom velocities have a parameterized bottom stress which can be a choice between linear, quadratic, or logarithmic terms (Hedstrom, 2009). The Bottom friction is perscribed as:

$$\tau_b^x = (\zeta_1 + \zeta_2 \sqrt{u^2 + v^2}).u \tag{3.20}$$

$$\tau_b^y = (\zeta_1 + \zeta_2 \sqrt{u^2 + v^2}).v \tag{3.21}$$

where,

- ρ_{air} is the density of atmospheric air $[\frac{\partial kg}{\partial m^3}]$.
- ζ_1 is the coefficient of linear bottom friction.
- ζ_2 is the coefficient of quadratic bottom friction.
- C_D is non-dimensional wind-drag coefficient.
- u_{10}, v_{10} are the horizontal components of the wind vector in x and y respectively measured at 10 m above sea level.

3.1.3 Domain specifics

The model is a ROMS based configuration which has been implemented in the South West Indian Ocean, focused on the Mozambique Channel. It has been designed to investigate the effect of tidal forcing on the upper ocean properties in this region. The configuration was built using ROMSTOOLS (Penven et al., 2008). The geographical domain lies between 5-28 ^{o}S and 30-50 ^{o}E (Figure 1.1) and encompasses some of the main ocean currents, namely : the North East Madagascar current, the South East Madagascar current. It also includes the eddy field associated with the Mozambique Channel. The model was configured at a horizontal resolution of 1/12^{o} to be able to resolve mesoscale features and associated processes. The model is closed at the western boundary. The vertical resolution in the model is defined by 40 σ-coordinate levels, distributed according to $\theta_b = 0$ and $\theta_s = 6$ resulting in an increased concentration towards the surface. The transition depth between the horizontal surface layers and the minimum depth was set to $h_c = 10m$ which gives a better depiction of outflows in shallow straits. The model topography was bilinearly interpolated onto the grid from the high resolution dataset, gridded at 1-minute, derived from the Global Earth Bathymetric Chart of the Oceans (GEBCO1) global topography data set. The pressure gradient errors as stated previously, are reduced by smoothing the bathymetry where the smoothing parameter, r, is less than a critical value of 0.2 (Haidvogel and Beckmann, 1999). A selective hanning filter was applied to remove any steep topographic features in the deep ocean that could possibly cause some numerical instabilities into the system.

3.1.4 Surface forcing

The daily averaged surface forcing used in the ROMS simulations is derived from the Climate Forecast System Reanalysis (CFSR, Saha et al., 2010). The CFSR is global and consists of models of the atmosphere, ocean, land surface, and sea ice and an assimilation system to combine the model first-guess fields with observations. The spectral atmospheric model is T382 (resolution, 38 km) with 64 vertical levels. The ocean part of CFSR, which is the Modular Ocean Model (MOM, version 4), has a steady vertical resolution of 0.5^{o} longitude, but a variable horizontal resolution that increases from 0.25^{o} between 10^{o}N and 10^{o}S to 0.5^{o} at 30^{o} latitude, but remains constant from there to the poles. Outputs from the MOM has been stored on a 0.5^{o} latitude × 0.5^{o} longitude grid. There are 40 vertical levels with 27 in the upper 400 m. Preliminary analyses show that the CFSR output is better to previous NCEP reanalyses although some biases are still present (Higgins et al., 2010; Saha et al.,

2010). The CFSR was initially generated for the years 1979–2009, but the period used in this study spans between 1990 to 2008.

3.1.5 Lateral boundaries and initial conditions

The initial and boundary conditions for temperature T and salinity S are acquired from the monthly Simple Ocean Data Analysis (SODA; (Carton et al., 2000; Carton and Giese, 2008)). The ocean general circulation model used in SODA (version 2.2.4) has an average horizontal resolution of 0.25^{o} latitude $\times$ 0.4^{o} longitude with 40 vertical levels. A few versions of SODA (v2.0.2, v2.0.4, and v2.2.4) are combined to make a longer time series of T/S to extrapolate the period of the ROMS simulations from 1979 to 2008. The T and S values are used to compute the currents at the initial time and along the boundaries, where the off-equatorial currents are computed assuming geostrophy. However, within 2^{o} of the equator the currents are obtained by linear interpolation between the off-equatorial values. SODA is used instead of CFSR since the upper-ocean temperature in CFSR is kept as daily SST and salinity available as monthly climatology. This may therefore create large imbalances in the density field which may generate spurious currents.

3.1.6 Tidal parameterization

One of the most important forcing for bottom currents over the Mozambique Channel is from tides. The barotropic tides were introduced at the model lateral open boundaries using an inverse modeling technique,the Flather radiation condition (Flather, 1987) to force velocities and sea surface elevations from the TPXO global tidal solution (Egbert and Erofeeva 2002). The top 10 constituents (M2, S2, N2, K2, K1, O1, P1, Q1, Mf, Mm ; ordered by their amplitudes in the Mozambique Channel) for elevation and barotropic flow were interpolated from TPXO.7, with a horizontal resolution of 0.25 degrees. Two runs were performed to assess the role of tidal forcing in the Mozambique Channel. The main difference between the two runs was that one included tidal forcing (***Tide***) while the other did not (***NoTide***). Other parameters and forcing functions remain identical between both runs.

3.2 Tropical Cyclone data

3.2.1 IBTrACS

The best track analysis used in the present study is version v03r09 from the International Best Track Archive for Climate Stewardship (IBTrACS) dataset (Knapp et al., 2010), developed by the NOAA National Climatic Data Center, which were the first to synthese and combine best track data worldwide from all official Tropical Cyclone Warning Centers (TCWCs) and the WMO Regional Specialized Meteorological Centers (RSMCs). The dataset contains the position in terms of latitudes and longitudes, maximum winds attained by the storm, minimum central pressure, and storm nature for every tropical cyclone globally at every 6-hr interval in UTC. The dataset is freely available from 1848 to the present but here, the interannual variability of tropical cyclones was investigated over the period 1979-2010 (ftp://eclipse.ncdc.noaa.gov/pub/ibtracs/v03r10/all/netcdf/year/), where 1979 represents the time where routine use of satellite data allowed a consistent monitoring of tropical cyclones.This study is restricted to the austral summer season covering the South West Indian Ocean (west of 100 ^{o}E).

3.2.2 Meteo-France

In the thesis (Chapter 4 and 5), to analyze the daily evolution of Tropical cyclone BANSI (formed around North East of Madagascar in January 2015) and JAPHET (generated in the Mozambique Channel in February 2003), TC characteristics (position, wind speed and cyclone intensity) were collected from Météo-France La Reunion (MFR)/La Réunion Regional Specialized Meteorological Center (RSMC) as the South West Indian Ocean is their official region of responsibility (WMO 2002) (http://www.meteofrance.re/cyclone/trajectoire). The intensity scale used by Meteo-France is mentioned in table 2.1

3.3 Reanalysis data

3.3.1 SODA

Monthly mean temperature and salinity data from the Simple Ocean Data Assimilation reanalysis (SODA) v2.2.4, mapped onto a uniform 0.5^{o} zonal x 0.5^{o} meridional x 40 vertical levels for the period 1980–2010 were used to compute Tdy and BLT. This oceanic reanalysis dataset consist of gridded state variables (e.g. temperature, salinity, zonal and meridional

velocities and sea level) and different derived fields (such as heat content) for the global ocean (http://apdrc.soest.hawaii.edu/datadoc/soda_2.2.4.php/).

3.3.2 HYCOM

To analyze the upper ocean thermal and salinity structure during the transit of a TC, which occurred after the period for which SODA data are available, daily temperature and salinity profiles from HYCOM 1 NCODA Global data (https://hycom.org/dataserver/glb-analysis) were used. The Hybrid Coordinate Ocean Model (HYCOM) is a data assimilative isopycnal-sigma-pressure coordinate ocean model developed to improve the representation of oceanic processes [Bleck, 2002; Wallcraft et al.,2002]. The present configuration has a horizontal resolution of 0.08^{o} x 0.08^{o}, 33 vertical layers and uses a nonlocal K-profile parameterization (KPP) for the boundary layer mixing scheme [Large et al., 1994, 1997].

3.3.3 NCEP/NCAR

Monthly wind stress, geopotential height at 850 HPa, moisture flux convergence and omega anomalies from the National Center for Atmospheric Research (NCEP/NCAR) reanalysis monthly means (Kalnay et al., 1996) are used to study the variability of atmospheric circulation over the South West Indian Ocean (https://www.esrl.noaa.gov/psd/data/gridded/data.ncep.reanalysis.derived.html).

3.4 Precipitation dataset

3.4.1 GPCC

To examine the relationship between the upper ocean characteristics and rainfall over the southern African mainland, a longer time series (1980-2013) for precipitation is used (monthly Global Precipitation Climatology Centre (GPCC) Version 7,http://www.esrl.noaa.gov/psd/). The Global precipitation analysis products of the GPCC provides high quality gridded monthly precipitation data for the global land- surface. This product contains monthly output with a spatial resolution of 0.5^{o}x0.5^{o} latitude by longitude.

3.5 Altimetry data

Satellite altimetry has been found to be one of the most functional tools to analyse the variations of global sea surface topography and velocity fields, with high spatial resolution and short temporal intervals. The altimeter products used in this study were produced by *Ssalto/Duacs* and distributed by the Archiving, Validation, and Interpretation of Satellite Oceanographic (AVISO), with support from CNES (http://www.aviso.altimetry.fr/duacs/). The data were $'allsatmerged'$ global daily mean sea level anomalies on a 0.25^{o} grid available over a time period of January 1993 through September 2017 (ftp://ftp.sltac.cls.fr/Core/SEALEVEL_GLO_PHY_L4_REP_OBSERVATIONS_008_047/dataset-duacs-rep-global-merged-allsat-phy-l4-2003/). The $'allsatmerged'$ data is composed of datasets with up to four satellites at a particular time, using all missions available at a certain time. Sampling and long wavelength errors determination are thus improved, therefore this dataset is better in quality but not homogeneous over the entire time span of the study. In this study, we used AVISO data to compare between a regional ocean model the position of an eddy for a particular day.

Chapter 4

Variability of upper ocean characteristics and tropical cyclones in the SW Indian Ocean

This chapter is based on the work published as:

Mawren, D., and C. J. C. Reason (2017), Variability of upper-ocean characteristics and tropical cyclones in the South West Indian Ocean, J. Geophys. Res. Oceans, 122. doi:10.1002/2016JC012028.

Abstract

Track and intensity are key aspects of tropical cyclone behaviour. Intensity may be impacted by the upper-ocean heat content relevant for TC intensification (known as Tdy) and barrier layer thickness (BLT). Here, the variability of Tdy and BLT in the South West Indian Ocean and their relationships with tropical cyclones are investigated. It is shown that rapid cyclone intensification is influenced by large Tdy values, thick barrier layers and the presence of anticyclonic eddies. For TC generation in the South West Indian Ocean, the parameter Tdy was found to be important.

Large BLT values overlay with large Tdy values during summer. Both fields are modulated by the westward propagation of Rossby waves, which are often associated with ENSO. For example, the 1997-1998 El Niño shows a strong signal in Tdy, SST and BLT over the South West Indian Ocean. After this event, an increasing trend in Tdy occurred over most of

the basin which may be associated with changes in atmospheric circulation. Increasing SST, Power Dissipation Index and frequency of Category-5 tropical cyclones also occurred from 1980 to 2010.

To further examine the links between tropical cyclones, Tdy and BLT, the ocean response to Category 5 Tropical Cyclone Bansi that developed near Madagascar during January 2015 was analysed. Its unusual track was found to be linked with the strengthening of the monsoonal northwesterlies while its rapid intensification from Category-2 to Category-4 was linked to a high-Tdy region, associated with a warm core eddy and large BLT.

4.1 Introduction

Tropical cyclones (TCs) are the most devastating weather phenomenon in nature with the powerful storm surge events occurring when severe and large TCs make landfall along coastlines. In the South West Indian Ocean (0^o-40^oS, 30^o-90^oE), tropical storms (including tropical cyclones) are generated mainly from late November through April, with on average 10 per season (Mavume et al., 2009) and typically peak during the months of January and February.

Although there have been significant strides in the TC track forecasts over the last 30 years, skills in TC intensity prediction still lag behind. Similar to cyclones in other tropical ocean basins, tropical cyclones in the South West Indian Ocean also cause significant social and economic damage in southeastern Africa and Madagascar. There have been marked cases in the South West Indian Ocean (e.g. TCs Eline and Favio) in the last two decades (Reason and Keibel, 2004; Klinman and Reason, 2008) where sudden intensification of storms has caused loss of life and major damage to property in Mozambique and Madagascar. Such intensification can happen when cyclones pass over regions of positive upper-ocean thermal anomalies (Scharroo et al., 2005; Lin et al., 2009b).

To forecast TC intensity more accurately, monitoring upper ocean conditions in the South Indian Ocean is of top priority. The factors controlling the intensity of TCs are poorly understood due to complex mechanisms (DeMaria et al., 2005), including internal dynamics (Gray, 1979; D'Asaro et al., 2011), upper-ocean interaction (Holliday and Thompson, 1979; Mainelli et al., 2008; Lin et al., 2005, 2008, 2009a,b, 2011; Pun et al., 2011; Lin et al., 2013b; Vincent et al., 2014; Balaguru et al., 2015) and TC interaction with the surrounding environment (Merrill, 1988; Emanuel and Živkovic-Rothman, 1999; Emanuel et al., 2004).

While tropical cyclone tracks are broadly determined by the large-scale steering flow, storm intensity is influenced to a greater extent by smaller-scale features both in the atmosphere and ocean (Emanuel, 1986). In order to establish useful warning systems for tropical cyclones, it is necessary to accurately predict both storm track and intensity.

One of the metrics for tropical cyclone-ocean interaction is the tropical cyclone heat potential (TCHP) (Leipper and Volgenau, 1972; Shay et al., 2000). It represents the integrated ocean heat content between the sea surface and the depth of 26^oC isotherm (Goni et al., 1996, 2009; Shay et al., 2000; Goni and Trinanes, 2003; Pun et al., 2007; Ali et al., 2013). Oceanic regions with deep mixed layers of temperature above 26^oC and hence large TCHP can fuel storm intensification by making more ocean heat energy available for uptake by the cyclone.

In recent years, intensity prediction in relation to the underlying thermodynamic structure has been an important problem for investigation. Ali et al. (2007) presented evidence that a well-mixed upper-ocean layer provides better information for TC prediction than do SST fields. Goni et al. (2009), argued that TC intensification can be linked to high TCHP contained in subsurface warm features such as eddies, assuming favourable atmospheric conditions are met. Malan et al. (2013) showed that the TCHP in the South West Indian Ocean has followed an upward tendency in recent decades with an associated increase in severe TC days but a decrease in overall TC frequency. Ocean heat content and vertically averaged water temperature have also been studied to improve TC intensity forecasting (Price, 2009; Ali et al., 2013; Lin et al., 2013a; Balaguru et al., 2015). Other studies have used different characteristics for calculating the integrated temperature over a depth of 80m (Lin et al., 2013b,a) or 100 m (Price, 2009). Recently, Balaguru et al. (2015) put forward a new metric of TC-ocean interaction, known as Tdy to compute the vertically averaged temperature over a variable mixing length. This parameter takes into account both the atmospheric and oceanic components which depend on the storm state and is investigated here for the South West Indian Ocean.

The impact and response of the ocean during the passage of a tropical cyclone may also be influenced by the ocean salinity stratification and Barrier Layer thickness (BLT). When the halocline is shallower than the thermocline, a layer is established between the density mixed layer depth (MLD) and the temperature mixed layer (ILD or Isothermal Layer Depth) which is known as the Barrier Layer. Several studies have reported the importance

of barrier layers related to TC (Sengupta et al., 2008; McPhaden et al., 2009). Wang et al. (2011) observed that the pre-existence of BLT can inhibit cyclone induced cooling in the surface and sub-surface layers by vertical mixing. Pailler et al. (1999) analyzed high vertical resolution measurements of salinity and temperature to show that high SSTs in the northwest Tropical Atlantic are often associated with low sea surface salinity and thick BLT ($>$40m). Balaguru et al. (2012) examined the effect of BLT on TC intensification to show that in the presence of a thick BLT and a favourable atmosphere, tropical storms are energized.

Several studies have highlighted the importance of the Seychelles-Chagos thermocline ridge (SCTR) in the tropical South West Indian Ocean for the regional climate (Hermes and Reason, 2008, 2009) and the intensification of tropical cyclones (Xie et al., 2002; Reason and Keibel, 2004; Malan et al., 2013). Hence, this study considers the variability in Tdy, BLT and other paramaters in the SCTR region (5-12^{o}S, 50-70^{o}E) as well as more generally over the South West Indian Ocean and their relationships with TC frequency. A case study of the intensification of TC Bansi in relation to Tdy, SST and BLT is also presented. Note that no studies have been conducted as yet to quantify the impact of BLT during the passage of a tropical cyclone in the South West Indian Ocean basin.

4.2 Data and Methods

Monthly mean temperature and salinity data from the Simple Ocean Data Assimilation reanalysis (SODA) v2.2.4 at 0.5^o zonal and 0.5^o meridional resolution for the period 1980 to 2010 were used to compute Tdy and BLT. BLT depends on the MLD which is defined as the uppermost layer of constant density and temperature, and acts as the interface for air-sea interactions. During high fresh water input, a uniform density mixed layer becomes shallower than the uniform temperature layer due to the influence of salinity. The region between the base of the mixed layer and the base of the isothermal layer is defined as the BLT:

$$BLT = ILD - MLD \tag{4.1}$$

The MLD determination is based on a density-based criterion that includes salinity but implying that the density changes from the ocean surface corresponding to a temperature change of 0.2^oC. A fixed temperature criterion of 0.2^oC is used to define the Isothermal Layer Depth (ILD; (Kara et al., 2003; de Boyer Montégut et al., 2007)). The barrier layer acts as a barrier to entrainment cooling and vertical mixing (Balaguru et al., 2012). Because this layer is a

prominent feature of warm regions of the tropical ocean where TCs are active, they may occur along TC tracks. SODA reanalysis (http://apdrc.soest.hawaii.edu/datadoc/soda_2.2.4.php) is used to quantify the impact of BLT on TC intensification.

The Power dissipation index (PDI, (Emanuel, 2005)) is used to investigate the relationship with TC intensity. This parameter is calculated by summing the cubes of the estimated maximum sustained wind speeds of every active tropical storm up to the point they reach Category 4 (the maximum wind speed 64 knots at six-hour intervals). The unit of PDI is 10^6 kt^3.

$$PDI = \int_0^\tau V_{max}^3 dt \tag{4.2}$$

A metric of TC-ocean interaction which gives a better representation of ocean stratification ((Balaguru et al., 2015)) and which is analysed in this study is Tdy. The variable mixing length (L) used to compute Tdy is based on the ocean state underneath the storm and is computed as follows :

$$L = h + (\frac{2\rho_o u_*^3 t}{\kappa g \alpha})^{\frac{1}{3}} \tag{4.3}$$

where h is the initial mixed layer depth, ρ_o is the sea water density, u_* is the friction velocity, t is the average time period of mixing under the storm (3hrs as in Balaguru et al. (2015)), κ is the von Kármán constant, g is the acceleration due to gravity and α is the rate of increase of potential density with depth beneath the mixed layer. The vertically averaged temperature over the mixing length L is calculated as:

$$T_{dy} = \frac{1}{L}\int_0^L T(z)dz \tag{4.4}$$

where T(z) is the temperature as a function of depth z. Tdy is averaged from November to April over the period 1980 to 2010, using temperature, salinity profiles from SODA reanalysis data and a wind speed of 60 ms^{-1} ($>$ 115 knots) for a Category 5 tropical cyclone (33 ms^{-1} for a Category 1 TC) (based on Meteo-France's intensity scale) and a duration of 3 hr. The spatial and temporal mean over the November to April season, as well as the standard deviation relative to this mean for both Tdy and BLT were calculated. The anomaly is computed as the difference between each parameter and its mean value. A strong positive (negative) anomaly represents an anomaly with magnitude larger than one positive (negative) standard deviation. Due to its greater spatial and temporal coverage in the South West Indian Ocean, the SODA dataset was chosen as the prefered reanalysis product to assess the role of Tdy and BLT in this basin.

The International Best Track Archive for Climate Stewardship (IBTrACS) dataset (Knapp et al., 2010) (1980-2010) is used to examine TC numbers, intensity and tracks as well as the main characteristics of tropical cyclone Bansi, the case study presented in Section 6. These data include the position of the TC center, TC central pressure, and 10-minute-average maximum sustained wind speed every 6 hours. To analyse the ocean structure during the transit of Tropical Cyclone Bansi, which occurred after the period for which SODA data are available, daily temperature and salinity profiles from HYCOM + NCODA Global data (https://hycom.org/dataserver/glb-analysis) were used. Briefly, the Hybrid Coordinate Ocean Model (HYCOM) is a data-assimilative isopycnal-sigma-pressure coordinate ocean model developed to improve the representation of oceanic processes (Bleck, 2002; Wallcraft et al., 2009). The present configuration has a horizontal resolution of 0.08^o x 0.08^o, 33 vertical layers and uses a nonlocal K-profile parameterization (KPP) for the boundary layer mixing scheme (Large et al., 1994, 1997).

4.3 Tdy and BLT influences on TC frequency

In order to better understand the upper-ocean's role and more specifically the salinity effect on TCs, Tdy was analysed by sub-sampling similar regions of high/low Tdy and stratifying them as regions of weak or strong BLT. All TCs generated in the South West Indian Ocean (5 - 20S; 40 E - 90 E) were analysed from 1980 to 2010 and based on their genesis location, their individual Tdy and BLT in time and space were investigated (Table 1). A total number of 131 TCs have been recorded over the study period, including 36 very intense tropical cyclones (VITCs; Category 5 TCs only). This approach provides a better understanding about the oceanic state under which TCs are generated.

Table. 4.1 indicates that the vast majority of TCs are generated under positive Tdy anomalies (77%) (15% occurring under strong positive anomalies).The common parameter statistics show that 47 % of TCs are generated under positive Tdy only while just 2% are being formed under BLT-favourable condition. The Tdy accounts for salinity not only through the MLD but more importantly through the stratification beneath the mixed layer. Thus, the temperature of the upper-ocean appears to be the main control parameter for the generation of TCs. An equivalent result is found for VITCs (line 2, Table 1). It is also interesting to note that a large portion of TCs (68 %) are generated under negative anomalies in BLT, 20 % of which are formed under adverse oceanic conditions (both negative Tdy and BLT anomalies).

		Strong (-ve)	Moderate (-ve)	Moderate (+ve)	Strong (+ve)
	TDY Ano / BLT Ano	0 0	29 - (~22 %) 5 - (~13 %)	82 - (~62 %) 27 - (~75 %)	20 - (~15 %) 4 - (~11 %)
Strong (-ve)	16 - (~12 %) 4 - (~11.5 %)	0 0	11 - (~8 %) 3 - (~9 %)	5 - (~4 %) 1 - (~2.5 %)	0 0
Moderate (-ve)	72 - (~56 %) 23 - (~64 %)	0 0	15 - (~12 %) 1 - (~2 %)	51 - (~38 %) 20 - (~56.5 %)	6 - (~5 %) 2 - (~5.5 %)
Moderate (+ve)	31 - (~23 %) 4 - (~10 %)	0 0	3 - (~2 %) 1 - (~2 %)	18- (~14 %) 3 - (~8 %)	10 - (~7 %) 0
Strong (+ve)	12 - (~19 %) 5 - (~13.5 %)	0 0	0 0	8 - (~6 %) 3 - (~8 %)	4 - (~3 %) 2 - (~5.5 %)

Table 4.1 The number and percentage of TCs (line 1: 131 TCs; line 2: 36 VITCs) generated from 1980 to 2010 according to their Tdy and BLT anomalies. Red box indicates Tdy-favourable condition (positive anomaly), Blue box represents BLT-favourable condition (positive anomaly), black box indicates favourable conditions for both variables and grey are the least favourable ones.

However, no TC is generated when both parameters are strongly negative. As shown below, BLT appears to be important for the intensification of TCs once they have generated.

4.4 Variability of Tdy, BLT and TC intensity

The South West Indian Ocean basin features a region of upwelling between $50-90^{o}$E and $5-12^{o}$S, known as the Seychelles-Chagos Thermocline Ridge (SCTR). This region has attracted attention due to its distinct oceanic variability at different time scales which can have a direct impact on weather and climate, in particular cyclogenesis in the tropical South Indian Ocean (Xie et al., 2002; Vialard et al., 2009; Malan et al., 2013). Using SODA data from 1980 to 2010, the climatological mean of Tdy, SST and BLT in the tropical Indian Ocean during November-April are calculated and shown in Fig. 4.1 (left column). Both Tdy and BLT show weak values across the SCTR region but high values in the southeastern part ($75-95^{o}$E and $12-22^{o}$S) and in the equatorial eastern region. Tdy also has large values near the East African Coast and extending across the equatorial zone whereas BLT has weak values in this zone between the coast and about 75^{o}E. Large number of TCs seem to be generated in and just south of the SCTR where there are are large values of Tdy and SST near 28^{o}C. Many VITCs (red circles) are generated close to areas of maximum Tdy values.

To understand the dominant variability patterns over the South West Indian Ocean, Tdy, SST and BLT are decomposed using Empirical Orthogonal Function (EOF) analysis. Fig. 4.1

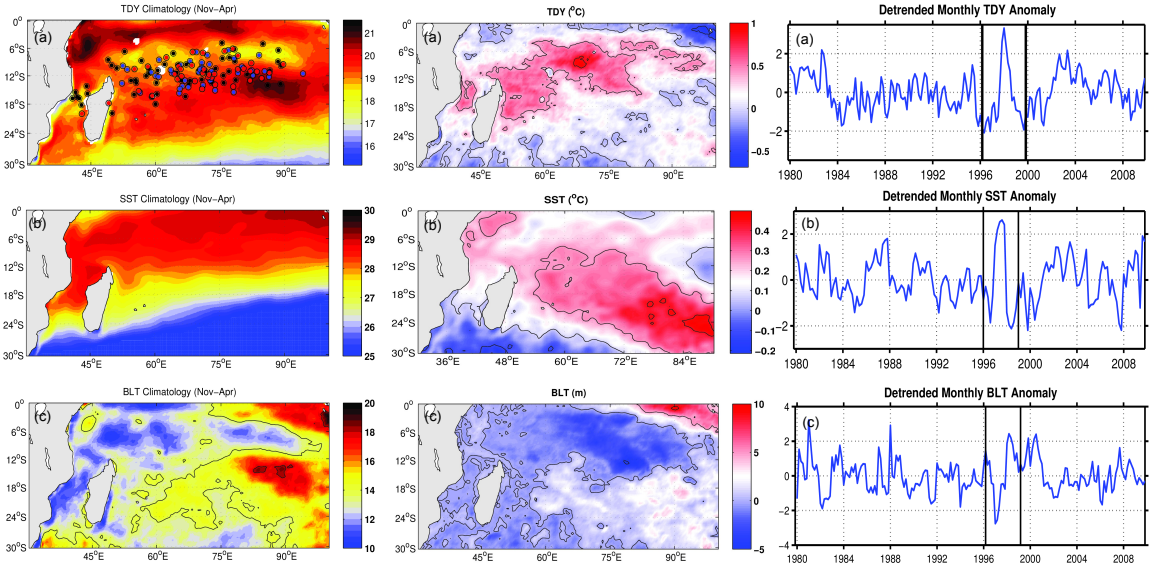

Fig. 4.1 Climatological maps (col 1), Spatial structures of EOF1 (col 2) and corresponding components (col 3) of (a) Tdy (SODA reanalysis) overlaid with genesis locations of (I) Cat 1-2 (black circles) (II) Cat 3-4 (blue circles) (III) Cat 5 (red circles), (b) sea surface temperature (SST; SODA reanalysis) and (c) barrier layer thickness (BLT; SODA reanalysis) over the South West Indian Ocean (SWIO) basin during the summer season (Nov-Apr) 1980 to 2010. The first EOF mode accounts for 6.1%, 25.3% and 6% of the variance respectively.

(middle column) shows the spatial patterns of the 1st EOF mode of the seasonally averaged (Nov-Apr) Tdy, SST and BLT anomalies, where the percentage of variance explained by each EOF1 is 6.1%, 25.3% and 6.0% respectively. Their corresponding time coefficients vary strongly on interannual timescales (Fig. 4.1 (right)), with the strongest signal recorded during the mature phase of the strong 1997-1998 El Niño. The Niño 3.4 index and the SST PC were found to correlate with a coefficient of 0.54 while the correlation of Niño 3.4 with Tdy was 0.42 (4 month lag), both significant at 99 %. The EOF1 of Tdy exhibits largest variation in the Mozambique Channel and in the central SCTR with maximum amplitude near 10^{o}S. The distinct pattern in Tdy (Fig. 4.1a) observed just south of the equator was also noted for upper ocean heat content by Ke et al. (2012). Fig. 4.1b shows a SST pattern typical of the response of the Indian Ocean to ENSO associated with westerly wind anomalies over the SCTR region (Reason et al., 2000). The EOF1 of BLT has some similarities in pattern with that of Tdy with largest values in the SCTR and in the far northeast (opposite sign).

Fig. 4.2 illustrates the normalized amplitudes of Tdy derived from SODA reanalysis using a 10 year running mean. The period of analysis stretches from 1980 to 2010 and focuses on

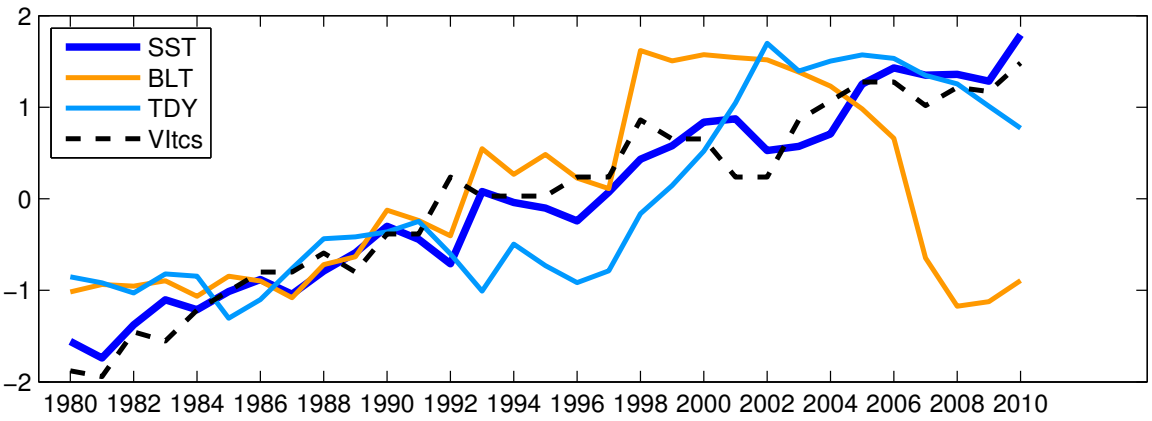

Fig. 4.2 10-year running mean of: very intense tropical cyclones over central SWIO (50^oE-90^oE,$0-40^o$S), SST, Tdy and BLT all computed across the SCTR region from 1980−2010 averaged over the peak cyclone season (November to April). All ocean metrics are normalized.

the November to April season so as to capture the highest signals of Tdy that coincide with cyclone activity in the South West Indian Ocean (5-20^oS; 40^oE-90^oE). Tdy is well correlated with normalized values of SST (SODA data), BLT (derived from SODA) and the number of very intense tropical cyclones (VITCs; Category 5 TCs only) with correlation coefficients of 0.84,0.47 and 0.77 respectively (significant at 99 %). Note that for all the statistical values estimated in this study, the significance level was assessed with a Monte Carlo technique by comparing the squared correlation to that of a randomly scrambled ensemble. A higher correlation value, 0.95 (99% significant) of SST with VITCs is noted. This result is not unexpected since a warmer upper ocean helps to sustain cyclone intensity over a much longer period of time by an uninterrupted supply of sensible and latent heat fluxes from the ocean to the surface.

During 1980-1998, VITC activity seems to strengthen with an increase in Tdy, SST and BLT values. However, a jump is observed in both the Tdy and BLT around 1997-1998. After 1997, the frequency of VITCs increases (0.08 year^{-1}) along with a warming in SST and Tdy of order 0.10^oC and 0.11^oC per year respectively. However, a decreasing tendency in BLT is noted after 1997(0.22m per year).These tendencies are statistically significant at the 99% significance level.

In order to investigate TC numbers and TC intensity in the South West Indian Ocean, the time series of the accumulated Power Dissipation Index (PDI; (Emanuel, 2005, 2007))

was examined. The PDI index is used to represent the total energy dissipated by tropical storms, incorporating their lifetime and their maximum sustained wind speed (>35 knots). Fig. 4.3a shows the annual accumulated PDI ($40-90^oE$; $5-20^oS$) computed from 1980 to 2010, averaged for the peak months (November-April). In addition to interannual variability, there is an upward trend in the annual accumulated PDI and number of VITCs of the order of 0.014 $kt^3 yr^{-1}$ and 0.031 per year respectively, indicating that storms are becoming more intense (statistically significant at 95 %). PDI was found to correlate strongly with VITC frequency with a correlation coefficent of 0.63 as compared to 0.44 with TC frequency (both statistically significant at 95 %). The power spectral density (Fig. 4.3b,c) performed for accumulated PDI and number of TCs over the period 1950-2010 reflects strong interannual to multi-decadal variability. Spectral peaks in the number of TCs (Fig. 4.3c are prominent near 2 yrs, 6 yrs and 8 yrs (all above 95% confidence level). The 2 and 6 year peaks are close to the frequencies at which ENSO and IOD are prominent (Saji et al., 1999; Allan et al., 2003). Although the power spectral density of PDI (Fig. 4.3b) has peaks at 2 yrs, and 6yrs, they are not statistically significant. A 20-year peak, close to the multidecadal signal found over the Indian Ocean (Allan et al., 1995) is also apparent in TC numbers but needs to be viewed with caution since these data only extend over 60 years. However, several studies (Allan et al., 1995, 2003; Reason, 2000; Han et al., 2014) have identified decadal to multidecadal variability in the Indian Ocean region during austral summer and such variability was observed in both atmospheric and oceanic parameters like temperature, wind, sea level pressure, salinity and sea level. These low frequency oscillations may then influence Tdy, and thermocline characteristics in the basin. Over the North Indian Ocean, Rao et al. (2008); Krishna (2009); Evan et al. (2011); Wang et al. (2012) have also observed that an intensification of Arabian Sea premonsoon TCs is related to decadal variations in SST over the whole Indian Ocean.

An important turning point in the climate of the Indian Ocean region occured around 1997/1998, which was shown to be associated with significant changes in sea surface temperature, chlorophyll and atmospheric circulation over the Indian Ocean (Manatsa et al., 2012; Dilmahamod et al., 2016) and indeed a jump can be seen about this time in Fig. 4.2 in Tdy and BLT, and to a lesser extent, SST. It is therefore of interest to look at the epochal variability, pre- and post-1997/1998 in Tdy over the Indian Ocean. The spatial trends of November-April averaged Tdy calculated using SODA data (Carton et al., 2000) for two different time periods, epoch 1: 1980-1996 and epoch 2:1998-2010, are shown in Fig. 4.4. The linear trends were computed using the least square linear regression that fits the data

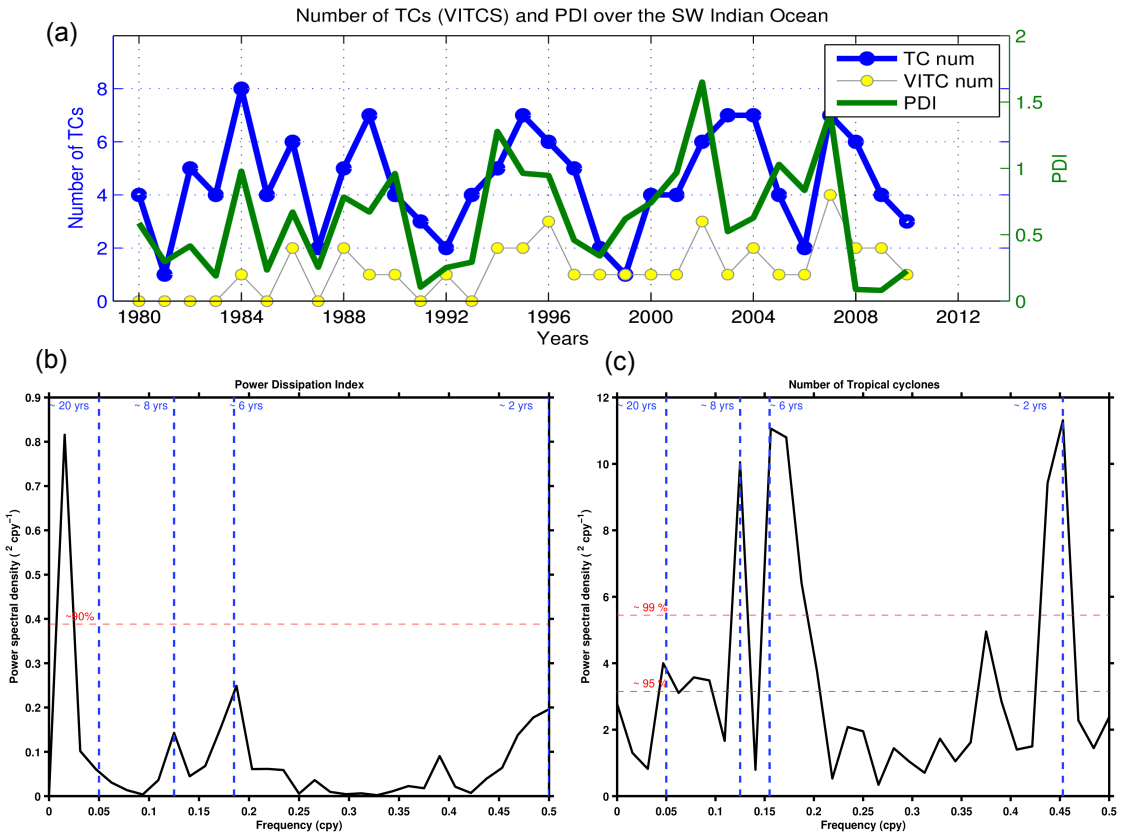

Fig. 4.3 (a) The annual values of the Power Dissipation Index (PDI, which accounts for cyclone strength, duration and frequency−green line) and the number of tropical cyclones (blue line) / cyclones (yellow circles). (b) Power spectral density of power dissipation index and (c) Power spectral density of number of TCs; the broken horizontal lines present an estimate of the 90% and 95-99% confidence limit in (b) and (c) respectively; blue vertical dashed lines are spectral peaks significant at 95%.

and the statistical significance of these trends (Fig. 4.4; black contours) was determined by performing a t-test. The first epoch (1980-1996; Fig. 4.4a) shows a declining Tdy trend over several areas in the Indian Ocean, particularly east of Madagascar and across the basin near 6-8^oS. During the second epoch (1998-2010; Fig. 4.4b), there is an increasing trend in Tdy in the Mozambique Channel, in the central South Indian Ocean (central to eastern SCTR) and in some areas in the North Indian Ocean, with trends reaching 0.2, 0.3 and 0.4^{o}C year^{-1} respectively, significant at 90%. Fig. 4.4 also reveals that more VITCs have occurred in the 1998-2010 epoch compared to the earlier one. Many but not all VITCs occur near regions of increasing Tdy trend. This result is consistent with the overall statistics indicated in Table 1, where TCs/ VITCs can also be generated over regions of shallow BLT.

On interannual time scales, climate modes such as ENSO and the Indian Ocean Dipole (IOD), which have a strong signal over the Indian Ocean (Saji et al., 1999; Reason et al., 2000), may influence tropical cyclone activity through their effect on the large-scale atmospheric and upper ocean environment in which the storms evolve. For example, there is large scale warming of the tropical Indian Ocean during positive IOD and El Niño events which may increase the number of tropical cyclones in the South West Indian Ocean, as observed on decadal scales for VITCs in Fig. 4.2. These climate modes induce interannual variations of the subsurface oceanic stratification which may enhance TC activity. However, some studies (*Girishkumar and Ravichandran,* 2012; Girishkumar et al. (2015)) have argued that although El Niño leads to positive SST anomaly in the Bay of Bengal, the number of tropical cyclones decreases due to changes in less favourable atmospheric conditions. In addition to ENSO, the Subtropical South Indian Ocean Dipole (SIOD) (Behera and Yamagata, 2001; Reason, 2001, 2002) is also known to influence the SST of the South Indian Ocean and regional rainfall over Southern Africa in summer. Ash and Matyas (2012) provided evidence of an influence of the SIOD on TC trajectories in the South West Indian Ocean while Matyas (2015) found relationships between the SIOD, TC tracks and formation in the Mozambique Channel. Seasonal correlations (NDJFM) of Tdy and BLT with the Niño 3.4 index (ENSO), DMI index (Indian Ocean Dipole; (Saji et al., 1999)), and SIOD (subtropical South Indian Ocean Dipole; (Behera and Yamagata, 2001)) were performed for the period 1980 to 2010. Tdy and BLT are positively correlated with the Niño 3.4 index with correlation coefficients of 0.42 (4 month lag) and 0.53 (2 month lag) respectively (significant at 99%). For the IOD, the correlation coefficients are 0.30 (6 month lag) and 0.36 (3 month lag) respectively, which are statistically significant at 99%. A weaker relationship exists with the SIOD, r = 0.17 for

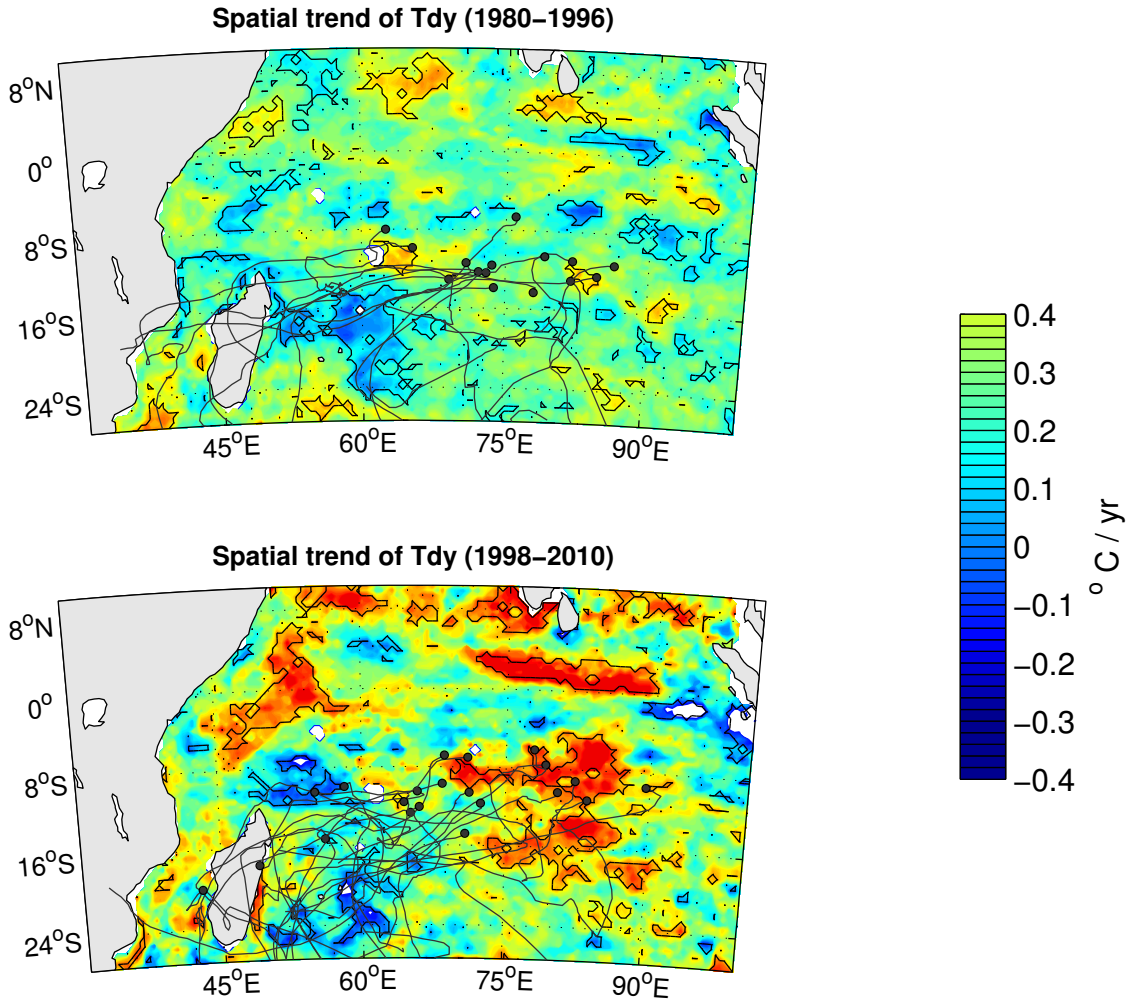

Fig. 4.4 Spatial trend of November−April averaged Tdy (SODA data) during the period 1980−1996 (top panel) and 1998−2010 (bottom panel) overlaid with very intense tropical cyclones tracks and their genesis locations; contours highlight areas at 90% significance

Tdy and r = 0.38 for BLT (99 % significant).

4.5 Rossby wave influences

Since Rossby wave propagation across the South West Indian Ocean including the SCTR (Hermes and Reason, 2008, 2009) is often prominent and is modulated by ENSO, the IOD and the SIOD, it is interesting to see how these waves impact on Tdy and BLT. A Hovmoller diagram of Tdy anomalies and SSH (Fig. 4.5 a,b) along 10^oS clearly shows the westward propagation of upper ocean signals with elevated values observed during 1997-1998,2002-2003 and 2006-2007. El Ni$\tilde{n}$o events occured during all these years. The speed of propagation of the increased Tdy and SSH signals (downwelling wave)(Fig. 4.5 a,b) was calculated as 0.28 ms^{-1}, which is roughly consistent with the phase speed of the first baroclinic mode Rossby waves, 0.21 ms^{-1} along 10^oS (Subrahmanyam et al., 2001). As the thermocline deepens, a thick barrier layer is established partly due to heavy precipitation or by anomalous westward advection of fresher water from the Indonesian throughflow (Vialard et al., 2009) via the South Equatorial Current (Gordon et al., 1997; Liu and Alexander, 2007). Although not as clear as the SSH signals, the BLT computed from SODA reanalysis (Fig. 4.5d) also reveals the westward migration of this layer due to the displacement of the thermocline depth associated with the downwelling Rossby wave, particularly in 1997-1998, 2002-2003 and 2006-2007.

The Indian Ocean ITCZ is located near the SCTR during austral summer and is therefore likely to be sensitive to changes in SST and Tdy. Increased SST as well as Tdy leads to strong positive precipitation anomalies (Xie et al., 2002)(TRMM+GPCC precipitation data at 0.25^o resolution) across the SCTR (Fig. 4.5c) during 1998, 2002, 2004, 2006 and 2008. Low-salinity values at the surface increase stratification of the water column, creating thick BLT formation (Chowdary et al., 2009), visible notably in 1998, 2002, 2003, 2004 and 2007. The vertical displacement of the thermocline depth associated with the downwelling Rossby wave is in turn forced by easterly wind stress all over the 10^o S band across the South West Indian Ocean (40-100^oE), as can be seen (negative anomalies) for 1998, 2002, 2003, 2004, 2007 (Fig. 4.5e). These easterly winds lead to anticyclonic wind stress curl over the tropical South East Indian Ocean and generate downwelling Rossby waves (Schott et al., 2009). The increased SSH, Tdy and BLT are then favourable for TC intensification. However, the variability of these parameters are more important along actual cyclone tracks and are

examined further in the case study of Bansi below.

4.6 Upper Ocean response to TC: A case study of Bansi

In this section, a case study of Severe TC Bansi is presented with the objective of investigating how changes in BLT and Tdy may have influenced its evolution. In the South Indian Ocean, most cyclones originate just south of the Inter Tropical Convergence Zone (ITCZ) and move westwards until near Madagascar before recurving east and back into the open South Indian Ocean. However, severe TC Bansi formed near northern Madagascar, intensified and moved towards the east-southeast during $11-18^{th}$ Jan 2015 (Fig. 4.6a). Several weeks of very heavy rainfall occured over Malawi and Mozambique, associated with the passage of TC Bansi and tropical storm Chedza, caused widespread flooding, which displaced more than 100 000 people and led to several deaths and considerable damage (http://www.bbc.com/news/magazine-30980324, http://edition.cnn.com/2015/01/17/africa/malawi-flooding/). The 850 hPa Geopotential height anomaly prior (5-10^{th} January) to Bansi (Fig. 4.6b), shows that strong anticyclonic conditions were present to the west-northwest of the formation region of Bansi, thus making propagation towards Madagascar unlikely. The movement of Bansi may be explained by the strengthening of the monsoonal north westerlies towards northern Madagascar, steering the storm towards the southeast (Fig. 4.6c).

On the 13^{th} January 2015, Bansi intensified to a Category 5 cyclone with maximum sustained wind speed of 220 km/h and minimum pressure of 923 hPa as monitored by Meteo France. Under WMO agreements, Meteo France through the RMSC at La Reunion, is responsible for forecasting TCs in the South West Indian Ocean. On the 14^{th} January 2015, the eye of Bansi was about twice as large as the size of Mauritius due to eyewall replacement (Moderate Resolution Imaging Spectroradiometer aboard NASA's Aqua satellite) and decreased its intensity to Category 2 before strengthening back to Category 4 within 24 hrs. On the 15^{th} January, the maximum sustained winds reached 185 km/h, with a minimum pressure of 940 hPa(http://www.meteofrance.re/cyclone/saisons-passees/2014-2015/dirre/BANSI). Thus, Bansi was one of the most powerful cyclones to occur in the South West Indian Ocean.

Maps of Tdy, SST and SSH for January 2015 overlaid by TC Bansi track are illustrated in Fig. 4.7. The storm was generated on the 11^{th} of January near $55^{o}E$, $16^{o}S$ in a region of relatively high Tdy and SST close to 28 ^{o}C.On 14^{th} January, it weakened in intensity while

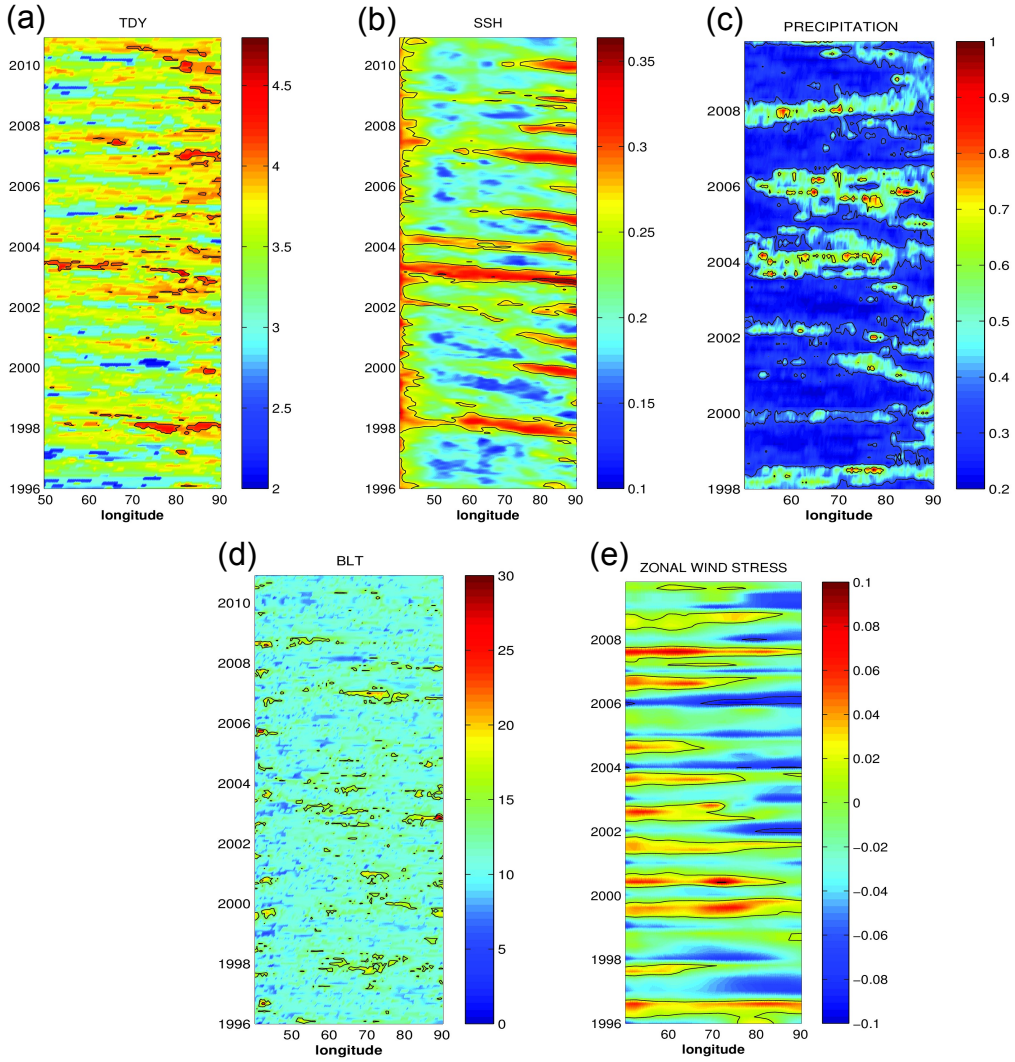

Fig. 4.5 Time−Longitude sections at 10^{o}S of (a) Tdy anomalies (^{o}C) (b) SSH (m) (c) Precipitation (mm/day) (d) BLT (m) (e) Zonal wind stress (N/m^2)

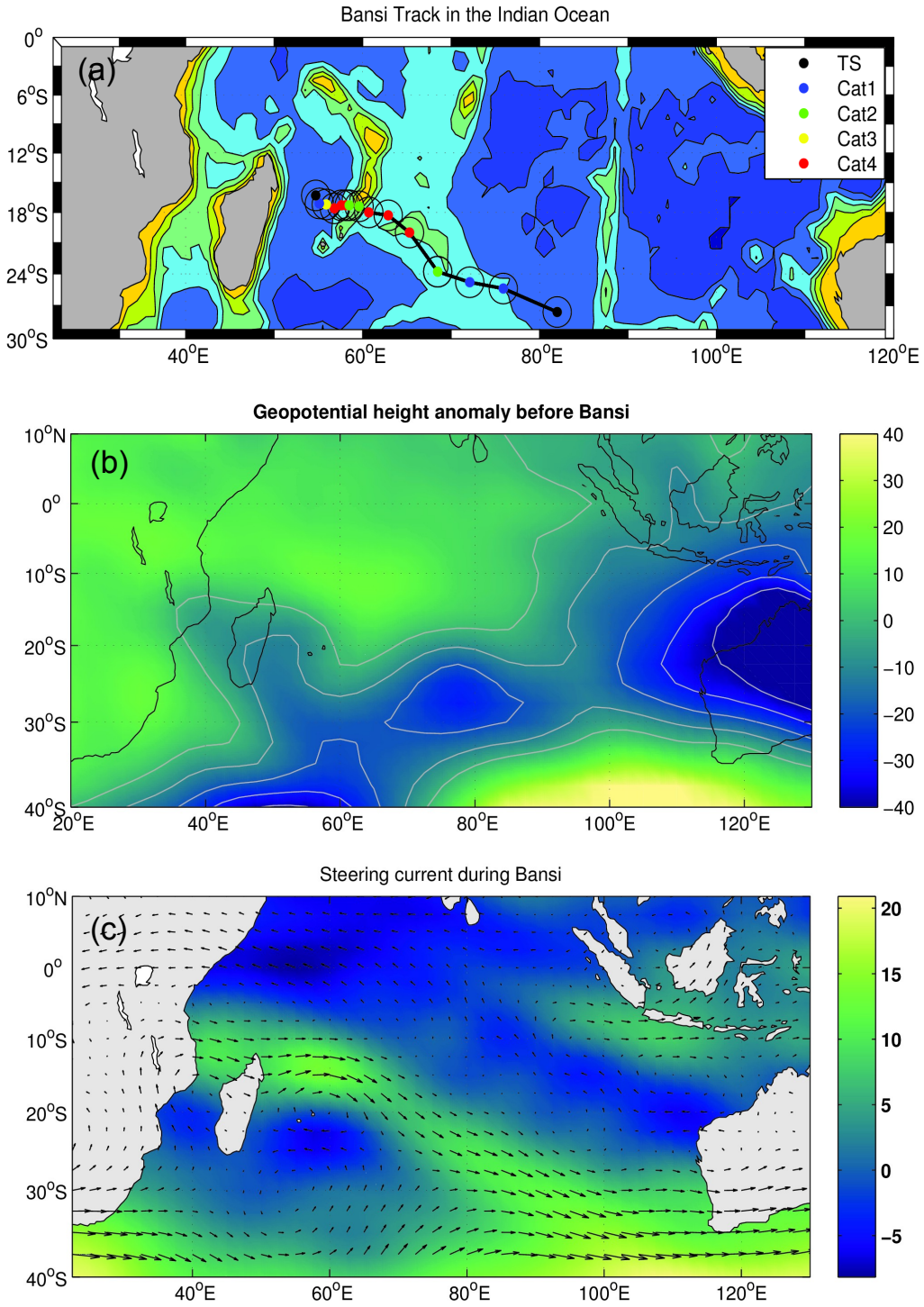

Fig. 4.6 (a) Track of TC Bansi from 11th to 18th Jan 2015, coloured circles represent the location and intensity of the cyclone on a daily basis plotted over the bathymetry, (b) Geopotential height anomaly before (5-10th) Bansi (NCEP/NCAR Reanalysis) (c) 500 hPa zonal winds (NCEP/NCAR Reanalysis) during Bansi

moving over lower Tdy values ($56^oE,17^oS$; Fig. 4.7a) and cooler SST (Fig. 4.7b,Fig. 4.8d). This decrease in Tdy implies that air-sea heat exchange (Price, 2009) may have played a major role in the weakening of TC Bansi. A link between SSH (Fig. 4.7c) and TC intensification is also apparent in this area, showing that Bansi weakened on the 14^{th} January while travelling over a cyclonic eddy ($58^oE,17^oS$) and went through a period of rapid intensification within 24 hrs (15^{th} January) after traversing over an anticyclonic feature ($60^oE,18^oS$). Several studies (Ali et al., 2007; Lin et al., 2013a; Vissa et al., 2013; Wu et al., 2007; Wada and Usui, 2010) in other regions have also shown how TC may intensify after passing over such eddies in the upper ocean. However, this is the first time this type of intensification has been analysed in the South West Indian Ocean. Fig. 4.8 indicates that the rapid intensification on the 15^{th} occurred in a region when the Tdy was higher than when Bansi was Category 2, and both SST and BLT were increased. The system maintained a Category 4 status on the Meteo-France scale on the 16^{th} January (high Tdy and thick BLT; Fig. 4.8a,c) until it left the warm eddy ($66^oE,20^oS$). Balaguru et al. (2012) suggested that when a TC passes over such regions, the mixing induced by it can cause water of similar temperature to enter the mixed layer. This process then leads to a weaker SST cooling (Fig. 4.8d) and an increase in Tdy (Fig. 4.8c), as happened with Bansi, which can then energize the TC through changes in air-sea enthalpy flux transfer.

The response of the upper ocean to the passage of Bansi including the role that the barrier layer had in modulating the surface cooling is now considered. A comparison between Bansi as Category 2 (14^{th} January) and as Category 4 TC (15^{th} January) is illustrated in Fig. 4.9. On the 14^{th} January, when Bansi started to lose its intensity, it caused further SST cooling (Fig. 4.8d) around the region with a shallow BLT (Fig. 4.9a) following stronger cooling evident on the 13^{th}. Bansi then gradually entered a region of deep BLT of 20m thick (Fig. 4.9b), high Tdy and SST (Fig. 4.8c,d) around 15^{th} January. This thicker barrier layer reduced the mixing up of deeper cooler waters. When Bansi started to dissipate near 72^oE 25^oS on 17^{th} January, no barrier layer existed.

The increase in BLT, Tdy and D26 values on the 15^{th} of January could be attributed to the presence of anticyclonic eddies (warmer SST) and the propagation of downwelling Rossby waves deepening the thermocline depth near 50-60^oE as shown on the D26 Hovmoller plot (Fig. 4.10a).The latter were computed from the monthly GODAS dataset at a horizontal resolution of $1/3^o$. The thick warm layer seems to have started around November 2013, near 85-90 ^oE, sloshing west across the basin. The thermocline was deepened (Fig. 4.10a) thus

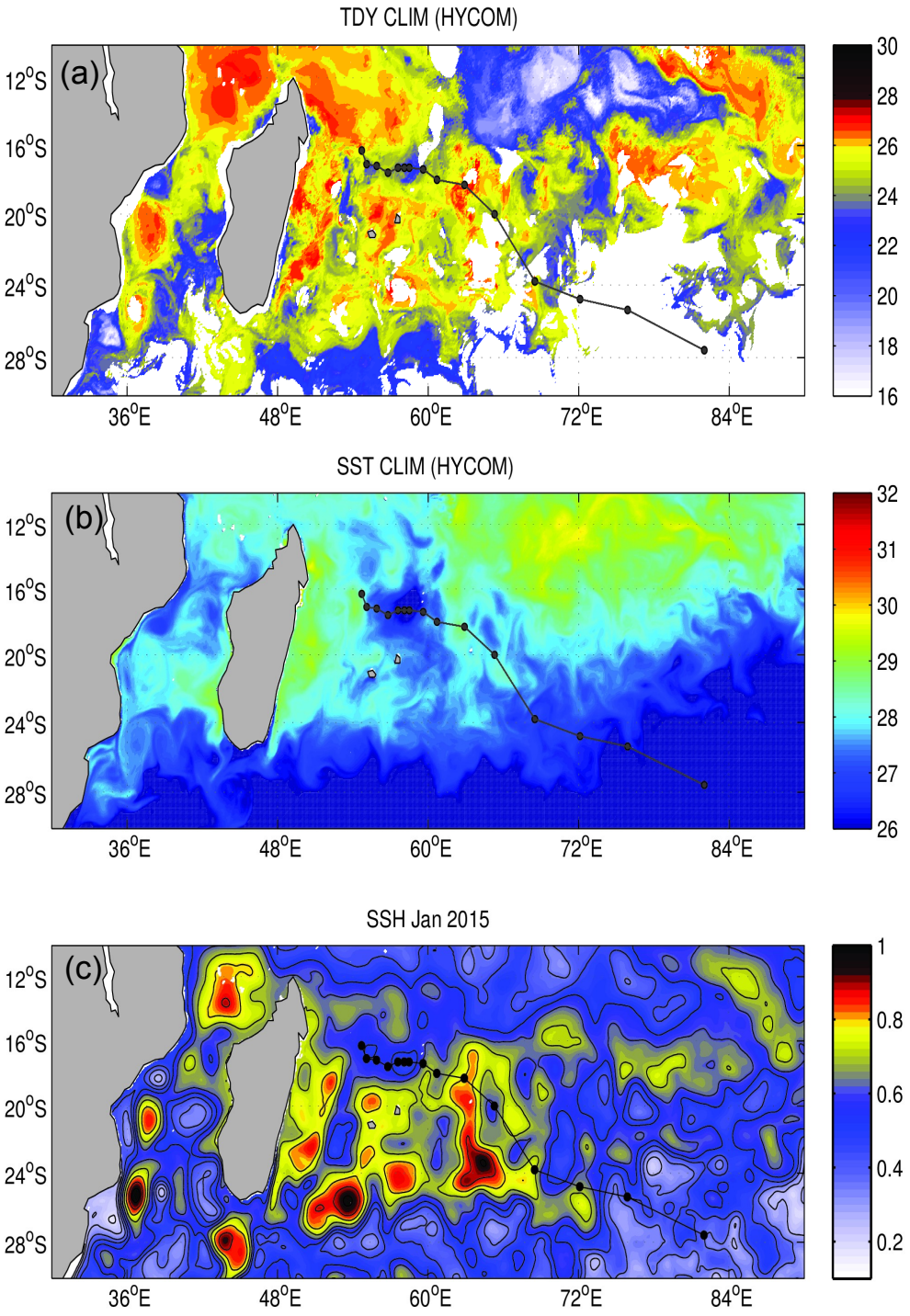

Fig. 4.7 Maps of (a) Tdy (^{o}C) (b) SST (^{o}C) and (c) SSH (m) (Aviso) mean January 2015 fields overlaid with the daily position of Bansi starting on 11^{th} January and ending on 18^{th} January 2015.

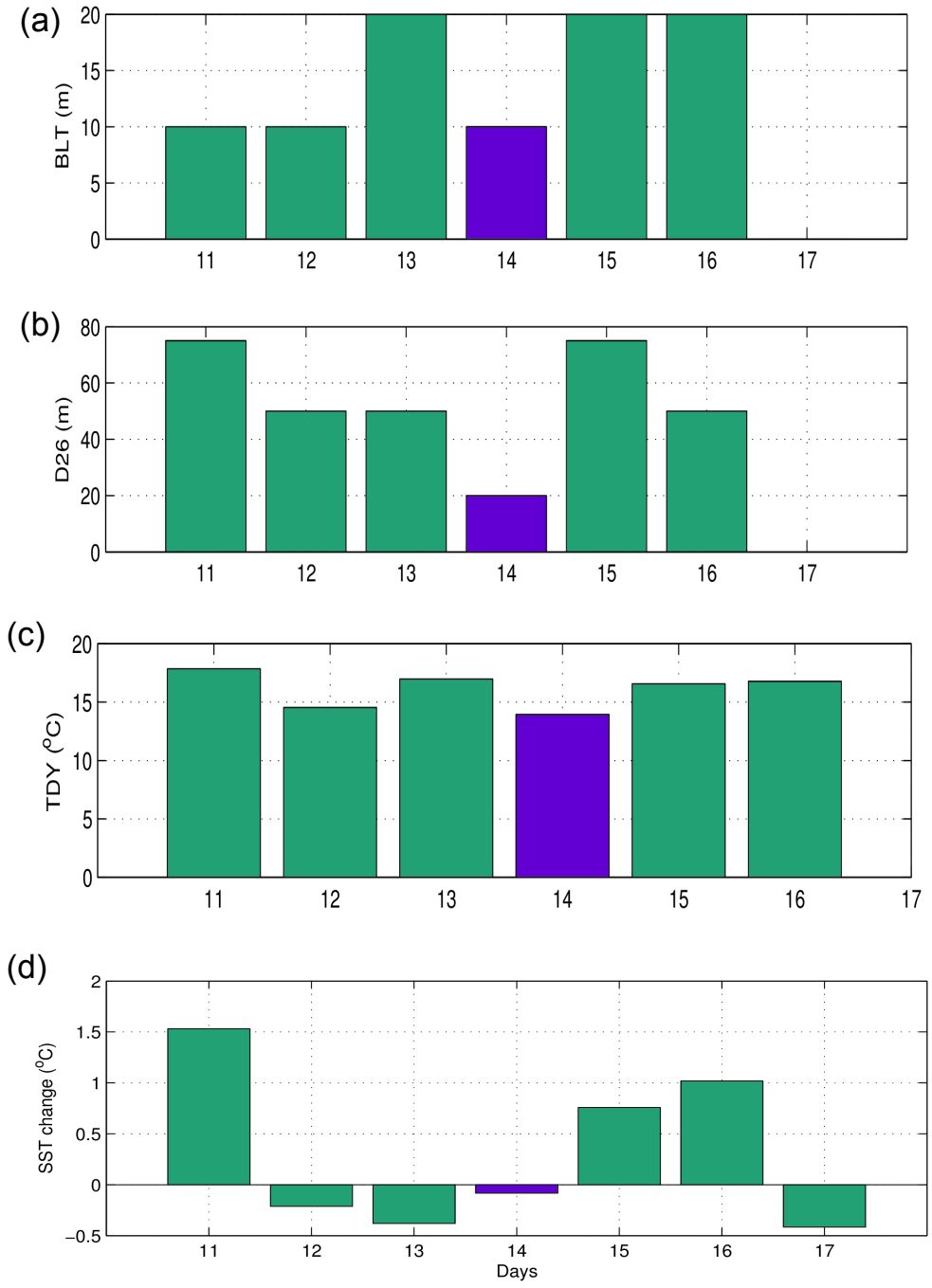

Fig. 4.8 Values of (a) Barrier Layer thickness (m) (b) D26 (m) (c) Tdy (^oC) and the (d) Difference between zonal SST average and SST (^{o}C) under Bansi. 14^{th} Jan shaded in purple indicate the weakening of TC Bansi as it encountered a cyclonic eddy.

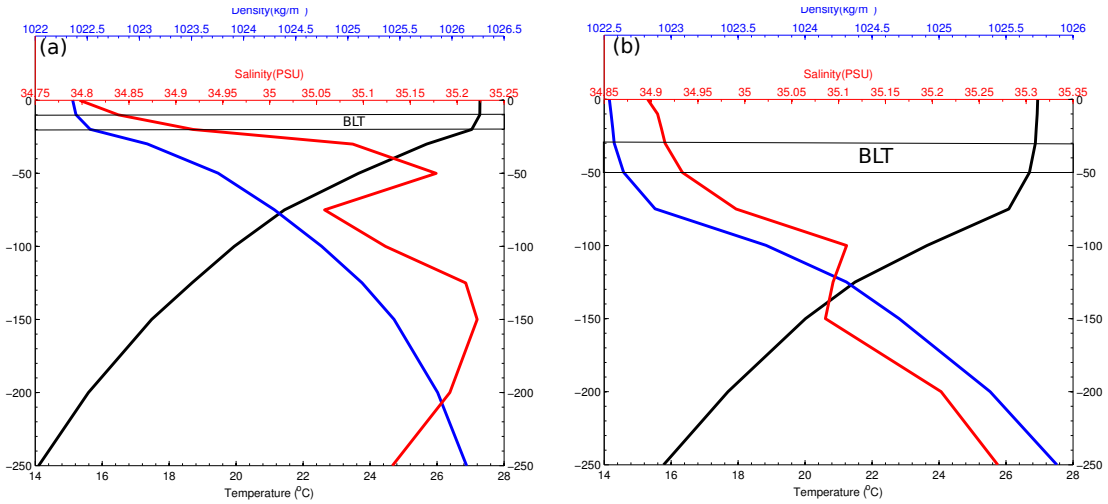

Fig. 4.9 BLT change during Bansi passage (a) Category 2 (b) Category 4 (bold red line: Salinity, blue: Density, black: Temperature).

making it harder for the deeper and colder water to mix with the surface waters. The deep warm subsurface layer observed around November 2014−January 2015, near 50-65^{o}E could have favoured the intensification of Bansi by constraining the cyclone's self-induced negative feedback from ocean surface cooling (Cione and Uhlhorn, 2003; Lin et al., 2009b). Fig. 4.10b illustrates the ocean heat content (OHC) anomalies calculated over the depths 0−300m for 50-100^{o}E along the 16^{o}S band (where Bansi reached Category 4), highlighting higher than average OHC values in January 2015 over the whole basin as compared to previous years. More energy therefore became available via latent heat flux exchange to fuel Bansi's sudden intensification. The results imply that in the presence of thicker BLT, deeper thermocline and higher Tdy (anticyclonic eddies), the intensification of Bansi was favoured.

4.7 Summary and Discussion

Assessing the interannual variability and trends of upper ocean characteristics has become increasingly important for understanding tropical cyclone intensity. Focusing on the Seychelles-Chagos Thermocline Ridge (an area of particular interest for cyclogenesis in the South Indian Ocean; (Vialard et al., 2009)), this study used monthly temperature and salinity profiles from SODA reanalysis dataset (40 vertical levels, 0.5^{o}x0.5^o horizontal resolution) to evaluate Tdy (Balaguru et al., 2015) and BLT variability over the past three decades (1980-2010) and relate that to TC characteristics.

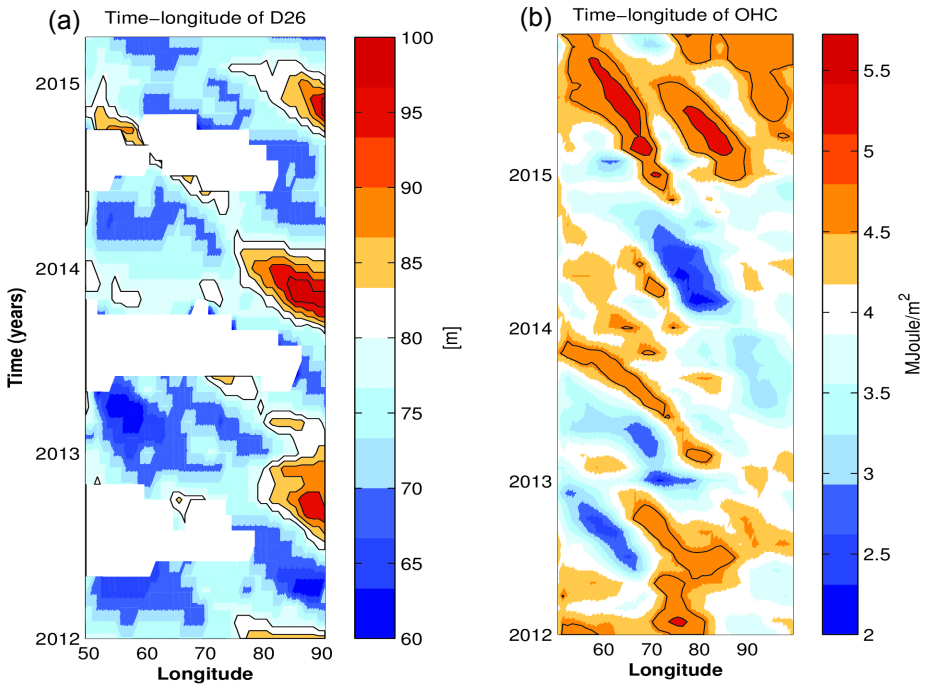

Fig. 4.10 Time-longitude of D26 (left) and ocean heat content anomalies (right) at latitude 16^{o}S. White patches on the left are missing values in winter due to temperature below 26 deg.

Empirical orthogonal function analysis of Tdy reveals the important role of the variability across the SCTR in the South West Indian Ocean. Time series of the seasonally-averaged (November to April) BLT and Tdy estimated from oceanic reanalysis data across the SCTR showed largest values around 1997-1998, 2003-2004, 2006-2007, which coincide with El Niño years. Downwelling Rossby waves propagate westwards across the basin and the associated warming in the upper ocean can enhance precipitation (Xie et al., 2002). Their speed of propagation determined in this study through lagged correlation is consistent with the phase speed of the first baroclinic mode Rossby wave. The Hovmoller plots of Tdy and BLT confirm the significance of Rossby wave propagation for upper ocean characteristics in the South West Indian Ocean that are important for tropical cyclone behaviour. BLT is sensitive to freshwater inputs by both precipitation and the advection of low salinity waters by the South Equatorial Current. During positive IOD or/and El Niño, the westward advection of negative SSS anomalies give rise to a thicker barrier layer due to increased salinity stratification. As mentioned in Vinayachandran and Nanjundiah (2009) and Grunseich et al. (2011), SSS anomalies take less than 2 months to travel across the Indian Ocean during El Niño events. The BLT responds quickly to precipitation and is also sensitive to atmospheric circulation anomalous associated with ENSO.

In order to understand the role of the upper-ocean, and more specifically the salinity effect on TCs, the Tdy parameter was analysed by subsampling regions of Tdy and stratifying them as regions of weak or strong BLT. All TCs generated in the South West Indian Ocean were analysed from 1980 to 2010 and based on their genesis location, their individual Tdy and BLT in time and space were investigated. This approach provides a better understanding of the oceanic state under which TCs are generated. The result indicates that the majority of TCs (77 %) were generated under positive Tdy anomalies while 68 % were formed under shallow BLT. Thus, the temperature of the upper-ocean appears to be most important for the generation of TCs while BLT may play a role in their intensification.

The analysis performed here suggests that an important change occured after the 1997/1998 El Niño, consistent with Manatsa et al. (2012) who provided evidence that a turning point in the climate of the Indian Ocean occurred around this time. An epochal variability of Tdy trends pre- and post- 1997/1998 shows large areas of decreasing trend near Madagascar pre-1997 and an increasing trend in the Mozambique channel and in the central tropical

South Indian Ocean after 1998, consistent with Goni et al. (2010) and Rajeevan et al. (2013). A 10 year running mean through the data across the SCTR region shows that VITC frequency, SST and Tdy have increased throughout the 1980-2010 period as has the Power Dissipation Index. However, the BLT only increased until 1997 after which it started to decline. Areas of increased Tdy, along with the warming in SST over most of the basin particularly around central SCTR region, are favourable for the occurrences of strong TCs, several of which have caused severe devastation and loss of life in the region (Reason and Keibel, 2004; Klinman and Reason, 2008).

A case study of TC Bansi and its relation to upper ocean heat content, Tdy and BLT was presented. This tropical cyclone is of interest due to its unusual track and also because of all the damage it caused. Anomalously deep thermocline and high Tdy values were observed around December 2014-January 2015 in the South West Indian Ocean and analysis of the upper ocean structure during Bansi showed that its rapid intensification to Category 4 was related to its passage over a high Tdy (warm core) eddy region and a deep barrier layer. The presence of a pronounced westward propagation of subsurface warming around November 2014 to February 2015 also may have contributed to its strengthening. This case study of Bansi further confirms that tropical cylone characteristics (both track and intensity) are strongly sensitive to upper ocean conditions.

The variability of the upper ocean characteristics and their relationships with tropical cyclones across the SCTR region has been investigated in Chapter 4. The next area of interest is the Mozambique Channel which is not only a region of relatively high TC activity with highly vulnerable coastal populations, but also very energetic in terms of mesoscale ocean eddies and tidal forcing. Several prominent TCs that crossed the Channel intensified just before they make landfall over Mozambique and therefore led to substantial loss of life and damage. Chapter 5 will look at the role of tides in influencing the upper ocean characteristics that are important for TC evolution and potential intensification.

Chapter 5

Effects of tidal mixing on the upper ocean structure and tropical cyclones in the Mozambique Channel

This chapter is based on the work submitted as:

Mawren, D., and C. J. C. Reason (2018), Effects of tidal mixing on the upper ocean structure and tropical cyclones in the Mozambique Channel. *submitted to J. Geophys. Res. Oceans*

Abstract

Ocean tides provide an important source of mechanical energy for the ocean circulation. Here, changes in upper ocean characteristics in the Mozambique Channel due to tidal forcing are examined as they may have significant impacts on the upper ocean structure and thus influence tropical cyclones which often occur here. Two experiments were conducted using the Regional Ocean Modelling System (ROMS); one forced with tides (***Tide***) and the other experiment without tidal forcing (***NoTide***). On seasonal time scales, the tidal forcing simulation shows warmer temperatures in the upper layer particularly near strong ocean currents (North East Madagascar Current and South East Madagascar Current). In tide, warming near these currents is intensified during winter due to the southeast trade winds, while in summer, poleward advection of warmer waters south of 16-17 ^{o}S seemed more prominent. On weather time scales, these changes in the upper ocean structure, especially

near the coast or in shallow regions can alter the intensity of passing tropical cyclones. When a storm encounters a warm anticyclonic eddy, as the case of TC Japhet examined here, the SST cooling by the cyclone is substantially reduced, the mixing length temperature is increased and the mixed layer is deepened. The difference between the two simulations shows that including tidal forcing deepens the mixed layer by 6m, raises the sea surface height by 0.2m and increases the eddy kinetic energy by 600 cm^2s^2.Furthermore, tide gives a better representation of the position of the eddy. These changes can be important for TC evolution.

5.1 Introduction

The Mozambique Channel in the southwestern Indian Ocean is found between Madagascar on the east and Mozambique on the west, the Comoros archipelago in the north and is linked to the greater Agulhas Current system to the south. Its particular geographic pattern and position make the Mozambique Channel peculiar in terms of ocean circulation, as it is found to be one of the most turbulent areas in the world's oceans (Ternon et al., 2014). The Channel receives input to the north via southward propagating eddies that are related to transport variability in the South Equatorial Current (Backeberg and Reason, 2010). It also contributes to inter-ocean exchanges due to its associatin with the Agulhas Current system that transports large amounts of heat and salt from the Indian to the Atlantic Oceans (Ruijter et al., 1999; Durgadoo et al., 2013; Loveday et al., 2014).

A detailed bathymetry of the Mozambique Channel area studied here is shown in Figure 5.1. The steep topography and the high surface tides of about 1 m for the M2 and S2 components (Le Provost, 2001) make the area conducive for the generation of internal tides. When compared to the South West Indian Ocean, tides in the Mozambique Channel are an important component of flow, with a gradual rise in tidal range from less than 2 m to the north and to the south of the channel to more than 5 m in its central part (Pugh, 1987; Robinson et al., 2006). Besides the upper ocean influences, tides are considered to be one of the most important sources of mechanical energy for driving ocean thermohaline circulations (Munk and Wunsch, 1998). Tides can contribute to about half of the total energy (1TW) required to drive the deep ocean circulation while the rest is due to the wind (Egbert and Ray, 2003).

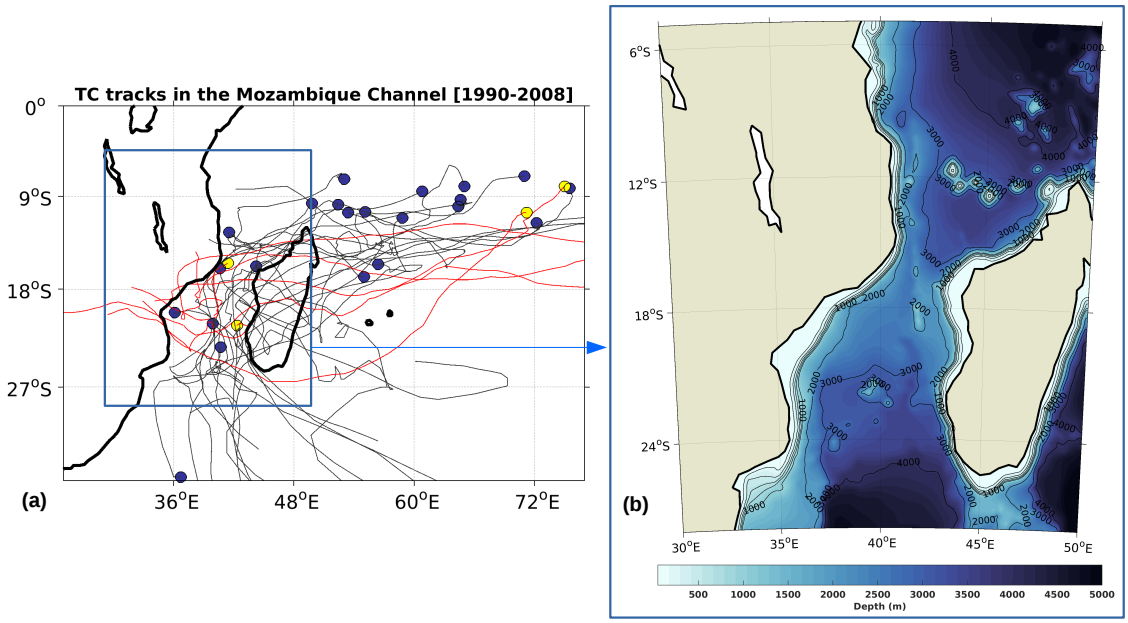

Fig. 5.1 (a) Map of Tropical cyclone trajectories crossing the Mozambique Channel during 1989/1990-2007/2008. Blue circles show the genesis location of TCs that crossed the Mozambique Channel and yellow circles are genesis locations of TCs that made landfall. Red tracks are landfalling TC tracks regardless of where they are formed. (b) Bathymetry of the Mozambique Channel (region of study). Contours are every thousand meters from 0 to 5000 m

.

According to Baines (1982), the energy fluxes computed from several shelf regions of the global oceans showed that the Mozambique Channel was amongst the 12 most energetic regions for tidal generation. The large–scale flows in the Mozambique Channel are intense and highly variable, especially in the central (narrowest) part, between 15 to 17 ^{o}S. Snapshots of the observations made by Schumann (1998) and DiMarco et al. (2002) suggested that eddies might be responsible for this high variability around this region. The Mozambique Channel is characterised by complex and variable surface and sub-surface circulation that is governed by mesoscale activity (e.g. (Biastoch and Krauss, 1999; de Ruijter et al., 2002; Ridderinkhof and De Ruijter, 2003; Schouten et al., 2003; Lutjeharms, 2006; Collins et al., 2014; Cossa et al., 2016)) and related to the large scale circulation in the Indian Ocean (Penven et al., 2006; Palastanga et al., 2006; Ridderinkhof et al., 2010; Backeberg and Reason, 2010). Eddies are generally generated where the Channel is the narrowest (16^{o}S) between the northern and central basins and propagate southward particularly along the coast of Mozambique

(Schouten et al., 2003; Backeberg and Reason, 2010; Collins et al., 2014; Halo et al., 2014; Malauene et al., 2014). Eddies are also formed at the southern tip of Madagascar and some of them migrate into the Channel northwards along the west coast of Madagascar (Quartly and Srokosz, 2004).

The ocean circulation in the Channel is also wind forced, presenting seasonal variations, which are strongest from October to February (Sætre, 1985). In summer, the average wind direction differs for the southern and northern part of the channel. The southern part is influenced by south-easterly winds and the northern part north-westerlies. Therefore, the northern part may be considered to form part of the monsoonal wind system of the Indian Ocean that exists north of 15 ^{o}S (Saetre and Da Silva, 1982) whereas the southern part does not. Also, during summer, the shelf waters of the Mozambique Channel may be affected by tropical storms (Figure 5.1a) that, as a rule, move poleward through the channel (van Heerden and Taljaard, 1998). Some of these storms intensify into Tropical Cyclones (TCs) and some TCs formed in the Channel, however, make landfall somewhere along the coast of Mozambique. Even if they do not make landfall, TCs generated in the Channel can still contribute significantly to rainfall over Mozambique and Madagascar (eg. TC Dera in 2001;(Reason, 2007)). During the period 1990-2008, 32 TCs (sustained winds $>$ 64 knots) crossed the Mozambique Channel, including 9 TCs which formed in the Channel and 7 TCs that made landfall over the southern African mainland (yellow circles and red tracks in Fig 1a). Several prominent TCs that crossed the Channel intensified before making landfall over Mozambique and led to substantial loss of life and damage (e.g. TC Eline in 2000,(Dyson and Van Heerden, 2001; Reason and Keibel, 2004); TC Favio in 2007,(Klinman and Reason, 2008); TC Japhet in 2003 analysed below). Since the Mozambique Channel is a region of strong tidal activity, it is worth investigating the role that tides may play in influencing the upper ocean characteristics that are important for TC evolution and potential intensification. Although the main focus here is on TCs, it is worth noting that other types of heavy rainfall events can also intensify over the Mozambique Channel and subsequently cause flooding over Mozambique and northeastern South Africa such as mesoscale convection complexes (Blamey and Reason, 2009, 2013) and tropical-extratropical cloudbands (Manhique et al., 2011, 2015). These systems are also sensitive to the SST of the channel and presumably to other upper ocean characteristics there.

Tidal currents in low lying coastal regions are important and mixing near the surface influences the properties of those water masses and the exchanges of heat and freshwater between the atmosphere and ocean, which in turn affect passing cyclones. The warm sea surface temperature (SST) in the Mozambique Channel serves as an important source of heat and moisture for rainfall over the southern African mainland (d'Abreton and Lindesay, 1993; Cook et al., 2004; Reason and Rouault, 2006). Therefore, small differences in the SST and upper ocean heat content here may lead to significant changes in the development of atmospheric deep convection and associated rainfall. Chevane et al. (2016) considered the effects of tidal currents on the vertical stratification in the Sofala Bank region of the western Mozambique Channel but the effects of tides on the upper ocean circulation and their potential significance for TC activity in the Mozambique Channel have not been investigated to date.

In this context, a three-dimensional numerical ocean model (ROMS) was configured to investigate the effects of tides on the upper ocean structure and to address the question of whether tidal forcing can influence upper ocean characteristics which are important for tropical cyclone genesis or intensification. The rest of the paper is organized as follows. Section 2 describes the regional ocean model, the data and the methods used to compute the upper ocean temperature related to TC intensification. Section 3 describes the seasonal evolution of the variables necessary for tropical cyclone intensification in a tidal forcing simulation and analyses the differences that exist between the two experiments; namely with and without tides. Section 4 describes a case study of tropical cyclone Japhet with underlying ocean characteristics such as SST, mixed layer depth, eddy activity and mixing length temperature (Tdy) which are important for storm evolution. Section 5 contains the discussion and summary.

5.2 Data and Methods

The ocean model

The model used in this study is the Regional Ocean Modelling System (ROMS), a realistic three-dimensional oceanographic model that solves the primitive equations with a stretched

terrain-following vertical coordinate (Shchepetkin and McWilliams, 2005; Debreu et al., 2012). The unresolved physical mixing processes are parameterised with a non-local K-profile parameterisation (Large et al., 1994) with both a surface and a bottom boundary layer parameterisation. The model explicitly allows free surface movements (important for tidal motions). ROMS has already been successfully applied to tidal problems in the Mozambique Channel (Chevane et al., 2016) as well as to the Zambezi River plume (Nehama and Reason, 2015). The numerics are based on finite differences, discretized horizontally in an Orthogonal-Curvilinear coordinate system. This can be used to follow the coastlines for irregular lateral boundaries, important for coastal processes. In the vertical it is discretized in a generalized σ-coordinate system: following the irregularities of the bottom topography (Song and Haidvogel, 1994) (important for flow topography interaction). The variables are computed on a numerical staggered Arakawa C grid (Arakawa and Lamb, 1977).

The model domain spans the entire Mozambique Channel and neighbouring South West Indian Ocean and captures the Mozambique Channel eddies as well as the Mozambique Channel outflow into the Agulhas current near 24 ^{o}S. The domain is an oblique grid, encompassing the region 30^{o}E – 50^{o}E and 5^{o}S – 35^{o}S with a 1/12^{o} horizontal resolution. The model bathymetry was derived from the Global Earth Bathymetric Chart of the Oceans (GEBCO) 1'-resolution dataset bilinearly interpolated onto the grid. The vertical grid was divided into 40 terrain-following layers with a resolution of about 5 m in the upper 100m. The model has open boundaries at three lateral faces, North, South and East. Boundary conditions are extracted from the Simple Ocean Data Assimilation reanalysis data (SODA) v2.1.6 (Carton and Giese, 2008) over a 1990-2008 interannual simulations. The daily averaged surface forcing used in the ROMS simulation is derived from the NCEP Climate Forecast System Reanalysis (CFSR). The interannual simuation, is initialised from January 1987, after which kinetic equilibrium is reached following a rapid 3 year adjustment period. The model is integrated for 18 years and the full 1990-2008 period is analysed at a daily resolution.

The barotropic tides were introduced at the model lateral open boundaries using a Flather radiation condition (Flather, 1987) to force velocities and sea surface elevations from the TPXO global tidal solution (Egbert and Erofeeva, 2002). Barotropic tidal data were obtained from TPXO 7.0 for the 10 principal constituents (M2, S2, N2, K2, K1, O1, P1, Q1, Mf, Mm). Two experiments were conducted using the model: one with the tidal forcing labeled ***Tide***

and another without the tidal forcing labeled ***NoTide***.

Tdy calculation

A novel approach used to analyze the ocean stratification in relation to TC activity involves the mixing length temperature, Tdy (Balaguru et al., 2015). Since the SST beneath the storm is difficult to measure, the SST ahead of the storm is normally used. However, the core SST can be much lower than the prestorm SST due to SST cooling induced by the storm and several studies (Balaguru et al., 2015; Foltz and Balaguru, 2016; Mawren and Reason, 2017) have shown that the Tdy, computed through a varying mixed layer depth gives a better estimate of the ocean state beneath the storm which is appropriate for TC generation and evolution. Therefore, compared to SST and vertically averaged temperature to fixed depth (Tropical Cyclone Heat Potential (TCHP);(Goni et al., 2010; Shay et al., 2000; Malan et al., 2013)), Tdy has brought significant improvement.

Tdy is the vertically averaged temperature over the TC-induced mixing length (L) defined as follows, using the turbulent kinetic energy approach (Foltz and Balaguru, 2016), based on a balance between the work done by the TC's wind forcing and the potential energy barrier created by ocean stratification as follows :

$$L = h + (\frac{2\rho_o u_*^3 t}{\kappa g \alpha})^{\frac{1}{3}} \tag{5.1}$$

where h is the initial mixed layer depth, u* is the friction velocity (obtained from the maximum wind speed of the TC), t represents the translation time of the TC, κ is the von Karman constant, g is the acceleration due to gravity and alpha is the rate of change of density beneath the mixed layer, which is a function of both oceanic and temperature (T) as well as salinity (S).

The vertically averaged temperature, Tdy over the mixing length L is then calculated as :

$$T_{dy} = \frac{1}{L}\int_0^L T(z)dz \tag{5.2}$$

where T(z) is the temperature as a function of depth z.

In the case of TC Japhet presented in Section 4, changes in Lagrangian computation of SST, MLD, Tdy and EKE under the TC gave a better representation of the underlying upper ocean structures. The SST change at each point along the TC track is evaluated as the difference between SST two days after the passage of the TC and the average SST over the 10-day period prior to the day before the storm passes over that point.

5.3 Results and discussions

5.3.1 Seasonal climatology

Figure 5.2 shows the seasonal evolution of climatological SST, MLD, TDY and EKE across the Mozambique Channel, obtained from the 18 year simulation with tides. These parameters are important in controlling the response of the upper ocean to the atmospheric forcing, which in turn, influences storm genesis and potential intensification of TCs. The seasonal meridional velocity and vorticity were also investigated to identify regions of potential instability in the flow. For the first time, the effects of tides on the upper ocean heat content related to tropical cyclone intensification will be investigated. Here, the seasonal average SST in Figure 5.2a increases by about 2-3 ^{o}C over the central Mozambique Channel (15 ^{o}S - 21 ^{o}S; 33 ^{o}E - 44 ^{o}E), where TCs are most common with warmest SST around March-April (29 - 30 ^{o}C) and coolest SST (25 - 26 ^{o}C) observed during September-October. Strong tidal mixing cools the SST along the Mozambican coast to about 24 - 25 ^{o}C in austral summer as it mixes the warm surface water with colder subsurface water. The signature of the North East Madagascar Current (NEMC) can be seen over the northern tip of Madagascar throughout the year, consistent with Manyilizu et al. (2014, 2016).

The mixed layer depth (MLD) is an important parameter connected with the amplitude of SST response to TCs (Vincent et al., 2012). During summer, when natural ocean convection is not effective, the mixed layer depth may be altered by wave-induced turbulence, especially during cyclone seasons. Conversely to SST, the MLD evolution does not have a smooth

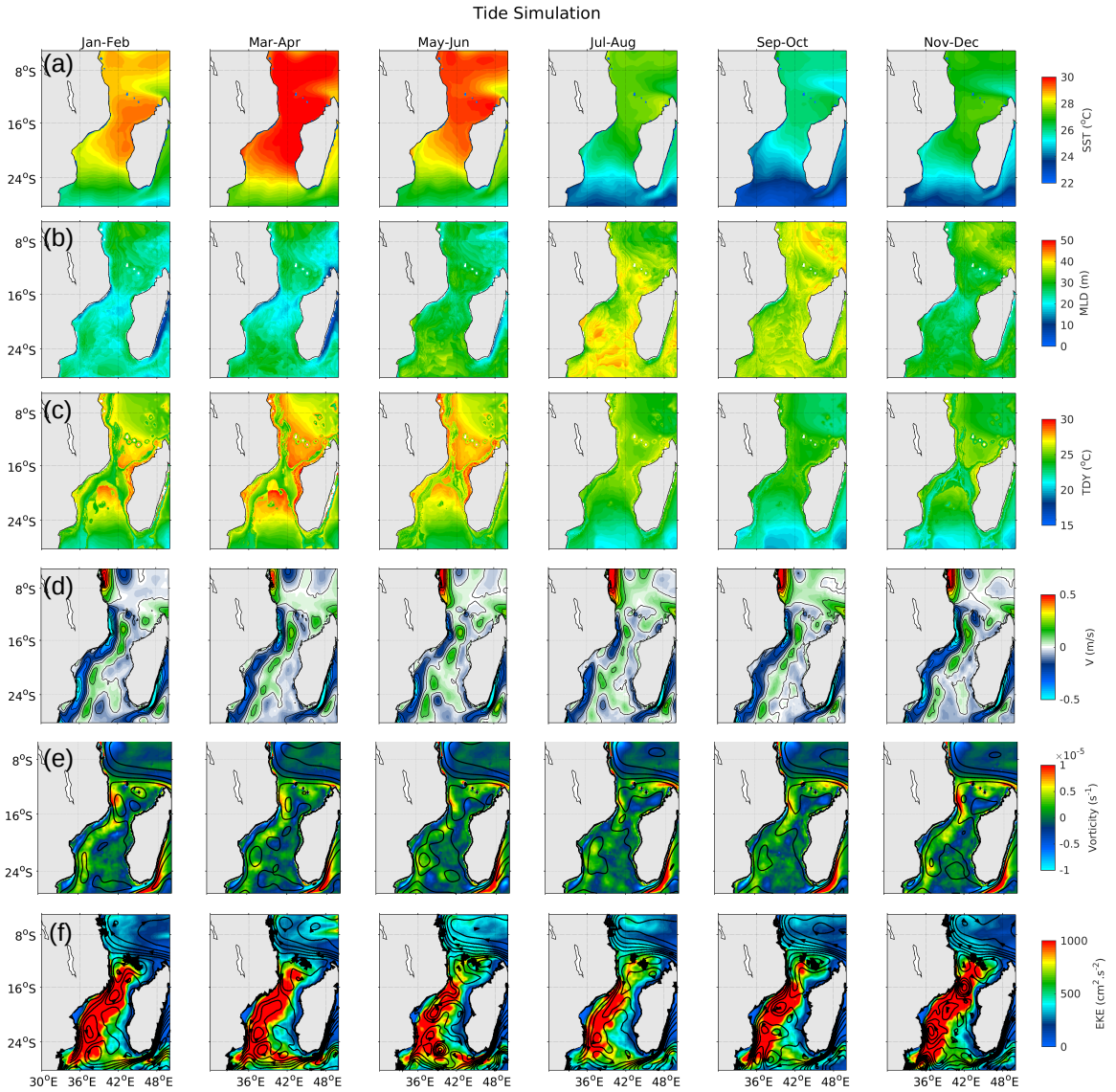

Fig. 5.2 Seasonal climatology of (a) SST, (b) MLD, (c) TDY, (d) meridional currents, (e) vorticity and (f) EKE in the Mozambique Channel based on the ROMS tidal run simulation.

annual cycle in the central Channel. At the beginning of spring, MLD is about 30 m over the central Channel and a bit deeper both to the north and the south (Figure 5.2b). In early summer (November-December), MLD over the central Channel shallows to 20-25 m and a narrow tongue of shallowest MLD is evident near the central Mozambican coast. This tongue became more prominent in summer progressing to less than 15 m in January-February while most of the rest of the central Channel exhibits MLD of about 20 m increasing to 25 m in

the south. The MLD starts to increase in March-April and reaches about 30 m in May-June when winter winds cool the surface and destabilise the upper layers. Deepest MLD occurs in late winter (July-August) reaching 40-50 m south of about 20^{o}S . The depth of the seasonal thermocline in the open ocean is set by the amount of wind mixing acting to deepen the surface mixed layer (Simpson and Sharples, 2012). On the shelf, the thermocline depth is a balance between wind mixing trying to deepen it, and tidal mixing attempting to push it back upward (Simpson and Sharples, 2012). Thus, the MLD along the Mozambican shelf tends to be shallower than that of the open channel.

Figure 5.2c plots Tdy (mixing length temperature) since a few studies (Toffoli et al., 2012; Balaguru et al., 2015, 2016) have demonstrated that using a variable mixed layer depth instead of a constant monthly value during summer months can lead to a significant improvement for the prediction of the upper ocean thermal structure, known as the mixing length temperature (Tdy in this study). The most noticeable feature in Figure 5.2c is the Tdy relation to the bathymetry, with four distinct regions apparent: (i) a warm well-mixed region on the inner shelf with relatively high Tdy, (ii) a well-mixed cooler region over the shelf edge; (iii) a stratified region in the central of the Channel and (iv) the Comoros islands region in the north near 12 ^{o}S which show higher Tdy than further offshore. The maximum Tdy is observed around March-April, during the latter part of the South West Indian Ocean TC season that runs from November through April with values varying between 27-30 ^{o}C in the central Channel. Minimum Tdy occurs between September-October (about 25 ^{o}C) in the central Channel. The annual cycle of Tdy is therefore similar to that of SST.

Figure 5.2d shows the seasonal varibility of the meridional velocity in the Mozambique Channel. Negative values (blue areas) indicate that the current is flowing poleward while positive values (red areas) are currents moving towards the equator. Throughout all the months, poleward currents seem to flow along the coast of Mozambique and east coast of Madagascar reflecting southward eddy propagation in the Channel and the South East Madagascar Current (SEMC) respectively. During the Southwest monsoon (austral winter), the NEMC has increased intensity around the Northern tip of Madagascar feeding into the East African Coastal Current (EACC), due to the increased southeast trade winds consistent with (Manyilizu et al., 2014, 2016). During the Northeast monsoon (austral summer), the poleward current along the coast of Mozambique is stronger (Figure 5.2d) than in winter. The

strengthening (weakening) of the poleward current during austral summer (winter) coincides with decreased (increased) local wind speeds (Nehama and Reason, 2015). Northwesterlies dominate over the Comoros Basin during summer and flow in the direction of the poleward current thus acting to strengthen this current along the coast of Mozambique. Conversely, southeasterlies dominate over the Comoros Basin during winter which exert an opposing force on the poleward current, thus weakening it.

However, on the shelf the situation is more complex. The poleward current seems to influence Tdy on the shelf since it carries warm waters from the tropical Indian Ocean. During summer, when the current is stronger (Figure 5.2d), its close relation with bathymetry indicates that vertical mixing is the major mechanism determining the summer Tdy climatology distribution in the Mozambique Channel. Since Tdy is inversely related to the mixing length and the initial MLD, any variations in the MLD would influence the upper ocean thermal structure. An overall shoaling of the MLD during summer results in part from intensified upper-ocean stratification caused by both surface warming and weakening of winds. Therefore, a decrease in the mixing length will imply a warmer Tdy (equation 2), vice versa in winter.

Similar patterns to Figure 5.2d are observed in Figure 5.2e, with increased vorticity along the coast of Mozambique, eastern and northern coast of Madagascar related to the SEMC and NEMC. Vorticity is maximum in summer south of 12 ^{o}S along the western part of the Channel which indicates the propagation of Mozambique channel eddies. The seasonal mean eddy kinetic energy (EKE) is presented in Figure 5.2f, with values exceeding 1500 $cm^2.s^{-2}$ south of 15 ^{o}S in the Mozambique Channel. Eddy activity in the Channel is most concentrated in the central and western part of the Channel. Figure 5.2f shows anticyclonic eddies in the Comoros Basin, generated west of the northern tip of Madagascar and which propagate westward towards the African coast, where they are deflected southwards into the Comoros Basin consistent with Backeberg and Reason (2010). The spatial pattern is rather similar throughout the year but maximum EKE strength is nevertheless reached during summer when TCs are active and minimum during July-August. It is also worth noting that weak EKE values are observed along coastal regions, particularly along the western coast of Madagascar.

5.3.2 Difference between Model Simulations with and without Tidal Mixing

Two experiments were conducted in this study; one with tidal forcing labeled ***Tide*** and another without the tidal forcing included labeled ***NoTide***. Figure 5.3a shows the seasonal evolution of differences in SST between the two simulations. In all months, tidal mixing cools the SST along the outer edge of the continental shelf of Mozambique and western Madagascar as it mixes the warm surface water with colder subsurface water. There are also large areas of cooling in the central channel offshore of the shelves in most months, particularly around November-December, January-February and July-August. Figure 5.3a shows that implementing tidal forcing cools the SST by 0.7 ^{o}C during winter (July-August) compared to 0.5 ^{o}C in summer (January-February) in the southern part of the channel, near 24 ^{o}S. In the central Channel, SST is cooled by about 0.4 ^{o}C in July-August and about 0.2-0.3 ^{o}C in January-February. Cooling of SST by about 0.2-0.5 ^{o}C in the areas of the Channel can be important for storm generation and intensification. In general, vertical mixing in the upper ocean can lead to a deepening of the ocean tropical thermocline and a reduction in the SST (Manucharyan et al., 2011). On the shelf, additional energy for vertical mixing from the sea floor up through the water column comes from currents that are controlled by the tides. Tidal currents create turbulence due to the shear produced by friction at the sea floor. A persistent cool bottom boundary layer exists in the model throughout all the months. Where the tides are stronger and/or where the water depth is shallower, they can mix the entire water column to the surface and this is a typical feature along coasts, in channels between reefs and in macro-tidal areas (Steinberg, 2007). Vertical mixing within a water column that is already well mixed from top to bottom, such as shallow waters, does not result in enhanced cooling ($<$-0.1 ^{o}C white areas in the northern part of the Channel in most months). In deeper regions, like the southeastern or northeastern part of the Channel, where the surface wind mixing does not co-occur with the tidal mixing from the sea floor, a core can result at the centre of the water column, displaying a reduced dissipation rate where there is minimal turbulence available for mixing (Steinberg, 2007) thus creating a warmer subsurface layer (observed in Figure 5.4).

Between 10-12 ^{o}S, a warm SST band is established along the NEMC feeding into the EACC. This positive SST difference between ***Tide*** and ***NoTide*** is present throughout the whole year reaching a maximum SST difference of about 0.30 ^{o}C in July-August. It is weakest during September-December, consistent with Manyilizu et al. (2016). Warming is

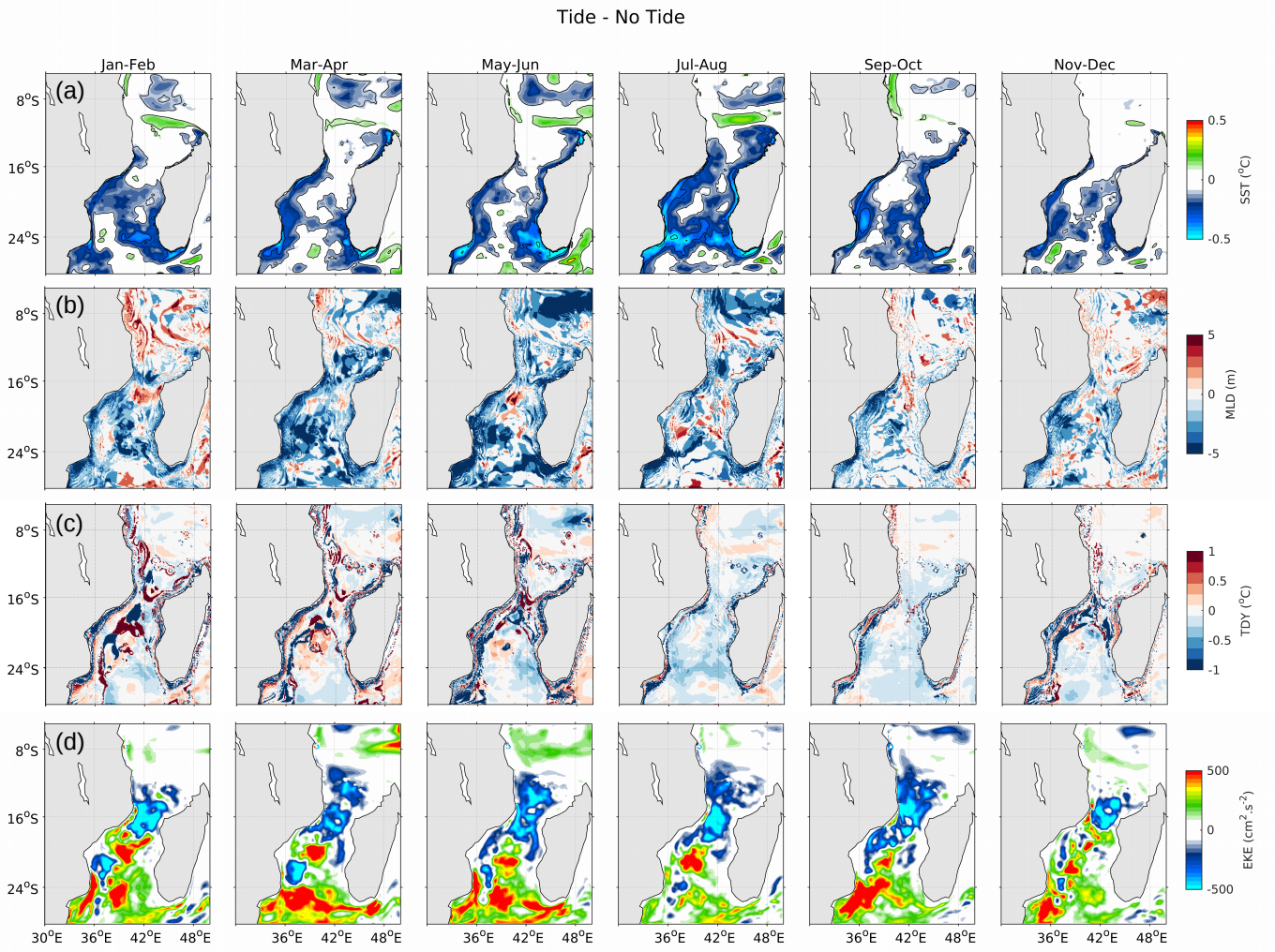

Fig. 5.3 Difference between the ***Tide*** and ***NoTide*** simulation of seasonal (a) SST, (b) MLD, (c) Tdy and (d) EKE

also visible along the SEMC, south of 24 °S where maximum warming (0.35 °C) occurs around May-June just to the southeast of southern Madagascar. Large circular warm features (0.2 °C) as shown in Figure 5.3a, suggest the shedding of eddies from the southern tip of Madagascar towards the African continent, where they most probably merge with Mozambique Channel Eddies and rings (Biastoch and Krauss, 1999; de Ruijter et al., 2002; Schouten et al., 2003; Ridderinkhof and De Ruijter, 2003; Halo et al., 2014).

Figure 5.3b indicates an overall deepening (positive values) of the MLD in the northern part of the Mozambique Channel starting around spring (September-October) reaching a

maximum MLD difference of about 10 m around January-February. It is also interesting to note that the spatial distribution of MLD difference between the two simulations across the Mozambique Channel indicates a deeper MLD by about 5 - 10 m along the NEMC, EACC and SEMC in most months. Introducing tidal forcing leads to deeper mixing or thermocline deepening occuring due to surface water convergence, entrainment generated by large turbulent eddies or current shear instabilities along the strong ocean currents (NEMC,EACC and SEMC). However most of the southern half (16 – 24 ^{o}S) of the Channel shows a shallower MLD throughout the year particularly in March-April and May-June.

Figure 5.3c shows differences in Tdy between the two simulations and suggests that the role of bathymetry is particularly important during summer and autumn. Along the coast and in shallow areas, the results show strong differences, ranging between -0.5 to -1^{o}C during winter and between 0.5 and 1^{o}C during summer. These differences are large enough to potentially influence tropical storms (Mawren and Reason, 2017). The Comoros Basin also exhibits large variations during this season. However, in deeper regions, in the south of the Channel (Figure 5.1), Tdy differences do not vary as much (-0.5 ^{o}C $<$ Tdy $<$ 0.5^{o}C). Similar to SST, a positive difference is mainly observed along the NEMC, EACC, SEMC and along the path of Mozambique eddies. In general, tidal forcing seems to introduce a distinct and consistent signal in all three parameters, SST, MLD and Tdy, particularly along ocean eddy paths in the Mozambique Channel (high EKE region in Figure 5.2f). It is therefore worth investigating the difference in eddy kinetic energy between the two simulations.

The difference in EKE (Figure 5.3d) indicates an intensification of eddy kinetic energy near the southern tip of Madagascar exceeding 1000 cm^{2}s^{-2}, due to more eddies advecting from there by the SEMC. This localized region appears to be high in vorticity (Figure 5.2e) and tidal stirring, providing enough energy to generate or sustain eddies in the Mozambique Channel (Halo et al., 2014). These eddies propagate west and northwest into the southern channel. Further north in the central channel, where southward propagating eddies often occur (Ridderinkhof and De Ruijter, 2003; Backeberg and Reason, 2010), the tidal run also shows large areas of increased EKE. The results also reveal that mesoscale eddy variability increases in strength in late summer (March-April), in accord with the increase in stratification. In contrast, the region 12 ^{o}S- 17 ^{o}S, shows a reduction in EKE (Figure 5.3d), probably due to the relatively minor role of tidal mixing in this region.

The results suggest that introducing tidal effects in an ocean model on a seasonal basis can lead to warming in some specific regions where there is high vorticity (Figure 5.2e) and high stirring, like ocean currents and turbulent eddies. The mixed layer depth in these regions is deepened by about 5-10m and shallowed elsewhere, which can be quite significant for tropical cyclones passing by. These changes in SST, MLD and Tdy are large enough therefore to potentially impact TCs occuring in the Channel. Furthermore, the tidal simulation showed increased EKE south of 17 ^{o}S during summer when TCs are active, the case study of TC Japhet below presents an example of an eddy in the channel influencing a tropical cyclone.

5.3.3 Impact of Tidal mixing on the upper ocean thermal structure

Figure 5.4a shows the differences in the vertical cross sections of potential temperature across longitude 42 ^{o}E (through the Mozambique Channel) between ***Tide*** and ***NoTide*** to investigate the effect of tides through the water column. The largest differences appear in the upper 200 m with lenses of warmer water apparent during summer in the central (between 15 ^{o}S and 20 ^{o}S) and northern channel (between 5 ^{o}S to 10 ^{o}S). Since the central part of the channel is the area where TCs are most active, it is of interest to analyse the vertical cross section of temperature in the upper 300 m at 17 ^{o}S throughout the different seasons (Figure 5.4b). The results indicate a warm subsurface feature in the upper 200 m, between 39-41 ^{o}E (in the western side of the Channel), reaching a maximum during January-February. Comparisons of the current speed for the upper 300 m (January-February climatology) between the 2 simulations, ***Tide*** and ***NoTide*** were shown in Figure 5.5a,b. A stronger current between January-February in the tidal run (Figure 5.5a) seems to match up with the subsurface warmer waters in this run during the same period. The increase in poleward currents (Figure 5.5c) advect warmer waters from the north and more towards the western side of the channel where the influence of tidal mixing is more significant.

Thus, including tides leads to substantial changes in the subsurface thermal structure of the ocean as well as SST, MLD, Tdy, EKE. It was also found (not shown) that negative sea surface salinity anomalies (SSS) were observed along the Mozambican coast in the tidal run, indicating the entrainment effect of river plumes like the Zambezi (Nehama and Reason,

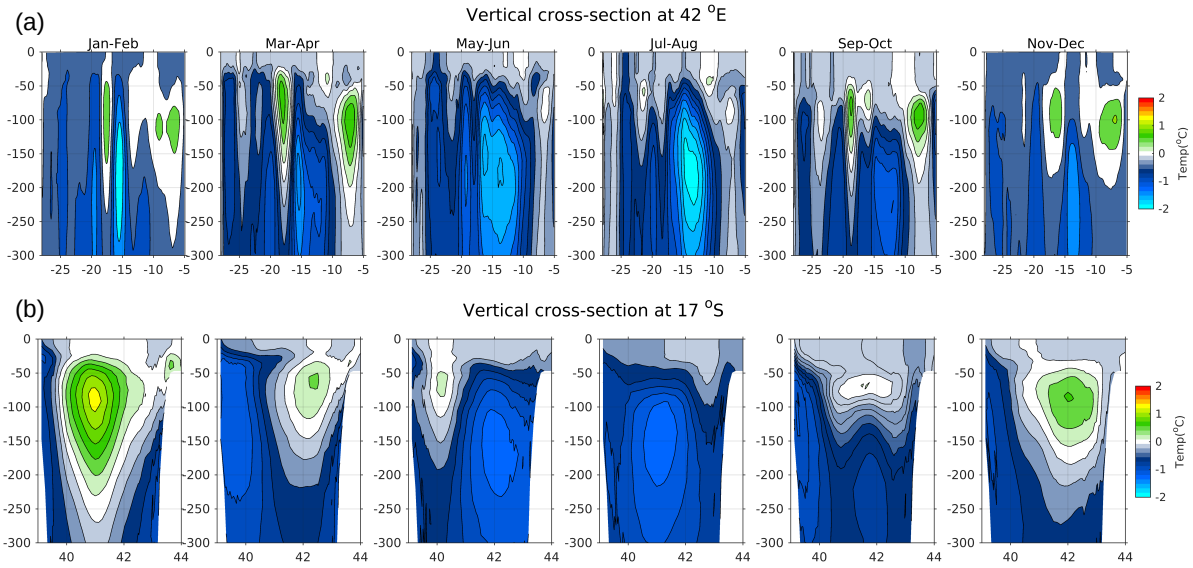

Fig. 5.4 Seasonal difference of the vertical cross-section of potential temperature between the ***Tide*** and ***NoTide*** simulation (a) at 42 °E and (b) at 17 °S.

2015) where this forcing is included. By contrast, saltier waters were observed along the west coast of Madagascar in ***Tide*** indicating a well-mixed layer of water induced by strong tidal currents there.

To see how including tides might be important on weather time scales, the next section considers a case study of TC Japhet. This tropical cyclone was one of the strongest (Category-4; maximum sustained wind speed of about 248 km hr^{-1}) and most damaging storms to occur in the Channel during the 18 year (1990-2008) period of the model integration and hence is interesting to study.

5.4 Case study of TC Japhet

To investigate the influence of tidal forcing on the daily evolution of the upper ocean characteristics important for tropical cyclones, daily output of SST, upper ocean heat content (Tdy), the mixed layer depth and the eddy kinetic energy from both ***Tide*** and ***NoTide*** were compared. TC Japhet formed in the channel on February 25th 2003 and later caused substan-

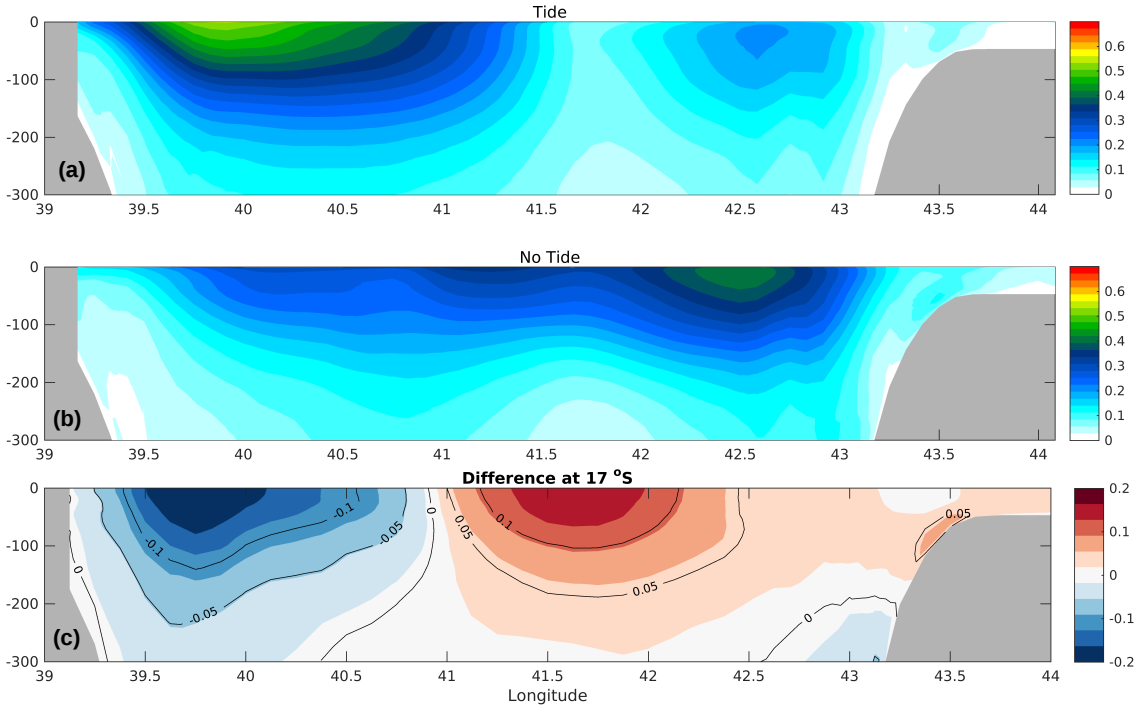

Fig. 5.5 Mean current computed for January-February climatology along latitude 17 °S for the upper 300 m across the Mozambique Channel between (a) ***Tide***, (b) ***NoTide*** simulation, (c) difference in meriodional current between the 2 simulations.

tial damage in southeastern Africa (Mozambique, Zambia and Zimbabwe) destroying more than 25,000 houses, leaving at least 23,000 people homeless. It also caused 25 fatalities in Mozambique and Zimbabwe. The main characteristics of TC Japhet, including its trajectory, wind speed and tropical cyclone intensity from the 25th February to 4th March 2003 were obtained from Meteo France (http://www.meteo.fr/temps/domtom/La_Reunion/webcmrs9.0/francais/archives/saisons_archivees/20022003/2002RE13.html).

TC Japhet was formed during the mature phase of the 2002-2003 El Niño event and its genesis location was in agreement with Ho et al. (2006). These authors derived a composite of all TCs formed during El Niño years and showed that during these events, TC genesis tends to shift westwards in the South West Indian Ocean, enhancing formation west of 75 °E and reducing it east of 75 °E. Another interesting aspect of TC Japhet is that it made landfall over Mozambique which is a rare occurrence during El Niño summers (Vitart et al., 2003; Klinman and Reason, 2008).

Figure 5.6 illustrates the day to day variation of SST, MLD, TDY and EKE change (see data and methods) beneath the storm during the evolution of TC Japhet for ***Tide***. The conditions were favourable on the 25th of February for TC Japhet to be formed, with a warming in SST by 0.5 ^{o}C and a deepening of the MLD by about 15 m compared to the week prior to its occurence. However a slightly cooler Tdy was noted, probably due to enhanced tidal mixing at the coast. As mentioned in the previous section, by definition, a deeper MLD will lead to a cooler Tdy. The EKE change however shows weak or nearly no eddy activity along the west coast of Madagascar on this day. As the TC began to strengthen from a tropical disturbance to a tropical storm between 26th - 27th February, the SST began to cool substantially deepening the mixed layer depth by about 5- 10m. However, in ***Tide***, the MLD on 26th and 27th was not as deep as on the 25th and 1st March when the storm was close to the Madagascar and Mozambican coasts respectively. This situation is because deeper waters are not influenced greatly by tidal currents thus leading to a decrease in vertical mixing. As the storm reached TC category on the 28th February, the SST cooling was reduced and the MLD became shallower which eventually led to a strong positive Tdy change. All these parameters, as well as an increase in the EKE on the 28th helped in strenghening Japhet. On the 1st of March, TC Japhet attained its maximum intensity as the cyclone interacted with an eddy (the highest EKE value was observed on that day). SST cooling was reduced and the Tdy was positive which impacted the TC evolution through an increase in air-sea enthalpy flux transfer (Price, 2009), leading to its rapid intensification. On the 2nd of March, as Japhet left the eddy (lower EKE), the SST and Tdy were largely reduced.

Figure 5.7 shows the spatial representation of TC Japhet and the different parameters influencing its evolution for the ***Tide*** simulation within a 5 degrees radius of the storm. The 6-hourly position of Japhet is shown by the small circles with green color indicating Tropical Storm strength, yellow - Tropical Cyclone strength, red - Intense Tropical Cyclone strength and the large black circles are the daily position. Figure 5.7a shows the SST change from the 25th February to the 2nd of March 2003 caused by TC Japhet. Initially, on the 25th February, as Japhet began to develop, the tidal forcing simulation shows a warming of nearly 0.5 ^{o}C and a deepening in the MLD by about 15 m near the west coast of Madagascar at 21.5 ^{o}S and 43.5 ^{o}E. An overall cooling was observed throughout the evolution of Japhet, except on the 25th, 28th February and 1st March as shown in Figure 5.7a. On the 28th February, Japhet gradually entered a region of shallower MLD (<5 m shallower) and positive Tdy (

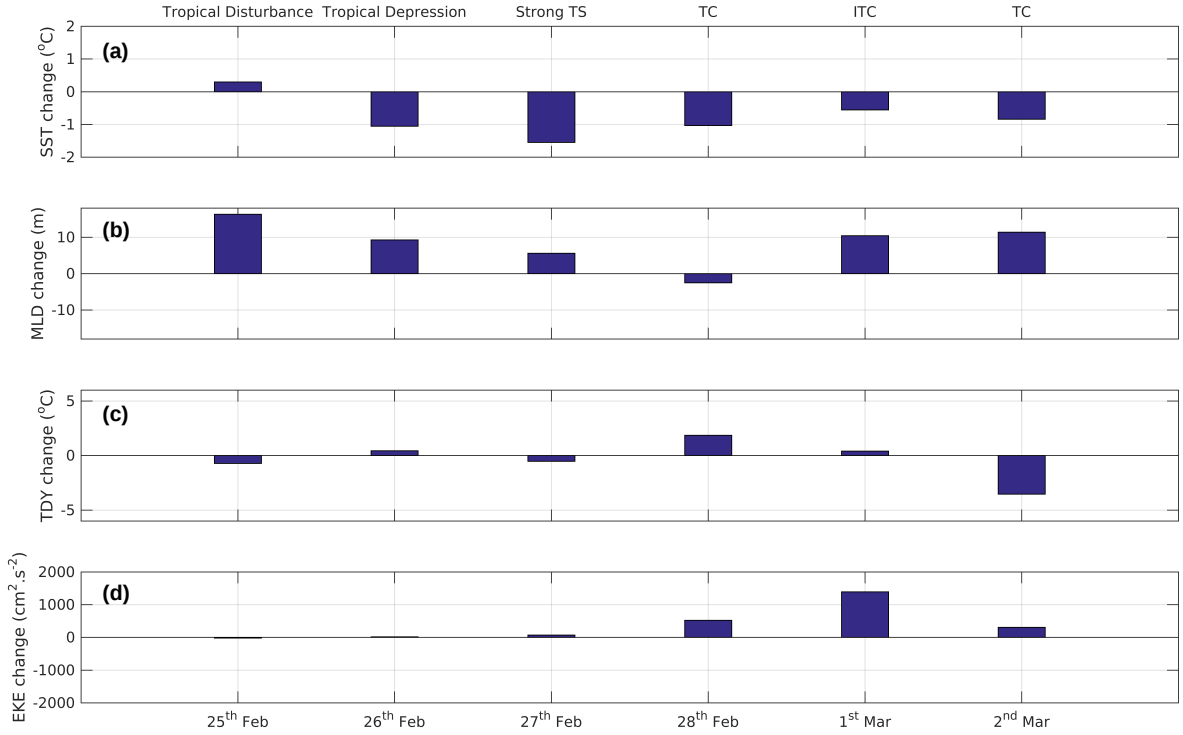

Fig. 5.6 Barchart representing the day to day variations of (a) SST, (b) MLD, (c) Tdy and (d) Eke change under TC Japhet during 25th February - 2nd March 2003 – for ***Tide*** simulation.

2^{o}C warmer), where it strengthened to a TC category. On the 1st of March, it encountered a warm anticyclonic eddy (37.7 ^{o}E; 23.8 ^{o}S) as shown in Figure 5.7d. On that day, the SST cooling was substantially reduced (Figure 5.7a, 5.6a) in the tidal run, the Tdy was increased by 0.5 – 1^{o}C (Figure 5.7c), the MLD was deepened by about 10m (Figure 5.7b) and the storm dropped to 935 hPa (Intense TC) as it moved across the eddy. The tidal forcing simulation highlights the regions with high turbulence or stirring, particularly around eddy paths and these regions were associated with significant warming and deepening of the mixed layer on the 1st of March. However, on March 2nd as the TC moved out of the eddy region towards the Mozambican coast, its strength was quickly reduced from an intense TC to a TC Category when it made landfall.

The actual values of SST, MLD, SSH, TDY and EKE are analyzed below for the 1st of March when TC Japhet reached its maximum intensity. As shown in Figure 5.8a, TC Japhet entered the eddy at 23.3 ^{o}S; 37.7 ^{o}E with EKE value reaching a maximum of 1557 cm^{2}s^2

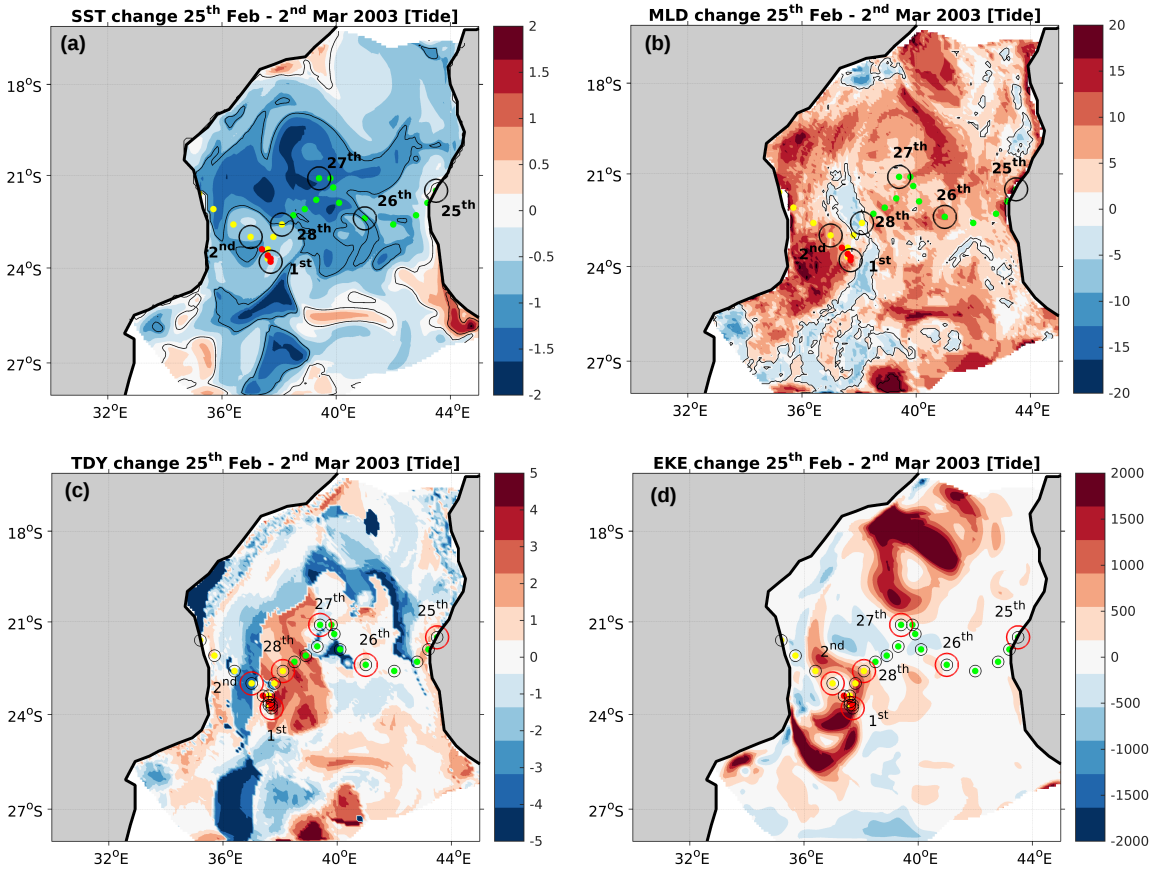

Fig. 5.7 (a) SST, (b) MLD, (c) Tdy and (d) EKE change for ***Tide*** simulation along the path of TC Japhet, where green circles represent Cat TS, yellow : Cat TC, red : Cat Intense TC.

in the ***Tide*** simulation. However, on the same day in the ***NoTide*** simulation (Figure 5.8c), the warm anticyclonic eddy was positioned slightly further north in the Channel therefore TC Japhet only encountered the edge of the eddy in ***NoTide*** (EKE 952 cm^2s^2). On the 2nd March, as the cyclone propagated to the western side of the Channel in ***Tide***, it left the eddy at 23 °S; 37 °E with EKE value at that point dropping down to 57 cm^2s^2. In constrast, on the same day in the ***NoTide*** simulation (Figure 5.8d), TC Japhet was found to be near the center of the eddy with maximum EKE value of 3988 cm^2s^2. Both ***Tide*** and ***NoTide*** show differences from AVISO but the ***Tide*** ones are smaller and also gets some representation of the cyclonic eddies further north which are not apparent in the ***NoTide***. Compared to AVISO (Figs 5.8 (e-f)), the results therefore show that the tidal simulation gives a better representation of the position of the eddy as it coincides with the day TC Japhet attained its maximum intensity. Figures 5.8 (g-j) all show the signature of the eddy in SST, Tdy, MLD

and EKE with the position of TC Japhet overlaid on the 1st of March.

The difference in the actual values of SST, MLD, SSH, TDY and EKE between the 2 simulations, during the evolution of TC Japhet are displayed in Figure 5.9a-e. The SST difference shows cooler temperatures due to tidal mixing (0.2 ^{o}C cooler) on the 25th February and on the 1st of March (0.3 ^{o}C cooler) when TC Japhet was closer to the Mozambican coast. As the TC strengthened from a Tropical Storm to a Tropical Cyclone on the 27th February, warmer SST (values up to 0.5 ^{o}C warmer), a decrease in SSH of 0.25 m, shallower MLD (values dropping down by 8m) and a decrease by 2^{o}C in Tdy were observed in the tidal simulation compared to ***NoTide***. Thus, as a result of TC Japhet passing over shallower region (Figure 5.9f), substantial changes in upper ocean characteristics occured. Deeper waters are not influenced greatly by tidal currents, leading to a decrease in vertical mixing therefore a decrease in MLD and SSH. As the TC propagated across the Channel, the EKE increases in both runs with the maximum value attained on the 1st of March in the ***Tide*** and 2nd of March in ***NoTide*** as explained in Figure 5.8. The MLD shows a deepening of about 6 m and an increase in SSH of about 0.2 m in the ***Tide*** simulation when Japhet encountered the eddy. A cooler surface and subsurface temperature of 0.3 ^{o}C was observed on that day due to strong tidal mixing. The difference of the EKE between the two runs is important since on the 1st of March when TC Japhet became an intense TC, stronger EKE occurred in the tide simulation compared to the simulation without tides.

In general, the oceanic mixed layer depth acts as an interface for ocean-atmosphere exchanges. However, in regions of high fresh water input where the uniform density mixed layer depth becomes shallower than the thermocline (because of salinity influences), the region between the based of the mixed layer and the base of the isothermal layer is defined as the barrier layer (Sprintall and Tomczak, 1992). The barrier layer thickness (BLT) has been showed by Balaguru et al. (2012); Mawren and Reason (2017), to be important for TC intensification since it acts as a barrier to entraining cooler subsurface water and vertical mixing. Since the barrier layer is a prominent feature in warm regions where TCs are active, a barrier layer may be present along their tracks. As such, the daily salinity and temperature profiles obtained from ***Tide*** and ***NoTide*** were analyzed under the path of TC Japhet to detect any presence of barrier layer on a day to day basis. Initially, as TC Japhet began to develop (Figure 5.10a), a barrier layer was established in both runs reaching a maximum of 20 m

in thickness, which may be due to fresh water input from local rivers or rainfall over the channel prior to Japhet (note that December-February are the main rainy months in the southern African region). The presence of a barrier layer implies that very little heat can pass into the ocean interior, causing a reduction in the SST cooling or a rise in SST change as observed in Figure 5.9a. However, as TC Japhet propagated into the channel, no barrier layers were present but the MLD was about 30-40 m or rather deep in both runs on 28th February and 1st March. On the 25th February, 28th February and 1st March (TC genesis and intensification), when TC Japhet was closer to the coast (Madagascar on the 25th February, Mozambique on the 1st March), the upper layer temperature profile appears to be cooler in the tidal simulation (Figure 5.10a,d,e) but it did not prevent the cyclone from losing its intensity. This is because the strong vertical mixing induced by tidal stirring caused the MLD to deepen and the subsurface temperature to become warmer. Together with TC Japhet encountering an ocean warm eddy, these were the main factors responsible for fueling enough energy to sustain and strengthen the cyclone.

Thus, introducing tides in a regional ocean model can lead to a larger impact on important upper ocean characteristics on a daily time scale, particularly for tropical cyclones crossing regions where tidal influences are significant such as the Mozambique Channel. On the day TC Japhet was generated, even though the SST difference was 0.5 ^{o}C cooler in the tidal simulation (which was expected), the storm still sustained its strength as it was formed in a region of a deep barrier layer. As it propagated across the Channel, no large differences between the model runs were noted as tidal mixing does not cause significant changes in deeper regions. However, as the storm encountered a warm anticyclonic eddy along the coast of Mozambique, the underlying upper ocean structures differ largely; with a deepening of the MLD by 6m, a rise of 0.2m in the SSH,an increase in the EKE by about 600 cm^{2}s^2 and a 0.3^{o}C decrease in the surface and subsurface temperature between the two model runs, which can be quite significant. The day to day variations of temperature and salinity profiles between ***Tide*** and ***NoTide*** show a difference of up to 1 ^{o}C and 0.3 psu respectively.

5.5 Conclusion and Discussion

A three-dimensional regional ocean model of the Mozambique Channel forced with tides was used to assess the effect of tides on upper ocean characteristics important for storms in this highly prevalent tropical cyclone region. To the best of our knowledge, tidal effects on TC ocean characteristics have not been previously studied. Given that Mozambique and Madagascar have suffered severe loss of life and subtantial damage from TCs in the Mozambique Channel in the last few decades, better analysis of upper ocean characteristics is of importance. On the seasonal scales, Figure 5.4 showed that turbulent mixing driven by tides leads to cooler surface waters, however such mixing can also cause significant warming in the subsurface layers. Deeper mixed layer depth (MLD) can occur in some specific regions where there are turbulent eddies and strong ocean currents (for instance the NEMC, EACC and SEMC in the Mozambique Channel). On a seasonal time scale, warming noted between the two runs along the NEMC and SEMC is heightened during winter due to the influence of southeast trade winds, while during summer, eddy activity south of 16-17 ^{o}S seemed to be more prominent in the tidal simulation. Bathymetry was found to play a role in Tdy with large differences observed in shallow regions, along the coast and in the Comoros Basin. In the northern and central part of the Channel, including tidal forcing may result in a cooler surface but warmer subsurface waters.

Introducing tides in a regional ocean model leads to changes in the upper ocean structure on a seasonal time scale but it can create a larger impact on a daily basis, particularly for passing tropical cyclones in regions where tidal influences are significant. For example, strong tidal mixing generates cooler water along the coast and when TCs are formed in these areas (e.g. of TC Japhet in this study), they may lose their intensity unless they are influenced by low salinity waters (due to the presence of fresh water or rainfall), creating a barrier layer. As Japhet encountered a warm anticyclonic eddy near the coast of Mozambique, the actual values of the underlying upper ocean structures may be quite different between the ***Tide*** and ***NoTide*** runs; with a decrease in SST of 0.3 ^{o}C, a deepening of the MLD by 7 m, a higher SSH of 0.2 m and a cooler Tdy of 0.3 ^{o}C and an EKE value of 500 cm^{2}s^2 on that day compared to AVISO. The results also show that the tidal simulation gives a better representation of the position of the eddy as it coincides with the day TC Japhet attained its maximum intensity.

The results presented here suggest that ocean models in regions like the Mozambique Channel (and possibly the Caribbean; NW shelf of Australia) need to include tidal effects to better simulate and understand the role of upper ocean in TC genesis and intensification. Tidal effects may therefore be important for forecasting TC intensification and for improving predictions of rainfall over TC affected regions like southeastern Africa.

About 5 % of the Tropical cyclones formed in the South West Indian Ocean make landfall over the southern African mainland and carry floods to the coastal lowlands. Often, the variability of the upper ocean heat content over the South West Indian Ocean influences the landfall frequency of tropical cyclones on Mozambique. In the next Chapter, the relationships between an index of southern African summer rainfall (SARI) and Tdy in the South Indian Ocean will be investigated with a focus on the frequency of TCs passing in the region.

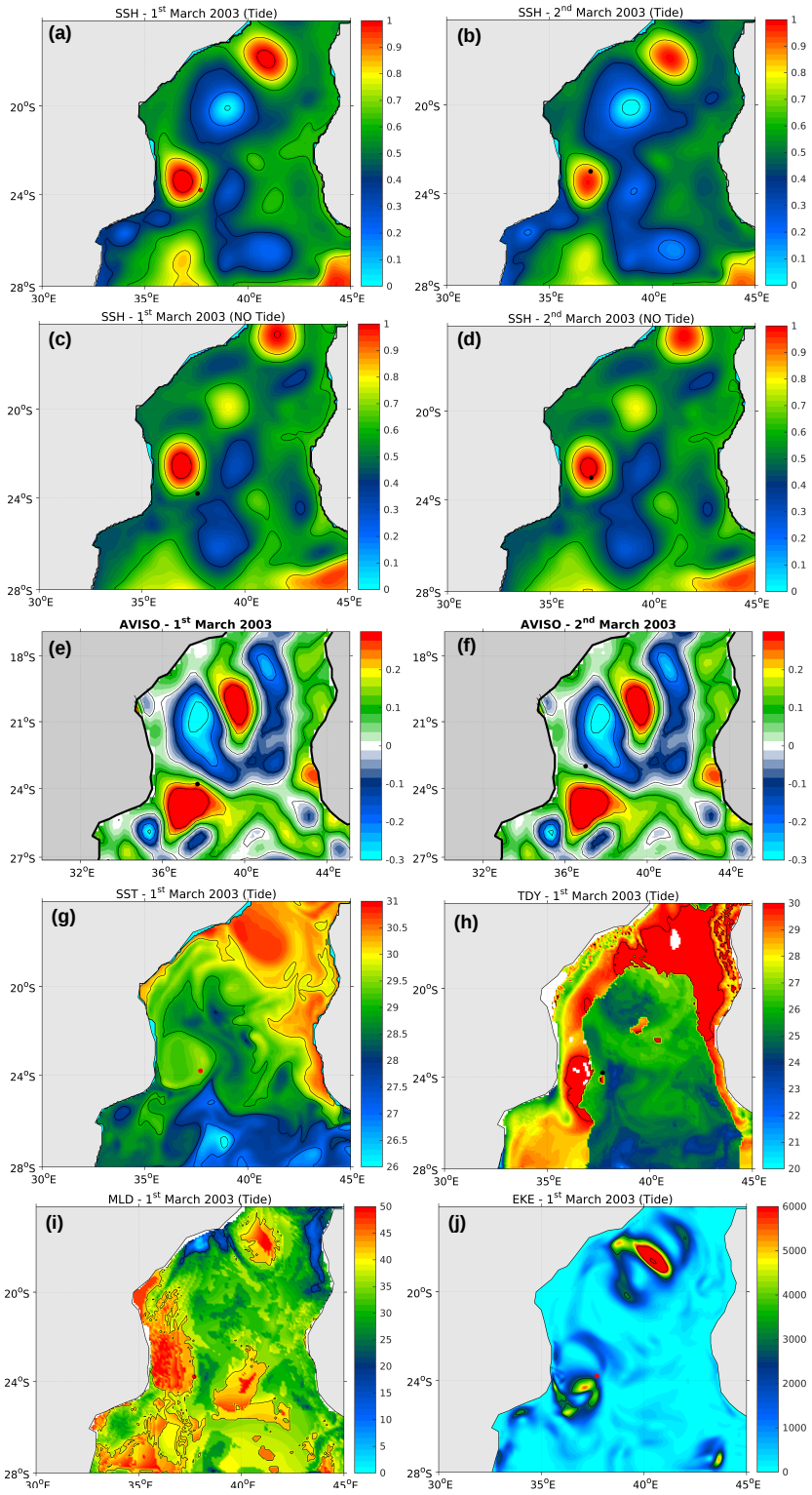

Fig. 5.8 Comparison between (a) SSH (m) (***Tide***),(c) SSH (m) (***NoTide***) and (e) SSH (m) from AVISO on the 1st of March, (b) SSH (***Tide***), (d) SSH (***NoTide***) and (f) SSH (m) from AVISO on the 2nd of March. Actual maps of (g) SST (^{o}C), (h) TDY (^{o}C), (i) MLD (m) and (j) EKE (cm^{2}s^2) in the ***Tide*** simulation on the 1st of March 2003, the day Tropical cyclone Japhet encountered an eddy in the western part of the Mozambique Channel (position of TC Japhet is represented by the red or black dot).

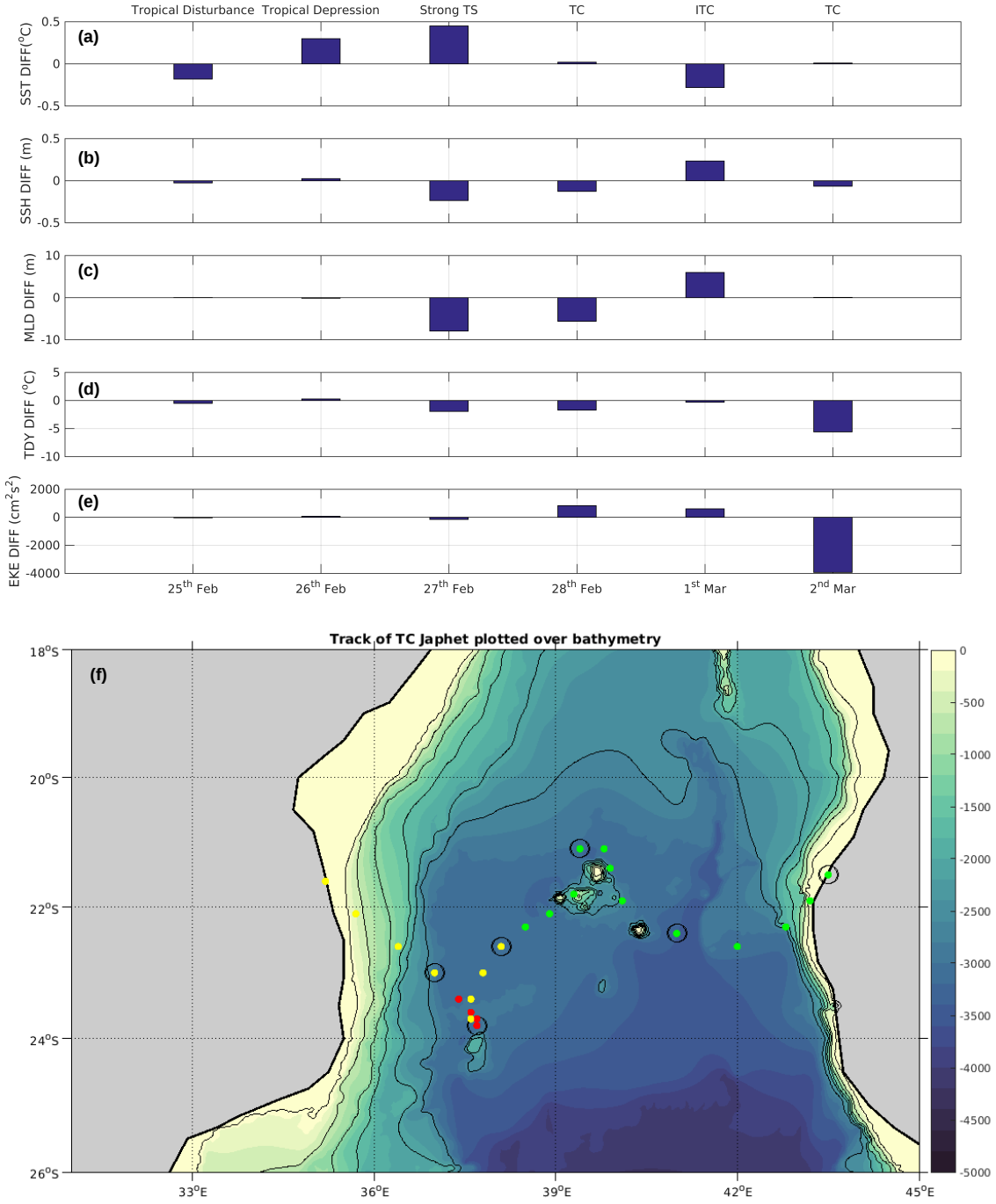

Fig. 5.9 Barchart representing the difference between the 2 simulations for actual values of (a) SST, (b) MLD, (c) Tdy and (d) Eke under TC Japhet during 25th February - 2nd March 2003, (f) track of TC Japhet overlaid over bathymetry

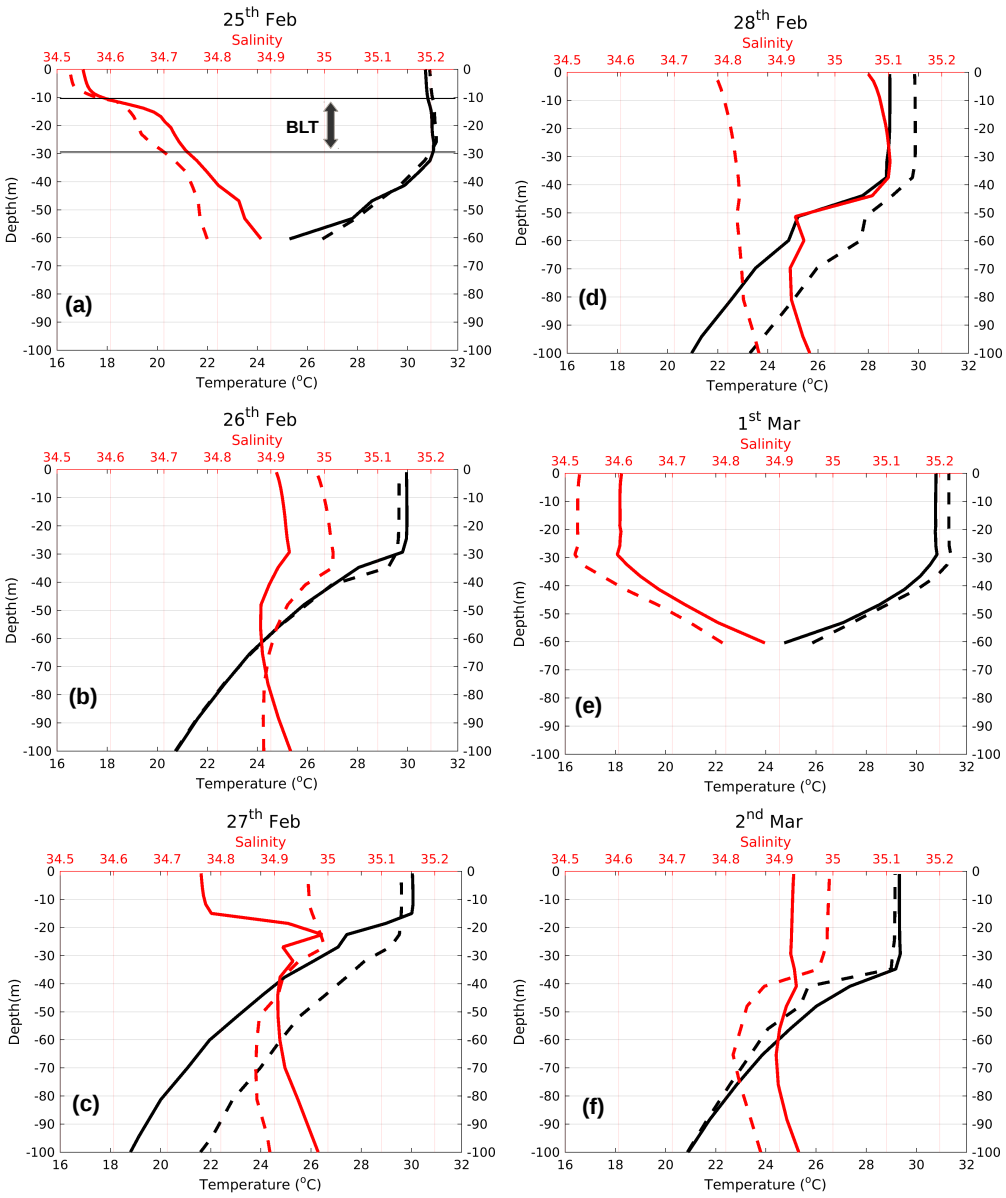

Fig. 5.10 Temp and Salinity profiles along the track of TC Japhet for - ***Tide*** (thick), ***NoTide*** (dotted) simulation

Chapter 6

Link between Upper Ocean Heat Content in the Tropical South Indian Ocean and Summer Precipitation over the southern African mainland

Abstract

Relationships between an index of southern African summer rainfall (SARI) and upper ocean temperature (using a new measure of mixing length temperature; Tdy) in the South Indian Ocean at zero (January-March) and one season (October-December) lag were analyzed. A region in the southern Mozambique Channel, termed as Tdy_{smc}, showed the strongest positive correlation with SARI at zero lag. Another strong but negative correlation with SARI at one season lag is found in the core of the Seychelles Chagos Thermocline Ridge region, termed as Tdy_{csctr}. Composite analysis (neutral with respect to ENSO) indicated that when Tdy_{smc} is enhanced over the South Mozambique Channel during JFM, positive rainfall anomalies prevail over large parts of subtropical southern Africa and the Congo Basin with reduced rainfall occuring over most of Madagascar and northern Mozambique. The rainfall differences are associated with enhanced easterly flow towards Madagascar transporting more moisture towards Mozambique and Tanzania, consistent with the increased rainfall. However, composite differences for Tdy_{csctr} OND seasons indicate increased precipitation particularly north of 10 ^{o}S, over Tanzania, Kenya and Congo Basin and reduced rainfall over most of subtropical Southern Africa. These negative rainfall anomalies over subtropical

southern Africa are associated with a weaker Angola Low as well as cyclonic anomalies along the south and east coasts of South Africa. The positive OND rainfall differences over tropical southern Africa can largely be matched up with relative ascent in these regions as well as westerly moisture fluxes over the Congo Basin and large areas of convergence.

During positive Tdy_{smc} JFM seasons, more tropical cyclones (TCs) were formed in the SWIO and more of them crossed the Mozambique Channel compared to negative Tdy_{smc} seasons. Furthermore, during positive Tdy_{smc} seasons, the landfalling TC was generated in the Mozambique Channel while during the negative Tdy_{smc} ones, it was formed in the central South Indian Ocean. Positive Tdy_{smc} seasons also have increased number of Category-5 TCs in the Mozambique Channel. Positive Tdy_{csctr} seasons indicate more TCs generated in the South West Indian Ocean and in the Mozambique Channel. Out of the 4 TCs that crossed the Channel during positive Tdy_{csctr} seasons, all 4 of them were formed in the channel itself, while out of the 3 TCs that crossed the channel during negative Tdy_{csctr} seasons, none were formed in the channel. These results suggest that changes in the mixing length temperature, Tdy_{smc} and Tdy_{csctr} indices which can be estimated from satellite data can be useful to monitor and potentially predict regional precipitation as well as the frequency and intensity of tropical cyclones that impact the southeastern coast of Africa.

6.1 Introduction

The rainy season over most of southern Africa extends from October to April, intensifying between December and March, when the atmospheric circulation favors transport of moist air from the western Indian Ocean to the southern African subcontinent. The two main sources are the northeast monsoonal flow over the western tropical Indian Ocean and easterly flow from the subtropical South Indian Ocean. During the summer months, as the South Atlantic and South Indian Ocean anticyclones migrate southwards, the influence of the mid-latitude circulation is reduced over the southern part of the subcontinent. On average, highest summer (November-April) precipitation occurs near the intertropical convergence zone (ITCZ; identified by large convective cloud structures) that lies across northern Madagascar and northern Mozambique, as well as over the convergence zone between the Angola Low and the southern Congo Basin (Figure 6.1a). Orographic enhancement of rainfall occurs over eastern Madagascar where the prevailing easterlies impact the mountains. In southeastern Africa, the highest summer mean precipitation occurs along the north and east coast of Madagascar (>1500 mm) and over northern Mozambique (>1000 mm) (Figure 6.1a).

The ITCZ moves southwards to approximately 17^{o}S over southeastern Africa (Taljaard and Phil, 1994) bringing tropical weather in the form of tropical cyclones, tropical lows and easterly waves which can make significant contributions to summer rainfall over southern Africa (e.g. (Dyson and Van Heerden, 2002; Reason and Keibel, 2004; Malherbe et al., 2012)). However, most of the rainfall over subtropical southern Africa results from cloud bands or tropical temperate throughs (Harrison 1984; Hart et al., 2010, 2013). Tropical cyclones (TCs) constitute one of the major natural disasters around the world. While it is well known that a cyclone's strong winds inflict damage directly upon human infrastructure,causing economic deficits and loss of human life (Sheets, 1990; Elsberry, 2002; Rappaport, 2000; Blake et al., 2007), heavy rainfall associated with TCs can also be a destructive factor. Approximately 119 million people are exposed to TC hazards every year (United Nation Development Program (UNDP), 2004). This is because half the world's population reside within 200 km of a coastline and the most cyclone-prone coastal regions are highly populated. Furthermore, an anticipated increase in coastal population within the next few years (Creel, 2003) would undoubtedly increase TC-related disasters (Pielke, 1990; Mendelsohn et al., 2012; Peduzzi et al., 2012).

Apart from negative infrastructural, societal and economical impacts, TCs bring a huge amount of rainfall and contribute largely to water resources. In 2007, the Intense TC Gamede established records for 72 h and 4 day rainfall accumulation of 3929 mm and 4869 mm respectively on the island of La Reunion in the South West Indian Ocean (Quetelard et al., 2009). On average, precipitation associated with TCs accounts for less than 10 % of the total precipitation over the global tropics and about 50 % of the total precipitation over a large part of ocean basins (Lin and Chan, 2015). Each year in the South West Indian Ocean, about 12-13 TCs are formed, accounting for about 14 % of the global total (Jury et al., 1993; Ho et al., 2006; Mavume et al., 2009). About 5% of the TCs make landfall over the southern African mainland (Vitart et al., 2003; Reason and Keibel, 2004) often leading to floods in the coastal lowlands (Crimp and Mason, 1999; Dyson and Van Heerden, 2002; Klinman and Reason, 2008; Malherbe et al., 2012). Regionally, the maximum mean rainfall due to TC occurs over the ocean in the Mozambique Channel (>40 mm) (Figure 6.1b), but on average, TC activity in the Mozambique Channel also provides substantial amounts to Mozambique, eastern Zimbabwe, south Malawi and northeastern South Africa. The contribution of TCs to the mean summer precipitation over the Mozambique Channel is 10-30% and 5-10 % over

the southeastern African mainland (mainly southern Mozambique, southeastern Zimbabwe and northeastern South Africa) (Figure 6.1c).

Although TCs contribute to about 5% of the summer rainfall occurring over southeastern Africa when averaged over 1998-2014, their relative contribution to local and widespread heavy rainfall events is highly significant in particular summers. About 50% of widespread heavy rainfall events over northeastern South Africa are caused by landfalling tropical systems (Matyas, 2015). During extreme years of TC activity, like 2000 and 2014, two TCs for both seasons made landfall over southeastern Africa contributing to 2 % and 3 % respectively to the summer southern African rainfall. When tropical systems make landfall in the eastern interior of southern Africa, their accumulated rainfall within a time span of a few days is often a very significant contribution to the annual total. Individual TC events can have massive impacts when they make landfall e.g. Hurricanes Irma (2017) in the US, TC Eline (2000) and TC Dineo (2017) in Mozambique and led to huge damage and loss of life (eg. over 1000 deaths in Mozambique in February 2000 mainly due to TC Eline). Due to the high vulnerability of populations in Mozambique, it is important to understand the contribution of TC to rainfall over the southern African mainland to mitigate risk.

SST over the South West Indian Ocean can also influence the regional atmospheric circulation (e.g. (Mason, 1995; Reason and Mulenga, 1999; Behera and Yamagata, 2001; Reason, 2001)) and hence can have an impact on the southern African summer rainfall and also the landfall frequency of tropical cyclones on Mozambique (Vitart et al., 2003). Besides SST, a link has recently been found between the tropical cyclone heat potential (a measure of upper ocean heat content) in the South West Indian Ocean and regional precipitation over southern Africa (Malan et al., 2013). Another measure of upper ocean heat content that is very important for TC-ocean interaction, has recently been proposed by Balaguru et al. (2015). This parameter known as Tdy, computes the vertically averaged temperature over a variable mixing length. This parameter takes into account both atmospheric and oceanic processes which are influenced by the storm state and gives a better representation of the ocean stratification important for the generation and intensification of TCs over the South West Indian Ocean (Mawren and Reason, 2017). Thus, it is now timely to assess whether there are any relationships between Tdy and summer rainfall over southern Africa and whether changes in Tdy influence the frequency and intensity of tropical cyclones in the

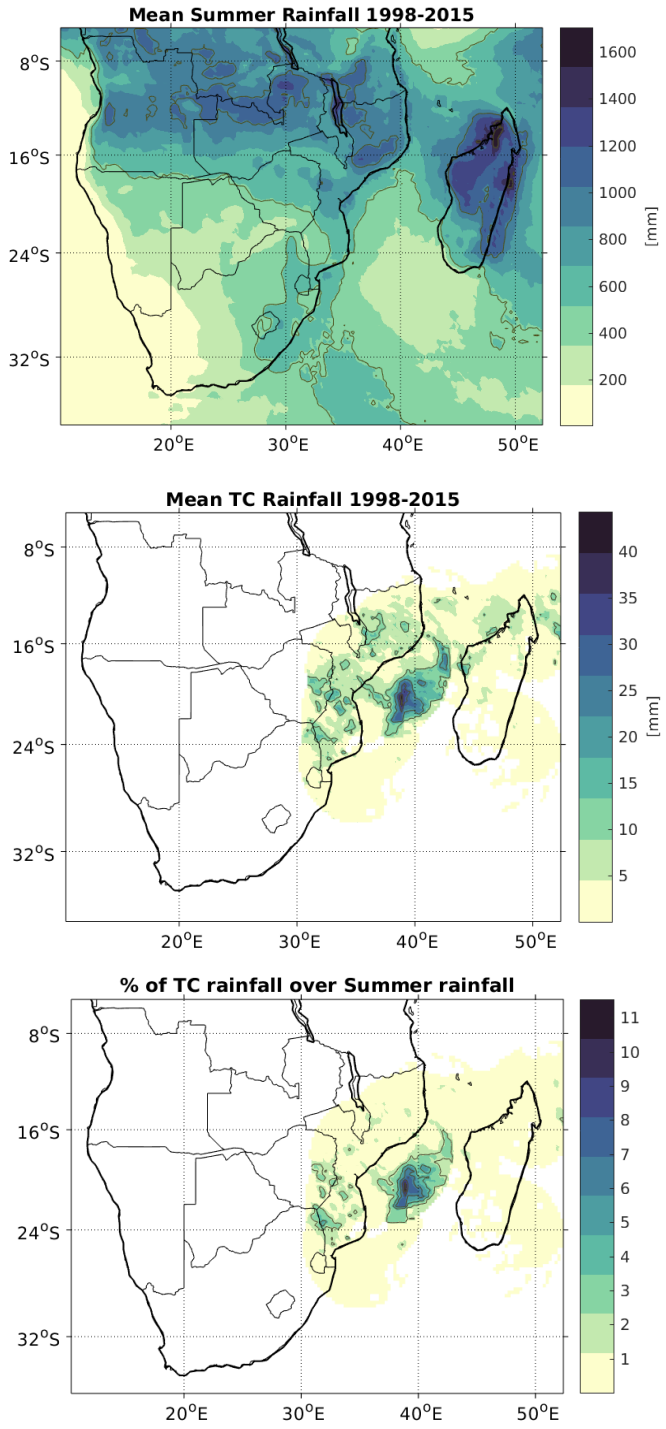

Fig. 6.1 (a) (a) Mean summer (Nov – Apr) rainfall, (b) mean TC rainfall and (c) TC contribution for Southeastern Africa for 1998-2014.

region.

6.2 Data and Methods

The precipitation dataset used in this study to characterize the rainfall originating from TCs over the Mozambique Channel is the daily TRMM multi-satellite precipitation analysis, at a spatial resolution of 0.25^o x 0.25^o. over the period 1998-2014. To examine the relationship between the upper ocean characteristics and rainfall over southern Africa, a longer time series (1980-2013) for precipitation is used (monthly GPCC Version 7, http://www.esrl.noaa.gov/psd/). TC track data and their generation sites are derived from the International Best Track Archive for Climate Stewardship (IBTrACS) data set (Knapp et al., 2010) for the period 1980-2014. Monthly zonal wind, geopotential height, moisture flux and omega from the National Center for Atmospheric Research (NCEP/NCAR) reanalysis (Kalnay et al., 1996) are used to study the variability of atmospheric circulation over the same period. Monthly mean temperature and salinity profiles obtained from the Simple Ocean Data Assimilation reanalysis (SODA) v3.3.1 product (Carton et al., 2000) at 1/2^o spatial resolution for the period 1980-2013 are used to compute the changes in upper ocean characteristics.

A novel approach used to analyze the ocean stratification in relation to TC activity involves the Tdy (Balaguru et al., 2015). Since the SST beneath the storm is difficult to measure, the SST ahead of the storm is normally used. However, the core SST can be much lower than the prestorm SST due to SST cooling induced by the storm. Several studies (Balaguru et al., 2015, 2016; Mawren and Reason, 2017) have found that the Tdy, computed through a varying mixed layer depth, gives a better estimate of the ocean state beneath the storm which is appropriate for TC generation and evolution.

Tdy is the vertically averaged temperature over the TC-induced mixing length (L) defined as follows, using the turbulent kinetic energy approach (Balaguru et al., 2016). It is based on a balance between the work done by the TC's wind forcing and the potential energy barrier created by ocean stratification as follows :

$$L = h + (\frac{2\rho_o u_*^3 t}{\kappa g \alpha})^{\frac{1}{3}} \tag{6.1}$$

where h is the initial mixed layer depth, u* is the friction velocity (obtained from the maximum wind speed of the TC), t represents the translation time of the TC, κ is the von Karman constant, g is the acceleration due to gravity and alpha is the rate of change of density beneath the mixed layer, which is a function of both oceanic and temperature (T) as well as salinity (S).

The vertically averaged temperature, Tdy over the mixing length L is then calculated as :

$$T_{dy} = \frac{1}{L}\int_0^L T(z)dz \tag{6.2}$$

where T(z) is the temperature as a function of depth z.

In this study, a partial correlation analysis was used to investigate potential relationships between Tdy and southern African summer rainfall by removing the impact of El Niño-Southern Oscillation (ENSO), the Subtropical Indian Ocean Dipole (SIOD) and Southern Annular Mode (SAM), since these modes can influence southern African rainfall (Lindesay, 1988; Reason et al., 2000; Behera and Yamagata, 2001; Reason, 2001, 2002; Reason and Rouault, 2005; Gillett et al., 2006). The formula for partial correlation is as follows:

$$r_{12(345)} = \frac{r_{12(34)} - (r_{15(34)} \cdot r_{25(34)})}{\sqrt{1 - r_{15(34)}^2} \cdot \sqrt{1 - r_{25(34)}^2}} \tag{6.3}$$

where,

- the coefficient $r_{12(345)}$ is used to characterize the correlations between two time series,1 and 2 representing Tdy and southern African summer rainfall with the influence of three other series 3,4,5 (ENSO,SIOD and SAM) removed.

- the coefficient $r_{12(34)}$ is used to characterize the correlation between Tdy and southern African summer rainfall with the influence of ENSO and SIOD removed.
- the coefficient $r_{15(34)}$ is used to characterize the correlation between Tdy and SAM with the influence of ENSO and SIOD removed.
- the coefficient $r_{25(34)}$ is used to characterize the correlation between southern African summer rainfall and SAM with the influence of ENSO and SIOD removed.

6.3 Summer Rainfall over southern Africa and Tdy anomalies in the tropical South Indian Ocean

Previous studies have shown evidence that SST anomalies in the South West Indian Ocean can influence southern African summer rainfall (Mason, 1995; Reason and Mulenga, 1999; Behera and Yamagata, 2001; Reason, 2000, 2002). Since Tdy is a measure of the upper ocean stratification, it seems possible that anomalies in Tdy may be linked with moisture flux anomalies and hence to regional precipitation. Furthermore, since Tdy can be approximated to some extent by sea surface height obtained from satellite, it offers another metric besides SST to investigate ocean influences on regional climate as well as potentially act as a predictor. To assess possible relationships, rainfall over the core southern African summer rainfall region (15 ^{o}S – 30 ^{o}S, 20 ^{o}E– 32 ^{o}E) was spatially averaged to form a precipitation index (SARI) for the period 1980-2014. This time series was then correlated with Tdy anomalies in the South Indian Ocean to identify regions having the strongest correlation coefficient values (Figure 6.2). To try and isolate the potential relationship between Tdy and atmospheric fields (due to climate modes), partial correlations were used to linearly remove the effects of ENSO, SIOD and SAM.

Figure 6.2a shows statistically significant (95 %) positive relationships between (January - March) SARI and (January - March) Tdy anomaly fields (at zero lag) over most of the western Indian Ocean, with stronger correlation values around 32 ^{o}E-44 ^{o}E, 18 ^{o}S-27 ^{o}S (defined as SMC - southern Mozambique Channel). Another large area of strong positive correlation exists in the central and southeastern South Indian Ocean. The normalized time series of Tdy anomalies extracted from box A (Figure 6.2a) is defined as the Tdy_{smc} index which extends over the period 1980 - 2013 (Figure 6.2c). The correlation between summer (January

- March) rainfall and one previous season (October - December) for Tdy anomalies in the South Indian Ocean was also analyzed. The results indicate a weaker positive correlation in the southern part of the Mozambique Channel but a stronger negative correlation around the core SCTR region (0^o - 9 ^{o}S; 62 ^{o}E - 80 ^{o}E), named as box B (Tdy_{csctr} index;Figure 6.2b). The Tdy_{smc} and Tdy_{csctr} indices are used below to investigate anomalous distributions of summer precipitation over the southern African mainland (Sections 6.6 and 6.7).

6.4 Interannual variability and trend of Tdy anomalies in the tropical South Indian Ocean

Over the 1980-2013 period, 12 neutral JFM seasons (excluding the influence of ENSO) were selected -(green bars in Figure 6.2c). However, on forming composites of anomalously positive and negative summers, a +/- 0.5 ^{o}C threshold (horizontal dotted line) was applied to the time series averaged over each box. Three positive Tdy_{smc} JFM seasons (1990,1997,2004) and three negative Tdy_{smc} JFM seasons (1981,1984,1993) were chosen for further analysis. Box B was also normalized over the period 1980 - 2012 as shown in Figure 6.2d. The period October to December (OND) over the SWIO region is typically a transition season before the main tropical cyclone season but is still significant rainfall over southern Africa. Figure 6.2d indicates that most of the positive values (negative values) coincide with El Niño (La Niña) years. Similar to box A, over these 32 years, 7 summers with a threshold of +/- 0.5 ^{o}C were selected for further analysis- 3 negative Tdy_{csctr} OND seasons (1984,1991,1993) and 4 positive Tdy_{csctr} OND seasons (1982,1994,1997,2002) - (green bars in Figure 6.2d).

A fitted linear regression through the data in Figure 6.2c indicates an increasing tendency of 0.02 ^{o}C/year, with prevailing negative (positive) Tdy_{smc} anomalies pre-1997/1998 (post-1997/1998). The result suggests that an important change occurred after the 1997-1998 El Niño, which is consistent with Manatsa et al., 2012 who provided evidence of a turning point in the climate of the Indian Ocean around this time. Tdy anomalies averaged over box B also indicate an increasing tendency of about 0.02 ^{o}C/year. The increasing tendency in both Tdy_{smc} and Tdy_{csctr} data also imply an increase in the occurrence of more positive Tdy_{smc} and Tdy_{csctr} seasons which may lead to a rise in the summer southern African rainfall

[15-30S; 20-32 E].

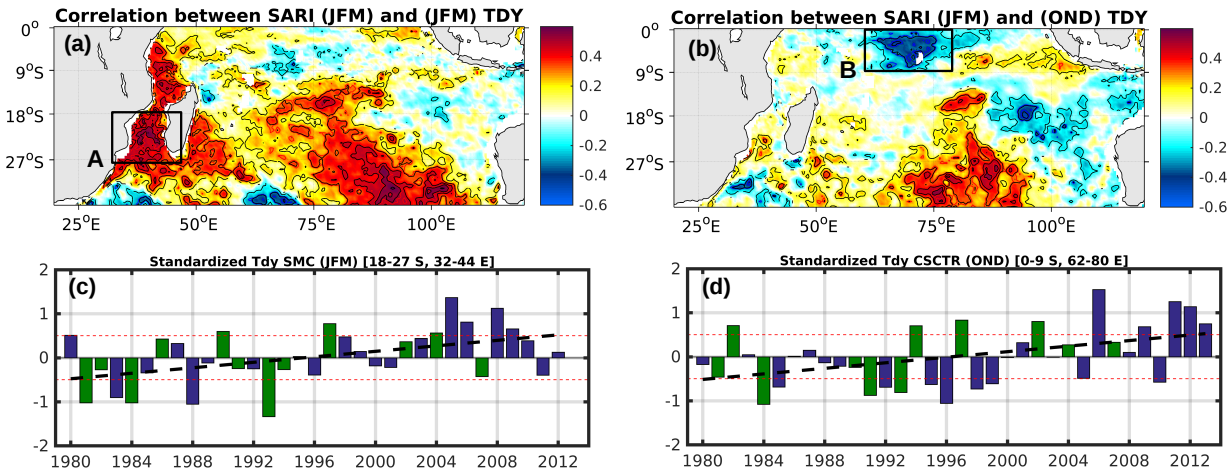

Fig. 6.2 (a) Correlation between summer (JFM) SA rainfall index (15 – 30 S, 20 – 32 E) and summer (JFM) Tdy anomalies in the South Indian Ocean. (b) Correlation between summer (JFM) SA rainfall index (15 – 30 S, 20 – 32 E) and one season lag (OND) Tdy anomalies in the South Indian Ocean. Regions with strongest negative and positive correlation coefficients were selected in box A (southern Mozambique Channel (SMC)) and box B (core SCTR (CSCTR)). Contours represent regions that are statistically significant at 95 %. (c) Time series of Tdy averaged over box A and (d) time series of Tdy averaged over box B. Dotted black lines indicate the fitted linear regression through the data. Dotted red lines indicate the +/- 0.5 ^{o}C. Green bars represent neutral (non-ENSO) years.

6.5 Anomalous oceanic and atmospheric features and possible mechanisms

Since SST influences surface evaporation and moisture transport, the SST-rainfall relationship was investigated through these fields. Partial correlations were used to linearly remove the effects of ENSO, SIOD and SAM and relationships between the SARI and the other fields (Tdy, SST, MLD, atmospheric circulation). The correlation between summer (January to March) SARI and (January to March) SST over the tropical South Indian Ocean is shown in Figure 6.3a. A similar pattern to that of Tdy in Figure 6.2a was observed but the statistically significant correlation coefficients were weaker in the Mozambique Channel and in the

southeastern Indian Ocean.

The relationship between summer SARI and (January-March) mixed layer depth at zero lag is shown in Figure 6.3c. From equation 6.2, since Tdy is inversely related to the mixing length and the initial MLD, any variations in the MLD would influence the upper ocean thermal structure. Therefore, a warmer Tdy will imply a shallower mixing length. This explains the negative correlation coefficient values with MLD observed in the southern Mozambique Channel and positive values across the CSCTR region (Figure 6.3c). However, only the negative values north and south of the Channel as well as east of Madagascar are statistically significant.

To explore the possible physical mechanisms linking Tdy in the South Indian Ocean with rainfall anomalies, moisture flux convergence anomalies computed from NCEP reanalyses were correlated with SARI at zero lag. Figure 6.3d shows a cyclonic anomaly over South Africa, a stronger Angola low and stronger easterly moisture flux anomalies towards eastern Madagascar carrying moisture from the tropical South Indian Ocean towards the northern half of the island. The intensification of the Angola Low is associated with enhanced local convection (Hermes and Reason, 2009) and increased westerly moisture transport from the southeast Atlantic (Rouault et al., 2003; Cook et al., 2004; Hermes and Reason, 2009) (Figure 6.3d). Over the northern Mozambique Channel, these easterly anomalies reflect a weaker NW monsoon towards NW Madagascar and hence less export of moisture away from northern Mozambique by the monsoonal westerlies, thus leading to more moisture convergence over most of central and eastern southern Africa and hence an increased SARI. Also, the enhanced easterlies east and north Madagascar may be more favourable to landfalling TCs.

These conditions are further reinforced by the anomalies in omega (pressure tendency) at 500hPa level (Figure 6.3b), indicating that there was relative uplift in the middle troposphere over southern South Africa and southern Mozambique and Zimbabwe implying favourable conditions for deep convection. The NW-SE orientation of the omega anomalies from the Angola Low region to the midlatitude South West Indian Ocean is very favourable for the development of the cloudbands that bring most of subtropical South Africa's summer rainfall (Harrison, 1984; Hart et al., 2010, 2013).

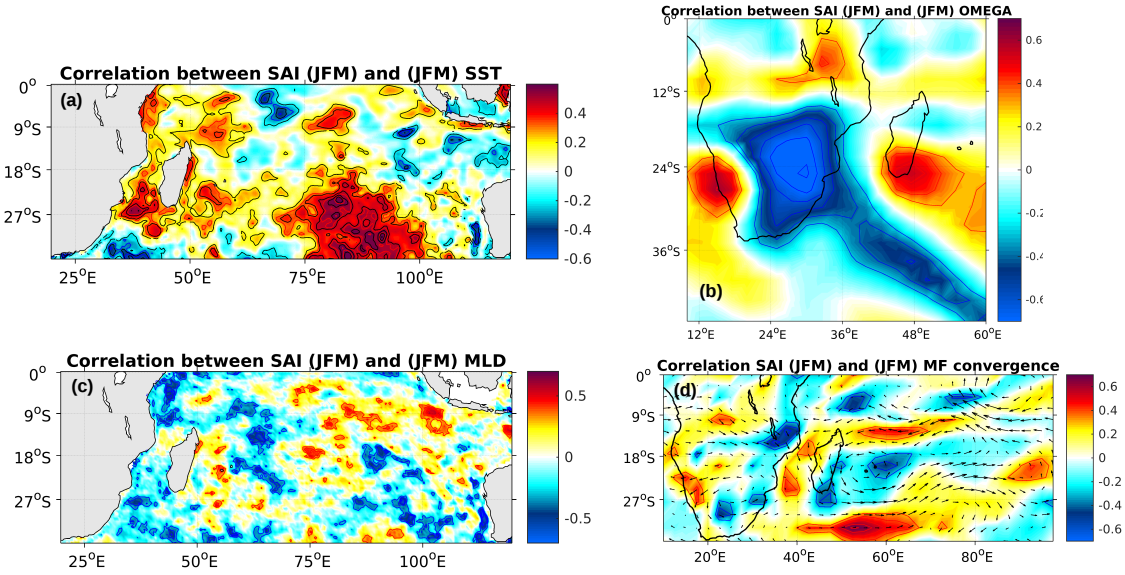

Fig. 6.3 Correlation between summer (JFM) SA rainfall index (15 – 30 S, 20 – 32 E) and summer (JFM) (a) SST, (b) Omega, (c) MLD and (d) Moisture Flux Convergence at 850 mb in the South Indian Ocean. Contours represent regions that are statistically significant at 95 %.

The correlation between summer SARI and SST in the South Indian Ocean at 1 season lag (October to December) is shown in Figure 6.4a. Significant positive coefficient values are observed along the eastern coast of Africa, in the Mozambique Channel and east of Madagascar as well as in the central South Indian Ocean. However, negative values were found over the CSCTR region but of weaker intensity compared to that of Tdy in Figure 6.2b.

The correlation map between summer SARI and mixed layer depth at 1 season lag (October to December) is plotted in Figure 6.4c. Statistically significant correlations exist over most of the central South Indian Ocean (negative) and in the core of the CSCTR (positive) where they reach 0.7.

The link between summer SARI and omega at 1 season lag (October to December) is shown in Figure 6.4b. Negative correlation values over South Africa indicate that there was relative uplift over the most of this country which imply favourable conditions for deep convection. There are also weaker uplift anomalies in the Angola Low region.

As expected, figure 6.4d shows a negative correlation in the moisture flux convergence present in the CSCTR region coinciding with negative SST and Tdy there. Easterly anomalies north of Madagascar imply increased moisture transport towards northern Mozambique/South Tanzania and relative moisture convergence over northern Tanzania/Kenya since they oppose the NE monsoon. There is also a small increase in westerly transport from the tropical SE Atlantic and a weak increase in convergence near the Angola Low. Then results suggest that when Tdy is increased (decreased) in the Mozambique Channel and east of Madagascar (central SCTR) during OND, the regional atmospheric circulation may be pre-conditioned to be favourable for increased rainfall in JFM. Figure 6.4a and Figure 6.1b suggest that some predictability of JFM rainfall over southern Africa may exist based on the previous season's Tdy and SST parts in the Mozambique Channel, SCTR and central South Indian Ocean.

6.6 Links between Tdy_{smc} index and summer rainfall over the southern African mainland

To assess rainfall relationships further, the time series extracted from box A in Figure 6.2b was analyzed. Composite rainfall differences between the anomalously positive (1990,1997,2004) and negative Tdy summers (JFM) (1981,1984,1993) that are neutral with respect to ENSO are presented in Figure 6.5a. These plots represent the total rainfall occuring throughout all these summers and not just the amounts directly associated with TCs. It is important to show the total rainfall since the circulation associated with a TC located away from southeastern Africa can still influence rainfall patterns over the landmass.

The results indicate positive rainfall anomalies prevailing over northern South Africa, Botswana, coastal Mozambique, Tanzania and Malawi. A large area of increased rainfall also occurs over most of the Congo basin and northern Angola. However, some negative

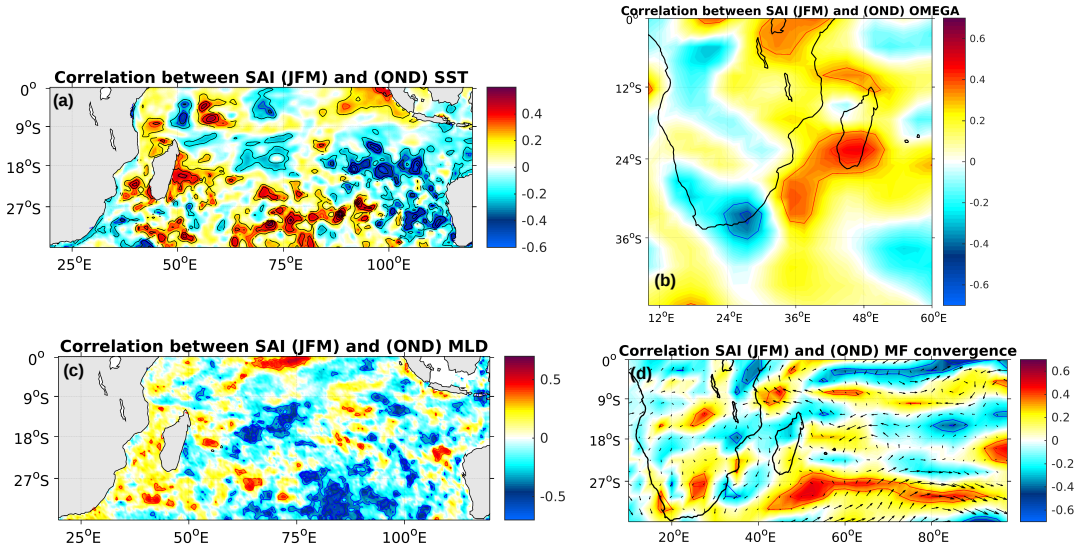

Fig. 6.4 Correlation between summer (JFM) SA rainfall index (15 – 30 S, 20 – 32 E) and 1 season lag (October to December) of (a) SST, (b) Omega, (c) MLD and (d) Moisture Flux Convergence at 850 mb in the South Indian Ocean. Contours represent regions that are statistically significant at 95 %.

values are observed over southern Zambia, southern Angola, Zimbabwe and most parts of Madagascar. This result implies that when Tdy is enhanced (reduced) over the southern Mozambique Channel, positive rainfall anomalies prevail over most of subtropical South Africa and the Congo basin with negative rainfall anomalies over Zimbabwe and some parts of Mozambique (Figure 6.5a).

To assess potential mechanisms, moisture flux convergence anomalies at 850 hPa, geopotential height at 850hPa, omega at 500hPa and latent heat flux are plotted in Figures 6.5b,c,d,e. The composite differences in circulation between JFM seasons with positive versus negative Tdy_{smc} index is analyzed in this section. Figures 6.5c indicates an anticyclonic anomaly east of Madagascar that acts to export more moisture from the tropical South Indian Ocean towards eastern Africa and which weakens the NW monsoon flow across the north Mozambique Channel that, in the climatological mean, transports moisture away from the mainland (Figure 6.5b). As a result, most of Madagascar shows negative rainfall differences. A strong cyclonic anomaly which exists southeast of South Africa favours the development of cold fronts which are the midlatitude input to the cloud bands that bring most of subtropical

southern African summer rainfall (Hart et al., 2010). Cloud band conditions are also favoured by weak cyclonic anomalies near the Angola Low and relative moisture flux convergence over Botswana and parts of Namibia and South Africa.

These conditions are further reinforced by the anomalies in omega (pressure tendency) at 500hPa level (Figure 6.5d), indicating that there was relative uplift in the middle troposphere over southern and central Mozambique, Botswana and most of South Africa implying favourable conditions for deep convection and cloud band development. However, positive omega anomalies correspond to dry conditions over northwestern Mozambique and Madagascar (Figure 6.5c).

Figure 6.5e shows the composite differences in latent heat flux. During positive Tdy_{smc} events, increased latent heat flux occurs over parts of the central and southern Mozambique Channel and ocean areas to the south as well as over the western tropical Indian Ocean along the path of the NE monsoon. This enhanced moisture is then advected over subtropical southern Africa leading to increased rainfall.

Relative uplift (Figure 6.5b) also exists over most of the Congo Basin, which together with some areas of convergence are consistent with the increased rainfall there (Figure 6.5a). Increased rainfall over Kenya and northern Tanzania is associated with relative uplift and easterly moisture flux from the tropical western Indian Ocean. These results suggest that changes in the Tdy over the southern Mozambique Channel may be related to rainfall (at zero lag) over large areas of southern Africa. Thus, the Tdy_{smc} index may be useful for monitoring and climate diagnostic purposes, particularly during neutral ENSO summers.

6.7 Links between Tdy_{csctr} index and summer rainfall over the southern African mainland

Similar to the previous section, the time series extracted from box B in Figure 6.2d was analyzed. Composite OND rainfall differences between the positive (1982, 1994, 1997, 2002)

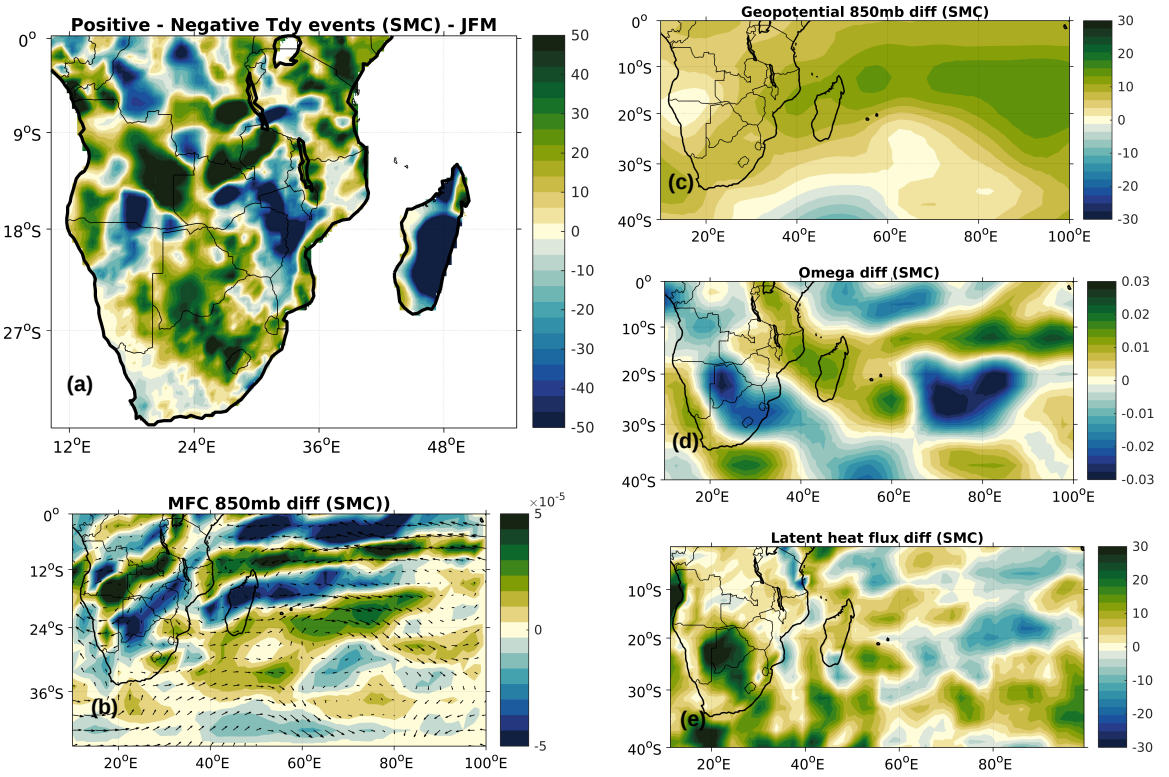

Fig. 6.5 Composite difference between positive (1990, 1997,2004) and negative (1981, 1984, 1993) summer Tdy MC index years that are neutral to ENSO for (a) rainfall, (b) moisture flux convergence at 850 mb, (c) geopotential height at 850 mb, (d) Omega at 500 mb and (e) latent heat flux.

and negative Tdy_{csctr} index (1984,1991, 1993) OND seasons are presented in Figure 6.6a. Note that unlike the previous section, the October to December season was used since Figure 6.2b indicated the strongest connection with CSCTR in this season.

Figure 6.6 shows composite differences of rainfall, 850 hPa moisture flux convergence, 850 hPa geopotential height, 500 hPa omega and latent heat flux for the CSCTR summers for OND. Composite rainfall differences indicate an increased precipitation particularly north of 10 ^{o}S, over Tanzania, Kenya and Congo Basin. Increased rainfall was also noted over Botswana, northern and southern Mozambique and parts of Madagascar. However, most of subtropical southern Africa shows negative rainfall differences. These negative differences are associated with a weaker Angola Low, unfavourable for cloud band development, as well as cyclonic anomalies along the east coast of South Africa which lead to cool,drier

South Atlantic air over South Africa unfavourable for rainfall (Mulenga et al., 2003) over most of the rest of southern Africa (Figure 6.6c). The positive rainfall differences over tropical southern Africa can largely be matched up with relative ascent in these regions (Figure 6.6d) as well as westerly moisture fluxes over the Congo Basin and large areas of convergence (Figure 6.6b). Previous work by Kijazi and Reason (2009) showed that floods over northern Tanzania were associated with similar westerly moisture flux anomalies over the Congo Basin. The region of strong uplift extends across the northern Mozambique Channel to northwestern Madagascar together with low level moisture convergence, helping to account for the large positive rainfall differences there. There is also relative ascent over northern Mozambique as well as low level moisture flux convergence in the northern channel consistent with the increased rainfall over parts of Mozambique and Madagascar (Figure 6.6a,b,d).

During positive TDY CSCTR events, positive latent heat flux differences are prevalent in the Mozambique Channel favourable to increase moisture availability over northern Mozambique, northern Madagascar and Tanzania (Figure 6.6e). Also, as expected stronger latent heat fluxes are found over the SCTR region coinciding with stronger Tdy and SST there. The results therefore suggest that OND rainfall over most of tropical (subtropical) South Africa may be related to positive (negative) anomalies in Tdy in the CSCTR region.

6.8 Relationship with Tropical cyclone activity

Since Tdy is a measure of the upper ocean stratification and has been associated with intensification of tropical cyclones (Mawren and Reason, 2017), it is of interest to look at tropical cyclone activity (genesis and landfalls) during summers of anomalous Tdy_{smc} index and Tdy_{csctr} index. Table 6.1 illustrates the differences in TC frequency between positive and negative JFM episodes of Tdy_{smc} index. The results show that a higher number of TCs were formed in the South West Indian Ocean (about 24 TCs over the period 1980-2013) during positive Tdy_{smc} summers compared to negative Tdy_{smc} summers with only 16 TCs. Also, more TCs crossed the Mozambique Channel during positive summers. Both positive and negative summers showed one landfalling TC; however, during positive summers, one was generated in the Mozambique Channel while during negative summers, that TC was formed in the central SW Indian Ocean. A higher number of Cat 5 TCs were formed in the SW Indian Ocean and a higher portion crossed the channel during positive summers compared to negative ones. The TCs during negative Tdy_{smc} summers tend to be formed further east in the SW Indian Ocean, follow straight southwestward trajectories and recurve

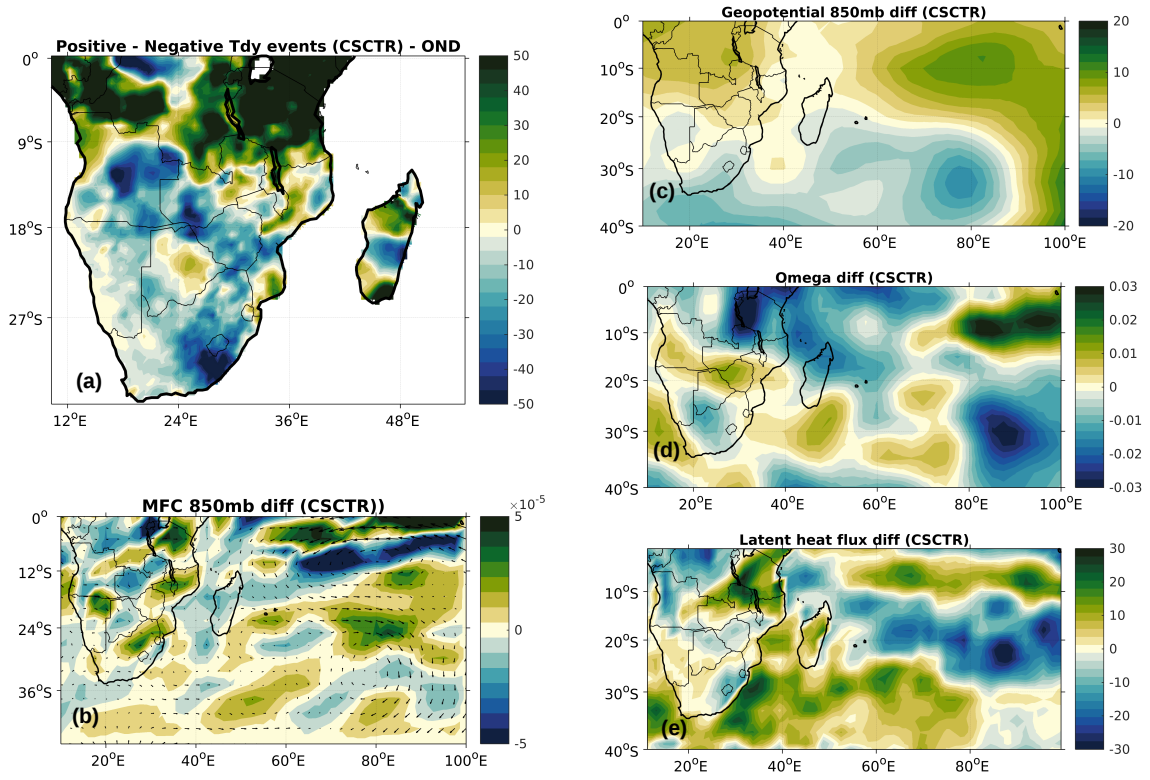

Fig. 6.6 Composite difference between positive (1982, 1994,1997,2002) and negative (1984, 1991, 1993) Tdy_{csctr} index years (October to December) that are neutral to ENSO for (a) OND rainfall, (b) (OND) moisture flux convergence at 850 mb (c) (OND) geopotential height at 850 mb, (d) (OND) Omega at 500 mb and (e) latent heat flux

just east of Madagascar, while during positive SMC summers, more TCs are formed east of 80 E and had more curved trajectories. Thus, positive Tdy in the southern Mozambique Channel are associated with more TCs crossing the Mozambique channel and these storms may be enhanced by the larger amount of latent heat flux over most of the Channel and east od Madagascar during these summers (Figure 6.5e).

Similar to Table 6.1, Table 6.2 illustrates the differences in TC frequency between positive and negative episodes of Tdy anomalies but over the CSCTR region. The results show that a higher number of TCs are formed in the South West Indian Ocean (about 24 TCs over the period 1980-2013) during positive Tdy_{csctr} episode compared to negative episode with only 16 TCs consistent with the influence that Tdy in this region has on SWIO TC numbers (Mawren and Reason, 2017). Out of the 4 TCs that crossed the Mozambique

Table 6.1 Number of TCs during Positive and Negative Tdy_{smc} JFM summers

Positive episode				**Negative episode**		
Landfalling TCs	MC TCs	SWIO TCs		Landfalling TCs	MC TCs	SWIO TCs
1	8	24	All TCs	1	6	18
1	4	13	Cat 1-2	1	4	9
0	1	6	Cat 3-4	0	1	6
0	3	5	Cat 5	0	1	3

Channel during positive Tdy_{csctr}, all 4 of them were formed in the Channel itself compared to zero TCs generated in the channel during negative CSCTR. This is because TCs during negative Tdy_{csctr} summers tend to be generated further east in the SW Indian Ocean.

The cyclonic anomalies east of Madagascar (Figure 6.6) and the positive latent heat flux differences in the central and southern Mozambique Channel may have accounted for the increase in TC numbers over the SWIO and Mozambique Channel during positive Tdy_{csctr}.

Table 6.2 Number of TCs during Positive and Negative Tdy_{csctr} OND

Positive episode				**Negative episode**		
Landfalling TCs	MC TCs	SWIO TCs		Landfalling TCs	MC TCs	SWIO TCs
1	4	24	All TCs	1	3	16
0	3	13	Cat 1-2	0	0	5
0	0	6	Cat 3-4	0	1	6
1	1	5	Cat 5	1	2	5

6.9 Conclusion and Discussion

Previous work has shown that there are relationships between SST anomalies in the South West Indian Ocean and summer rainfall over southern Africa (e.g., **?**Mason (1995); **?**); Reason and Mulenga (1999); Washington and Preston (2006). The mechanisms involve changes in moisture fluxes from this basin towards southern Africa. Such changes in moisture fluxes may occur through anomalies in heat exchange with the upper ocean and hence it is of interest to consider relationships between rainfall and upper ocean heat content. A measure of upper ocean heat content, important for tropical cyclones which frequently occur in summer in the South West Indian Ocean and which often impact on Madagascar and less

frequently mainland southeastern Africa, is the tropical cyclone heat potential and Malan et al. (2013) found some evidence of relationships between this heat potential and rainfall over parts of southern Africa. Following on from Malan et al. (2013), this study has chosen to investigate another parameter related to upper ocean heat content which has been shown to be very useful for tropical cyclones; namely, the upper ocean mixing length temperature, Tdy. Since Tdy can be monitored through satellites through its connection with sea surface height, it may then offer another parameter to assess for seasonal forecasting purposes. Although sea surface height offers the advantage of being directly monitored rather than being derived; it was found (not shown) that the correlations between Tdy and summer rainfall presented in this study were stronger than those between sea surface height and rainfall.

Correlation maps between spatially averaged southern African summer rainfall (using the SARI defined index) and Tdy anomalies in the South Indian Ocean at zero and one season lag were analyzed. Partial correlations were used to linearly remove the effects of ENSO, SAM and the subtropical South Indian Ocean Dipole. A region in the southern Mozambique Channel, Tdy_{smc}, showed the strongest positive link with SARI at zero lag. Another strong but negative correlation with SARI at one season lag was in the core of the SCTR region, termed Tdy_{csctr}. Using these times series, the difference between positive and negative neutral summers were assessed further. Composites of summer rainfall and other environmental parameters were investigated for both the southern Mozambique Channel and the SCTR regions. The results indicated that when Tdy_{smc} is enhanced over the southern Mozambique Channel, positive rainfall anomalies prevail over large parts of subtropical southern Africa and the Congo Basin with reduced rainfall occur over most of Madagascar and northern Mozambique.

Composite JFM differences in circulation during anomalous Tdy_{smc} seasons are associated with enhanced easterly flow towards northern Madagascar transporting more moisture towards Mozambique and Tanzania, a stronger Angola Low and relative uplift over most of South Africa, consistent with the increased rainfall. Positive latent heat flux anomalies over most parts of the western South Indian Ocean imply more favourable conditions for the existence of tropical storms over the central and southern Mozambique Channel.

For the OND composite rainfall differences during anomalous Tdy_{csctr} seasons increased precipitation occurs particularly north of 10 ^{o}S, over Tanzania, Kenya and Congo Basin with reduced rainfall over most of subtropical Southern Africa. These negative rainfall anomalies over subtropical southern Africa are associated with a weaker Angola Low as well as cyclonic anomalies along the south and east coasts of South Africa. The positive rainfall differences over tropical southern Africa can largely be matched up with relative ascent in these regions as well as westerly moisture fluxes over the Congo Basin and large areas of low level moisture flux convergence. The region of strong uplift extends across the northern Mozambique Channel to northwestern Madagascar together with low level moisture convergence, helping to account for the large positive rainfall differences there. There is also relative ascent over northern Mozambique consistent with the increased rainfall in that region.

During positive Tdy_{smc} summers, more TCs were formed in the SWIO and more of them crossed the Mozambique Channel compared to negative Tdy_{smc} summers. Both seasons have one landfalling TC but their TC genesis positions differ. During the positive Tdy_{smc} summers, the landfalling TC was generated in the Mozambique Channel while during the negative Tdy_{smc} summers, it was formed in the central South Indian Ocean. Stronger easterlies and large latent heat flux anomalies around Madagascar carried moisture from the tropical Indian Ocean towards the Mozambique Channel, favouring the existence of tropical cyclones in the area. Positive Tdy_{smc} summers also have increased number of Category-5 TCs in the Mozambique Channel. During positive Tdy_{csctr} seasons, more TCs were generated in the South West Indian Ocean and in the Mozambique Channel. Out of the 4 TCs that crossed the Channel during positive seasons, all 4 of them were formed in the channel itself, while out of the 3 TCs that crossed the channel during negative Tdy_{csctr} seasons, none were formed in the channel. These results suggest that changes in the Tdy_{smc} and Tdy_{csctr} indices can be useful to monitor and potentially predict regional precipitation as well as the frequency and intensity of tropical cyclones that impact the southeastern coast of Africa.

Chapter 7

Discussion and Conclusion

This study was designed to address the following key questions, as presented in Chapter 2 :

- Is the frequency and intensity of tropical cyclones increasing in the South West Indian Ocean? (**Chapter 4**)

- Is there any link between upper ocean characteristics and large-scale climate modes? (**Chapter 4**)

- What are the mechanisms of barrier layer thickness formation in the South West Indian Ocean? (**Chapter 4**)

- What are the upper ocean conditions necessary for tropical cyclone genesis and intensification? (**Chapter 4**)

- Are there any trend in the upper ocean characteristics in the South West Indian Ocean over the period 1980-2010? (**Chapter 4**)

- On the weather scale, how does the upper ocean characteristics influence the evolution of a tropical cyclone? (**Chapter 4**)

- How does tidal forcing influence the upper ocean characteristics? (**Chapter 5**)

- What impact does the tidal forcing has on the upper ocean characteristics on a seasonal and daily time scale? (**Chapter 5**)

- How does the upper ocean structure change when a cyclone encounters an eddy and how including tidal forcing can be important for TC evolution and intensification? (**Chapter 5**)

- Does the upper ocean heat content (Tdy) in the South Indian Ocean influence summer rainfall over southern Africa? (**Chapter 6**)

- Are there any links between atmospheric circulations and southern African rainfall?(**Chapter 6**)

- How does anomalous Tdy in the Mozambique Channel or over the SCTR region influence the formation, tracks and intensification of tropical cyclones in the SWIO? (**Chapter 6**)

The first result Chapter was focused on the Seychelles-Chagos Thermocline Ridge (an area of particular interest for cyclogenesis in the South Indian Ocean; (Vialard et al., 2009)), this study used monthly temperature and salinity profiles from SODA reanalysis dataset (40 vertical levels, 0.5^ox0.5^o horizontal resolution) due to its larger spatial and temporal coverage to evaluate Tdy (Balaguru et al., 2015) and BLT variability over the past three decades (1980-2010) and relate that to TC characteristics. Tdy is a novel approach used to analyze the ocean stratification in relation to TC activity. Since the SST beneath the storm is difficult to measure, the SST ahead of the storm is normally used. However, the core SST can be much lower than the prestorm SST due to SST cooling induced by the storm and several studies have found that the Tdy, computed through a varying mixed layer depth gives a better estimate of the ocean state beneath the storm which is appropriate for TC generation and evolution. Empirical orthogonal function analysis of Tdy reveals the important role of the variability across the SCTR in the South West Indian Ocean. Time series of the seasonally-averaged (November to April) BLT and Tdy estimated from oceanic reanalysis data across the SCTR showed largest values around 1997-1998, 2003-2004, 2006-2007,

which coincide with El Niño years.

Downwelling Rossby waves propagate westwards across the basin and the associated warming in the upper ocean can enhance precipitation (Xie et al., 2002). Their speed of propagation determined in this study through lagged correlation is consistent with the phase speed of the first baroclinic mode Rossby wave. The Hovmoller plots of Tdy and BLT confirm the significance of Rossby wave propagation for upper ocean characteristics in the South West Indian Ocean that are important for tropical cyclone behaviour. BLT is sensitive to freshwater inputs by both precipitation and the advection of low salinity waters by the South Equatorial Current. During positive IOD or/and positive El Niño, the westward advection of negative SSS anomalies give rise to a thicker barrier layer due to increased salinity stratification. As mentioned in Vinayachandran and Nanjundiah (2009) and Grunseich et al. (2011), SSS anomalies take less than 2 months to travel across the Indian Ocean during El Niño events. The BLT responds quickly to precipitation and is also sensitive to atmospheric circulation anomalous associated with ENSO.In order to understand the role of the upper-ocean, and more specifically the salinity effect on TCs, the Tdy parameter was analysed by subsampling regions of Tdy and stratifying them as regions of weak or strong BLT. All TCs generated in the South West Indian Ocean were analysed from 1980 to 2010 and based on their genesis location, their individual Tdy and BLT in time and space were investigated. This approach provides a better understanding of the oceanic state under which TCs are generated. The result indicates that the majority of TCs (77 %) were generated under positive Tdy anomalies while 68 % were formed under shallow BLT. Thus, the temperature of the upper-ocean appears to be most important for the generation of TCs while BLT may play a role in their intensification.

The analysis performed in chapter 4 suggests that an important change occured after the 1997/1998 El Niño, consistent with Manatsa et al. (2012) who provided evidence that a turning point in the climate of the Indian Ocean occurred around this time. An epochal variability of Tdy trends pre- and post- 1997/1998 shows large areas of decreasing trend near Madagascar pre-1997 and an increasing trend in the Mozambique channel and in the central tropical South Indian Ocean after 1998, consistent with Goni et al. (2010) and Rajeevan et al. (2013). A 10 year running mean through the data across the SCTR region shows that VITC frequency, SST and Tdy have increased throughout the 1980-2010 period as has the Power Dissipation Index. However, the BLT only increased until 1997 after which it started to decline. Areas of increased Tdy, along with the warming in SST over most of the basin

particularly around central SCTR region, are favourable for the occurrences of strong TCs, several of which have caused severe devastation and loss of life in the region (Reason and Keibel, 2004; Klinman and Reason, 2008). A case study of TC Bansi and its relation to upper ocean heat content was presented. This tropical cyclone is of interest due to its unusual track and also because of all the damage it caused. Anomalously deep thermocline and high Tdy values were observed around December 2014-January 2015 in the South West Indian Ocean and analysis of the upper ocean structure during Bansi showed that its rapid intensification to Category 4 was related to its passage over a high Tdy (warm core) eddy region and a deep barrier layer. The presence of a pronounced westward propagation of subsurface warming around November 2014 to February 2015 also may have contributed to its strengthening. This case study of Bansi further confirms that tropical cyclone characteristics (both track and intensity) are strongly sensitive to upper ocean conditions.

The second result Chapter developed a three-dimensional regional ocean model of the Mozambique Channel forced with tides used to assess the effect of tides on upper ocean characteristics important for storms in this highly prevalent tropical cyclone region. To the best of our knowledge, tidal effects on TC ocean characteristics have not been previously studied. Given that Mozambique and Madagascar have suffered severe loss of life and substantial damage from TCs in the Mozambique Channel in the last few decades, better analysis of upper ocean characteristics is of importance. On the seasonal scales, Figure 5.4 showed that turbulent mixing driven by tides leads to cooler surface waters, however such mixing can also cause significant warming in the subsurface layers. Deeper mixed layer depth (MLD) can occur in some specific regions where there are turbulent eddies and strong ocean currents (for instance the NEMC, EACC and SEMC in the Mozambique Channel). On a seasonal time scale, warming noted between the two runs along the NEMC and SEMC is heightened during winter due to the influence of southeast trade winds, while during summer, eddy activity south of 16-17 ^{o}S seemed to be more prominent in the tidal simulation. Bathymetry was found to play a role in Tdy with large differences observed in shallow regions, along the coast and in the Comoros Basin. In the northern and central part of the Channel, including tidal forcing may result in a cooler surface but warmer subsurface waters.

Introducing tides in a regional ocean model leads to changes in the upper ocean structure on a seasonal time scale but it can create a larger impact on a daily basis, particularly for

passing tropical cyclones in regions where tidal influences are significant. For example, strong tidal mixing generates cooler water along the coast and when TCs are formed in these areas (e.g. of TC Japhet in this study), they may lose their intensity unless they are influenced by low salinity waters (due to the presence of fresh water or rainfall), creating a barrier layer. As Japhet encountered a warm anticyclonic eddy near the coast of Mozambique, the actual values of the underlying upper ocean structures may be quite different between the ***Tide*** and ***NoTide*** runs; with a decrease in SST of 0.3 ^{o}C, a deepening of the MLD by 7 m, a higher SSH of 0.2 m and a cooler Tdy of 0.3 ^{o}C and an EKE value of 500 cm^{2}s^2 on that day compared to AVISO. The results also show that the tidal simulation gives a better representation of the position of the eddy as it coincides with the day TC Japhet attained its maximum intensity.The results presented here suggest that ocean models in regions like the Mozambique Channel (and possibly the Caribbean; NW shelf of Australia) need to include tidal effects to better simulate and understand the role of upper ocean in TC genesis and intensification. Tidal effects may therefore be important for forecasting TC intensification and for improving predictions of rainfall over TC affected regions like southeastern Africa.

Since Tdy is a measure of upper ocean heat content and can be monitored from satellite through its connection with sea surface height, it is opportune to investigate its possible relationships with the southern African rainfall, which is discussed in the third result Chapter. Correlation maps between spatially averaged southern African summer rainfall (using the SARI defined index) and Tdy anomalies in the South Indian Ocean at zero and one season lag were analyzed. Partial correlations were used to linearly remove the effects of ENSO, SAM and the subtropical South Indian Ocean Dipole. A region in the southern Mozambique Channel, Tdy_{smc}, showed the strongest positive link with SARI at zero lag. Another strong but negative correlation with SARI at one season lag was in the core of the SCTR region, termed Tdy_{csctr}. Using these times series, the difference between positive and negative neutral summers were assessed further. Composites of summer rainfall and other environmental parameters were investigated for both the southern Mozambique Channel and the SCTR regions. The results indicated that when Tdy_{smc} is enhanced over the southern Mozambique Channel, positive rainfall anomalies prevail over large parts of subtropical southern Africa and the Congo Basin with reduced rainfall occur over most of Madagascar and northern Mozambique.

Composite JFM differences in circulation during anomalous Tdy_{smc} seasons are associated with enhanced easterly flow towards northern Madagascar transporting more moisture towards Mozambique and Tanzania, a stronger Angola Low and relative uplift over most of South Africa, consistent with the increased rainfall. Positive latent heat flux anomalies over most parts of the western South Indian Ocean imply more favourable conditions for the existence of tropical storms over the central and southern Mozambique Channel. For the OND composite rainfall differences during anomalous Tdy_{csctr} seasons increased precipitation occurs particularly north of 10 ^{o}S, over Tanzania, Kenya and Congo Basin with reduced rainfall over most of subtropical Southern Africa. These negative rainfall anomalies over subtropical southern Africa are associated with a weaker Angola Low as well as cyclonic anomalies along the south and east coasts of South Africa. The positive rainfall differences over tropical southern Africa can largely be matched up with relative ascent in these regions as well as westerly moisture fluxes over the Congo Basin and large areas of low level moisture flux convergence. The region of strong uplift extends across the northern Mozambique Channel to northwestern Madagascar together with low level moisture convergence, helping to account for the large positive rainfall differences there. There is also relative ascent over northern Mozambique consistent with the increased rainfall in that region.

During positive Tdy_{smc} summers, more TCs were formed in the SWIO and more of them crossed the Mozambique Channel compared to negative Tdy_{smc} summers. Both seasons have one landfalling TC but their TC genesis positions differ. During the positive Tdy_{smc} summers, the landfalling TC was generated in the Mozambique Channel while during the negative Tdy_{smc} summers, it was formed in the central South Indian Ocean. Stronger easterlies and large latent heat flux anomalies around Madagascar carried moisture from the tropical Indian Ocean towards the Mozambique Channel, favouring the existence of tropical cyclones in the area. Positive Tdy_{smc} summers also have increased number of Category-5 TCs in the Mozambique Channel. During positive Tdy_{csctr} seasons, more TCs were generated in the South West Indian Ocean and in the Mozambique Channel. Out of the 4 TCs that crossed the Channel during positive seasons, all 4 of them were formed in the channel itself, while out of the 3 TCs that crossed the channel during negative Tdy_{csctr} seasons, none were formed in the channel. These results suggest that changes in the Tdy_{smc} and Tdy_{csctr} indices can be useful to monitor and potentially predict regional precipitation as well as the frequency and intensity of tropical cyclones that impact the southeastern coast of Africa.

7.1 Suggestions for future work

- It would be useful to implement a coupled regional model (e.g. ROMS-WRF) or any other coupled atmosphere-ocean-wave model to look at the air-sea interaction during the evolution of a tropical cyclone in more details. Use of tidal hydrodynamic and wave models to simulate the impacts of cyclones on coastal communities.

- The next step would be to use better parameterization of tidal mixing and increase ROMS resolution.

- Rainfall results in Chapter 6 can be tested with CMIP5 models.

- Another interesting work would be to investigate the variability of fresh water flux in the South West Indian Ocean with a focus on the intensity of tropical cyclones. Create tools to improve ROMS river forcing files to reduce any salinity biases.

References

Ali, M., Jagadish, P., and Jain, S. (2007). Effect of eddies on Bay of Bengal cyclone intensity. *Eos Trans. AGU*, 88(8).

Ali, M. M., Swain, D., Kashyap, T., McCreary, J., and Nagamani, P. (2013). Relationship between cyclone intensities and sea surface temperature in the Tropical Indian Ocean. *Geoscience and Remote Sensing Letters, IEEE*, 10(4):841–844.

Allan, R., Reason, C., Lindesay, J., and Ansell, T. (2003). Protracted'enso episodes and their impacts in the indian ocean region. *Deep Sea Research Part II: Topical Studies in Oceanography*, 50(12):2331–2347.

Allan, R. J., Lindesay, J. A., and Reason, C. J. (1995). Multidecadal variability in the climate system over the indian ocean region during the austral summer. *Journal of Climate*, 8(7):1853–1873.

Annamalai, H. and Murtugudde, R. (2004). Role of the indian ocean in regional climate variability. *Earth's Climate*, pages 213–246.

Arakawa, A. and Lamb, V. R. (1977). Computational design of the basic dynamical processes of the ucla general circulation model. *Methods in computational physics*, 17:173–265.

Ash, K. D. and Matyas, C. J. (2012). The influences of enso and the subtropical indian ocean dipole on tropical cyclone trajectories in the southwestern indian ocean. *International Journal of Climatology*, 32(1):41–56.

Backeberg, B. and Reason, C. (2010). A connection between the south equatorial current north of madagascar and mozambique channel eddies. *Geophysical Research Letters*, 37(4).

Baines, P. G. (1982). On internal tide generation models. *Deep Sea Research Part A. Oceanographic Research Papers*, 29(3):307–338.

Balaguru, K., Chang, P., Saravanan, R., Leung, L. R., Xu, Z., Li, M., and Hsieh, J.-S. (2012). Ocean barrier layers' effect on tropical cyclone intensification. *Proceedings of the National Academy of Sciences*, 109(36):14343–14347.

Balaguru, K., Foltz, G. R., Leung, L. R., Asaro, E. D., Emanuel, K. A., Liu, H., and Zedler, S. E. (2015). Dynamic potential intensity: An improved representation of the ocean's impact on tropical cyclones. *Geophysical Research Letters*, 42(16):6739–6746.

Balaguru, K., Foltz, G. R., Leung, L. R., and Emanuel, K. A. (2016). Global warming-induced upper-ocean freshening and the intensification of super typhoons. *Nature communications*, 7:13670.

Balaguru, K., Taraphdar, S., Leung, L. R., Foltz, G. R., and Knaff, J. A. (2014). Cyclone-cyclone interactions through the ocean pathway. *Geophysical Research Letters*, 41(19):6855–6862.

Beal, L. M., Chereskin, T. K., Lenn, Y. D., and Elipot, S. (2006). The sources and mixing characteristics of the agulhas current. *Journal of physical oceanography*, 36(11):2060–2074.

Beal, L. M., De Ruijter, W. P., Biastoch, A., Zahn, R., Cronin, M., Hermes, J., Lutjeharms, J., Quartly, G., Tozuka, T., Baker-Yeboah, S., et al. (2011). On the role of the agulhas system in ocean circulation and climate. *Nature*, 472(7344):429.

Beal, L. M., Ffield, A., and Gordon, A. L. (2000). Spreading of red sea overflow waters in the indian ocean. *Journal of Geophysical Research: Oceans*, 105(C4):8549–8564.

Behera, S., Salvekar, P., and Yamagata, T. (2000). Simulation of interannual SST variability in the tropical Indian Ocean. *Journal of Climate*, 13(19):3487–3499.

Behera, S. K. and Yamagata, T. (2001). Subtropical sst dipole events in the southern indian ocean. *Geophysical Research Letters*, 28(2):327–330.

Bender, M. A. and Ginis, I. (2000). Real-case simulations of hurricane–ocean interaction using a high-resolution coupled model: Effects on hurricane intensity. *Monthly Weather Review*, 128(4):917–946.

Bender, M. A., Ginis, I., and Kurihara, Y. (1993). Numerical simulations of tropical cyclone-ocean interaction with a high-resolution coupled model. *Journal of Geophysical Research: Atmospheres*, 98(D12):23245–23263.

Bessafi, M. and Wheeler, M. C. (2006). Modulation of south indian ocean tropical cyclones by the madden–julian oscillation and convectively coupled equatorial waves. *Monthly Weather Review*, 134(2):638–656.

Biastoch, A., Böning, C. W., and Lutjeharms, J. (2008). Agulhas leakage dynamics affects decadal variability in atlantic overturning circulation. *Nature*, 456(7221):489.

Biastoch, A., Böning, C. W., Schwarzkopf, F. U., and Lutjeharms, J. (2009). Increase in agulhas leakage due to poleward shift of southern hemisphere westerlies. *Nature*, 462(7272):495.

Biastoch, A. and Krauss, W. (1999). The role of mesoscale eddies in the source regions of the agulhas current. *Journal of Physical Oceanography*, 29(9):2303–2317.

Blake, E. S., Rappaport, E. N., Jarrell, J. D., Landsea, C., and Center, T. P. (2007). *The deadliest, costliest, and most intense United States tropical cyclones from 1851 to 2006 (and other frequently requested hurricane facts)*. NOAA/National Weather Service, National Centers for Environmental Prediction, National Hurricane Center Miami.

Blamey, R. and Reason, C. (2009). Numerical simulation of a mesoscale convective system over the east coast of south africa. *Tellus A*, 61(1):17–34.

Blamey, R. and Reason, C. (2013). The role of mesoscale convective complexes in southern africa summer rainfall. *Journal of climate*, 26(5):1654–1668.

Bleck, R. (2002). An oceanic general circulation model framed in hybrid isopycnic-Cartesian coordinates. *Ocean modelling*, 4(1):55–88.

Cadet, D. (1979). Meteorology of the indian summer monsoon. *Nature*, 279(5716):761.

Callahan, J. E. (1972). The structure and circulation of deep water in the antarctic. In *Deep Sea Research and Oceanographic Abstracts*, volume 19, pages 563–575. Elsevier.

Camargo, S. J., Emanuel, K. A., and Sobel, A. H. (2007). Use of a genesis potential index to diagnose enso effects on tropical cyclone genesis. *Journal of Climate*, 20(19):4819–4834.

Carton, J. A., Chepurin, G., Cao, X., and Giese, B. (2000). A simple ocean data assimilation analysis of the global upper ocean 1950-95. Part I: Methodology. *Journal of Physical Oceanography*, 30(2):294–309.

Carton, J. A. and Giese, B. S. (2008). A reanalysis of ocean climate using Simple Ocean Data Assimilation (SODA). *Monthly Weather Review*, 136(8):2999–3017.

Chan, J. C. (2009). Thermodynamic control on the climate of intense tropical cyclones. In *Proceedings of the Royal Society of London A: Mathematical, Physical and Engineering Sciences*, volume 465, pages 3011–3021. The Royal Society.

Chang-Seng, D. S. and Jury, M. R. (2010a). Tropical cyclones in the SW Indian Ocean. Part 1: inter-annual variability and statistical prediction. *Meteorology and atmospheric physics*, 106(3-4):149–162.

Chang-Seng, D. S. and Jury, M. R. (2010b). Tropical cyclones in the SW Indian Ocean. Part 2: structure and impacts at the event scale. *Meteorology and atmospheric physics*, 106(3-4):163–178.

Chevane, C., Penven, P., Nehama, F., and Reason, C. (2016). Modelling the tides and their impacts on the vertical stratification over the sofala bank, mozambique. *African journal of marine science*, 38(4):465–479.

Chiodi, A. and Harrison, D. (2007). Mechanisms of summertime subtropical southern indian ocean sea surface temperature variability: On the importance of humidity anomalies and the meridional advection of water vapor. *Journal of Climate*, 20(19):4835–4852.

Chowdary, J. S., Gnanaseelan, C., and Xie, S. (2009). Westward propagation of barrier layer formation in the 2006–07 Rossby wave event over the tropical southwest Indian Ocean. *Geophysical Research Letters*, 36(4).

Cione, J. J. and Uhlhorn, E. W. (2003). Sea surface temperature variability in hurricanes: Implications with respect to intensity change. *Monthly Weather Review*, 131(8):1783–1796.

Clemens, S., Prell, W., Murray, D., Shimmield, G., and Weedon, G. (1991). Forcing mechanisms of the indian ocean monsoon. *Nature*, 353(6346):720.

Collins, C., Hermes, J., and Reason, C. (2014). Mesoscale activity in the comoros basin from satellite altimetry and a high-resolution ocean circulation model. *Journal of Geophysical Research: Oceans*, 119(8):4745–4760.

Collins, C., Hermes, J., Roman, R., and Reason, C. (2016). First dedicated hydrographic survey of the comoros basin. *Journal of Geophysical Research: Oceans*, 121(2):1291–1305.

Cook, C., Reason, C. J., and Hewitson, B. C. (2004). Wet and dry spells within particularly wet and dry summers in the south african summer rainfall region. *Climate Research*, 26(1):17–31.

Cossa, O., Pous, S., Penven, P., Capet, X., and Reason, C. (2016). Modelling cyclonic eddies in the delagoa bight region. *Continental Shelf Research*, 119:14–29.

Creel, L. (2003). *Ripple effects: population and coastal regions*. Population Reference Bureau Washington, DC.

Crimp, S. and Mason, S. (1999). The extreme precipitation event of 11 to 16 february 1996 over south africa. *Meteorology and atmospheric physics*, 70(1-2):29–42.

Cronin, M. F., Bond, N. A., Farrar, J. T., Ichikawa, H., Jayne, S. R., Kawai, Y., Konda, M., Qiu, B., Rainville, L., and Tomita, H. (2013). Formation and erosion of the seasonal thermocline in the kuroshio extension recirculation gyre. *Deep Sea Research Part II: Topical Studies in Oceanography*, 85:62–74.

d'Abreton, P. and Lindesay, J. (1993). Water vapour transport over southern africa during wet and dry early and late summer months. *international Journal of Climatology*, 13(2):151–170.

D'Asaro, E., Lee, C., Rainville, L., Harcourt, R., and Thomas, L. (2011). Enhanced turbulence and energy dissipation at ocean fronts. *science*, 332(6027):318–322.

D'Asaro, E. A. (2003). The ocean boundary layer below hurricane dennis. *Journal of Physical Oceanography*, 33(3):561–579.

D'Asaro, E. A., Sanford, T. B., Niiler, P. P., and Terrill, E. J. (2007). Cold wake of hurricane frances. *Geophysical Research Letters*, 34(15).

de Boer, W. F., Rydberg, L., and Saide, V. (2000). Tides, tidal currents and their effects on the intertidal ecosystem of the southern bay, inhaca island, mozambique. *Hydrobiologia*, 428(1):187–196.

de Boyer Montégut, C., Mignot, J., Lazar, A., and Cravatte, S. (2007). Control of salinity on the mixed layer depth in the world ocean: 1. general description. *Journal of Geophysical Research: Oceans*, 112(C6).

de Ruijter, W. P., Ridderinkhof, H., Lutjeharms, J. R., Schouten, M. W., and Veth, C. (2002). Observations of the flow in the mozambique channel. *Geophysical Research Letters*, 29(10).

de Sousa, L. P., Brito, A., Abdula, S., and Caputi, N. (2006). Research assessment for the management of the industrial shallow-water multi-species shrimp fishery in sofala bank in mozambique. *Fisheries research*, 77(2):207–219.

Debreu, L., Marchesiello, P., Penven, P., and Cambon, G. (2012). Two-way nesting in split-explicit ocean models: algorithms, implementation and validation. *Ocean Modelling*, 49:1–21.

DeMaria, M., Mainelli, M., Shay, L. K., Knaff, J. A., and Kaplan, J. (2005). Further improvements to the statistical hurricane intensity prediction scheme (SHIPS). *Weather and Forecasting*, 20(4):531–543.

Dickey, T., Frye, D., McNeil, J., Manov, D., Nelson, N., Sigurdson, D., Jannasch, H., Siegel, D., Michaels, T., and Johnson, R. (1998). Upper-ocean temperature response to hurricane felix as measured by the bermuda testbed mooring. *Monthly Weather Review*, 126(5):1195–1201.

Dilmahamod, A., Hermes, J. C., and Reason, C. J. C. (2016). Chlorophyll-a variability in the Seychelles–Chagos Thermocline Ridge: Analysis of a coupled biophysical model. *Journal of Marine Systems*, 154:220–232.

DiMarco, S. F., Chapman, P., and Nowlin, W. D. (2000). Satellite observations of upwelling on the continental shelf south of madagascar. *Geophysical Research Letters*, 27(24):3965–3968.

DiMarco, S. F., Chapman, P., Nowlin Jr, W. D., Hacker, P., Donohue, K., Luther, M., Johnson, G. C., and Toole, J. (2002). Volume transport and property distributions of the mozambique channel. *Deep Sea Research Part II: Topical Studies in Oceanography*, 49(7-8):1481–1511.

Donohue, K. A. and Toole, J. M. (2003). A near-synoptic survey of the southwest indian ocean. *Deep Sea Research Part II: Topical Studies in Oceanography*, 50(12-13):1893–1931.

Durgadoo, J. V., Loveday, B. R., Reason, C. J., Penven, P., and Biastoch, A. (2013). Agulhas leakage predominantly responds to the southern hemisphere westerlies. *Journal of Physical Oceanography*, 43(10):2113–2131.

Duvel, J. P., Roca, R., and Vialard, J. (2004). Ocean mixed layer temperature variations induced by intraseasonal convective perturbations over the indian ocean. *Journal of the atmospheric sciences*, 61(9):1004–1023.

Dyson, L. and Van Heerden, J. (2001). The heavy rainfall and floods over the northeastern interior of south africa during february 2000. *South African Journal of Science*, 97(3-4):80–86.

Dyson, L. and Van Heerden, J. (2002). A model for the identification of tropical weather systems over south africa. *Water SA*, 28(3):249–258.

Egbert, G. D. and Erofeeva, S. Y. (2002). Efficient inverse modeling of barotropic ocean tides. *Journal of Atmospheric and Oceanic Technology*, 19(2):183–204.

Egbert, G. D. and Ray, R. D. (2003). Semi-diurnal and diurnal tidal dissipation from topex/poseidon altimetry. *Geophysical Research Letters*, 30(17).

Elsberry, R. L. (2002). Predicting hurricane landfall precipitation: Optimistic and pessimistic views from the symposium on precipitation extremes. *Bulletin of the American Meteorological Society*, 83(9):1333–1339.

Emanuel, K. (2001). Contribution of tropical cyclones to meridional heat transport by the oceans. *Journal of Geophysical Research: Atmospheres*, 106(D14):14771–14781.

Emanuel, K. (2005). Increasing destructiveness of tropical cyclones over the past 30 years. *Nature*, 436(7051):686–688.

Emanuel, K. (2007). Environmental factors affecting tropical cyclone power dissipation. *Journal of Climate*, 20(22):5497–5509.

Emanuel, K., DesAutels, C., Holloway, C., and Korty, R. (2004). Environmental control of tropical cyclone intensity. *Journal of the atmospheric sciences*, 61(7):843–858.

Emanuel, K. A. (1986). An air-sea interaction theory for tropical cyclones. Part I: Steady-state maintenance. *Journal of the Atmospheric Sciences*, 43(6):585–605.

Emanuel, K. A. (1999). Thermodynamic control of hurricane intensity. *Nature*, 401(6754):665–669.

Emanuel, K. A. and Živkovic-Rothman, M. (1999). Development and evaluation of a convection scheme for use in climate models. *Journal of the Atmospheric Sciences*, 56(11):1766–1782.

Emery, W. (2001). Water types and water masses. *Encyclopedia of ocean sciences*, 6:3179–3187.

Evan, A. T., Kossin, J. P., Ramanathan, V., et al. (2011). Arabian sea tropical cyclones intensified by emissions of black carbon and other aerosols. *Nature*, 479(7371):94–97.

Evans, J. L. (1993). Sensitivity of tropical cyclone intensity to sea surface temperature. *Journal of Climate*, 6(6):1133–1140.

Fauchereau, N., Trzaska, S., Rouault, M., and Richard, Y. (2003). Rainfall variability and changes in southern africa during the 20th century in the global warming context. *Natural Hazards*, 29(2):139–154.

Fennessy, S. and Isaksen, B. (2007). Can bycatch reduction devices be implemented successfully on prawn trawlers in the western indian ocean? *African Journal of Marine Science*, 29(3):453–463.

Fine, R. A. (1993). Circulation of antarctic intermediate water in the south indian ocean. *Deep Sea Research Part I: Oceanographic Research Papers*, 40(10):2021–2042.

Fink, A. H. and Speth, P. (1998). Tropical cyclones. *Naturwissenschaften*, 85(10):482–493.

Flather, R. (1987). A tidal model of the northeast pacific. *Atmosphere-ocean*, 25(1):22–45.

Foltz, G. R. and Balaguru, K. (2016). Prolonged el niño conditions in 2014–2015 and the rapid intensification of hurricane patricia in the eastern pacific. *Geophysical Research Letters*, 43(19).

Foltz, G. R., Balaguru, K., and Hagos, S. (2018). Interbasin differences in the relationship between sst and tropical cyclone intensification. *Monthly Weather Review*, 146(3):853–870.

Gadgil, S. (2003). The indian monsoon and its variability. *Annual Review of Earth and Planetary Sciences*, 31(1):429–467.

Gammelsrød, T. (1992). Variation in shrimp abundance on the sofala bank, mozambique, and its relation to the zambezi river runoff. *Estuarine, Coastal and Shelf Science*, 35(1):91–103.

Gillett, N. P., Kell, T. D., and Jones, P. (2006). Regional climate impacts of the southern annular mode. *Geophysical Research Letters*, 33(23).

Girishkumar, M., Prakash, V. T., and Ravichandran, M. (2015). Influence of pacific decadal oscillation on the relationship between enso and tropical cyclone activity in the bay of bengal during october–december. *Climate Dynamics*, 44(11-12):3469–3479.

Goni, G., DeMaria, M., Knaff, J., Sampson, C., Ginis, I., Bringas, F., Mavume, A., Lauer, C., Lin, I., Ali, M., et al. (2009). Applications of satellite-derived ocean measurements to tropical cyclone intensity forecasting. Technical report, DTIC Document.

Goni, G., Kamholtz, Garzoli, S., and Olson, D. (1996). Dynamics of the Brazil-Malvinas Confluence based on inverted echo sounders and altimetry. *Journal of Geophysical Research*, 101(C7):16273–16289.

Goni, G., Mavume, A., Mehra, A., Sampson, C., Lauer, C., Chassignet, E., Bringas, F., Halliwell, G., Lin, I., Ginis, I., et al. (2010). The ocean observing system for tropical cyclone intensification forecasts and studies. *Proceedings of the" OceanObs*, 9.

Goni, G. J. and Trinanes, J. A. (2003). Ocean thermal structure monitoring could aid in the intensity forecast of tropical cyclones. *Eos, Transactions American Geophysical Union*, 84(51):573–578.

Gordon, A. L., Ma, S., Olson, D. B., Hacker, P., Ffield, A., Talley, L. D., Wilson, D., and Baringer, M. (1997). Advection and diffusion of Indonesian Throughflow Water within the Indian Ocean South Equatorial Current. *Geophysical Research Letters*, 24(21):2573–2576.

Gordon, A. L. and McClean, J. L. (1999). Thermohaline stratification of the indonesian seas: model and observations. *Journal of Physical Oceanography*, 29(2):198–216.

Gray, W. M. (1979). Hurricanes: Their formation, structure and likely role in the tropical circulation. *Meteorology over the tropical oceans*, 77:155–218.

Gründlingh, M. L. (1995). Tracking eddies in the southeast atlantic and southwest indian oceans with topex/poseidon. *Journal of Geophysical Research: Oceans*, 100(C12):24977–24986.

Grunseich, G., Subrahmanyam, B., Murty, V., and Giese, B. S. (2011). Sea surface salinity variability during the indian ocean dipole and enso events in the tropical indian ocean. *Journal of Geophysical Research: Oceans*, 116(C11).

Haidvogel, D. B. and Beckmann, A. (1999). *Numerical ocean circulation modeling*. World Scientific.

Halo, I., Backeberg, B., Penven, P., Ansorge, I., Reason, C., and Ullgren, J. (2014). Eddy properties in the mozambique channel: A comparison between observations and two numerical ocean circulation models. *Deep Sea Research Part II: Topical Studies in Oceanography*, 100:38–53.

Han, W. and McCreary, J. P. (2001). Modeling salinity distributions in the indian ocean. *Journal of Geophysical Research: Oceans*, 106(C1):859–877.

Han, W., Vialard, J., McPhaden, M. J., Lee, T., Masumoto, Y., Feng, M., and De Ruijter, W. P. (2014). Indian ocean decadal variability: A review. *Bulletin of the American Meteorological Society*, 95(11):1679–1703.

Harris, T. (1972). Sources of the agulhas current in the spring of 1964. In *Deep Sea Research and Oceanographic Abstracts*, volume 19, pages 633–650. Elsevier.

Harrison, M. (1984). The annual rainfall cycle over the central interior of south africa. *South African Geographical Journal*, 66(1):47–64.

Hart, N., Reason, C., and Fauchereau, N. (2010). Tropical–extratropical interactions over southern africa: Three cases of heavy summer season rainfall. *Monthly weather review*, 138(7):2608–2623.

Hart, N. C., Reason, C. J., and Fauchereau, N. (2013). Cloud bands over southern africa: seasonality, contribution to rainfall variability and modulation by the mjo. *Climate dynamics*, 41(5-6):1199–1212.

Hastenrath, S. and Greischar, L. (1991). The monsoonal current regimes of the tropical indian ocean: Observed surface flow fields and their geostrophic and wind-driven components. *Journal of Geophysical Research: Oceans*, 96(C7):12619–12633.

Heirtzler, J. R. (1977). *Indian Ocean Geology and Biostratigraphy: Studies Following Deep-sea Drilling Legs 22-29*. American geophysical union.

Hermes, J. and Reason, C. J. C. (2005). Ocean model diagnosis of interannual coevolving SST variability in the South Indian and South Atlantic Oceans. *Journal of Climate*, 18(15):2864–2882.

Hermes, J. and Reason, C. J. C. (2008). Annual cycle of the South Indian Ocean (Seychelles-Chagos) thermocline ridge in a regional ocean model. *Journal of Geophysical Research: Oceans*, 113(C4).

Hermes, J. C. and Reason, C. J. C. (2009). The sensitivity of the Seychelles–Chagos thermocline ridge to large-scale wind anomalies. *ICES Journal of Marine Science: Journal du Conseil*, page fsp074.

Higgins, R., Kousky, V., Silva, V., Becker, E., and Xie, P. (2010). Intercomparison of daily precipitation statistics over the united states in observations and in ncep reanalysis products. *Journal of climate*, 23(17):4637–4650.

Ho, C.-H., Kim, J.-H., Jeong, J.-H., Kim, H.-S., and Chen, D. (2006). Variation of tropical cyclone activity in the south indian ocean: El niño–southern oscillation and madden-julian oscillation effects. *Journal of Geophysical Research: Atmospheres*, 111(D22).

Holland, G. J. and Lander, M. (1993). The meandering nature of tropical cyclone tracks. *Journal of the atmospheric sciences*, 50(9):1254–1266.

Holliday, C. R. and Thompson, A. H. (1979). Climatological characteristics of rapidly intensifying typhoons. *Monthly Weather Review*, 107(8):1022–1034.

Hong, X., Chang, S. W., Raman, S., Shay, L. K., and Hodur, R. (2000). The interaction between hurricane opal (1995) and a warm core ring in the gulf of mexico. *Monthly Weather Review*, 128(5):1347–1365.

Huang, B. and Shukla, J. (2007). Mechanisms for the interannual variability in the tropical indian ocean. part ii: Regional processes. *Journal of climate*, 20(13):2937–2960.

Jackett, D. R. and Mcdougall, T. J. (1995). Minimal adjustment of hydrographic profiles to achieve static stability. *Journal of Atmospheric and Oceanic Technology*, 12(2):381–389.

Jaimes, B. and Shay, L. K. (2009). Mixed layer cooling in mesoscale oceanic eddies during hurricanes katrina and rita. *Monthly Weather Review*, 137(12):4188–4207.

Jullien, S., Marchesiello, P., Menkes, C. E., Lefèvre, J., Jourdain, N. C., Samson, G., and Lengaigne, M. (2014). Ocean feedback to tropical cyclones: climatology and processes. *Climate dynamics*, 43(9-10):2831–2854.

Jury, M. R., Pathack, B., and Parker, B. (1999). Climatic determinants and statistical prediction of tropical cyclone days in the southwest Indian Ocean. *Journal of Climate*, 12(6):1738–1746.

Jury, M. R., Valentine, H. R., and Lutjeharms, J. R. (1993). Influence of the agulhas current on summer rainfall along the southeast coast of south africa. *Journal of Applied Meteorology*, 32(7):1282–1287.

Kako, S. and Kubota, M. (2007). Variability of mixed layer depth in kuroshio/oyashio extension region: 2005–2006. *Geophysical research letters*, 34(11).

Kalnay, E., Kanamitsu, M., Kistler, R., Collins, W., Deaven, D., Gandin, L., Iredell, M., Saha, S., White, G., Woollen, J., et al. (1996). The ncep/ncar 40-year reanalysis project. *Bulletin of the American meteorological Society*, 77(3):437–471.

Kara, A. B., Rochford, P. A., and Hurlburt, H. E. (2003). Mixed layer depth variability over the global ocean. *Journal of Geophysical Research: Oceans*, 108(C3).

Karstensen, J. and Quadfasel, D. (2002). Formation of southern hemisphere thermocline waters: Water mass conversion and subduction. *Journal of Physical Oceanography*, 32(11):3020–3038.

Ke, H., Qi-Long, Z., Qiang, X., and Dong-Xiao, W. (2012). Relationship between upper-ocean heat content in the tropical Indian Ocean and summer precipitation in China. *Atmospheric and Oceanic Science Letters*, 5(4):306–313.

Kijazi, A. L. and Reason, C. (2009). Analysis of the 2006 floods over northern tanzania. *International Journal of climatology*, 29(7):955–970.

Klinman, M. and Reason, C. (2008). On the peculiar storm track of tc favio during the 2006–2007 southwest indian ocean tropical cyclone season and relationships to enso. *Meteorology and Atmospheric Physics*, 100(1-4):233–242.

Knapp, K. R., Kruk, M. C., Levinson, D. H., Diamond, H. J., and Neumann, C. J. (2010). The international best track archive for climate stewardship (IBTrACS) unifying tropical cyclone data. *Bulletin of the American Meteorological Society*, 91(3):363–376.

Kossin, J. P. and Sitkowski, M. (2009). An objective model for identifying secondary eyewall formation in hurricanes. *Monthly Weather Review*, 137(3):876–892.

Krishna, K. M. (2009). Intensifying tropical cyclones over the north indian ocean during summer monsoon-global warming. *Global and Planetary Change*, 65(1):12–16.

Kuleshov, Y., Chane-Ming, F., Qi, L., Chouaibou, I., Hoareau, C., and Roux, F. (2009). Tropical cyclone genesis in the southern hemisphere and its relationship with the enso. In *Annales Geophysicae*, volume 27, pages 2523–2538.

Kuleshov, Y. and de Hoedt, G. (2003). Tropical cyclone activity in the southern hemisphere. *Bull. Aust. Met. Oceanogr. Soc*, 16:135–7.

Kuleshov, Y., Qi, L., Fawcett, R., and Jones, D. (2008). On tropical cyclone activity in the southern hemisphere: trends and the enso connection. *Geophysical Research Letters*, 35(14).

Kumar, S. P. and Prasad, T. (1999). Formation and spreading of arabian sea high-salinity water mass. *Journal of Geophysical Research: Oceans*, 104(C1):1455–1464.

LaCasce, J., Nøst, O., and Isachsen, P. (2008). Asymmetry of free circulations in closed ocean gyres. *Journal of Physical Oceanography*, 38(2):517–526.

Large, W. G., Danabasoglu, G., Doney, S. C., and McWilliams, J. C. (1997). Sensitivity to surface forcing and boundary layer mixing in a global ocean model: Annual-mean climatology. *Journal of Physical Oceanography*, 27(11):2418–2447.

Large, W. G., McWilliams, J. C., and Doney, S. C. (1994). Oceanic vertical mixing: A review and a model with a nonlocal boundary layer parameterization. *Reviews of Geophysics*, 32(4):363–403.

Le Provost, C. (2001). Ocean tides. In *International Geophysics*, volume 69, pages 267–303. Elsevier.

Leipper, D. F. and Volgenau, D. (1972). Hurricane heat potential of the Gulf of Mexico. *Journal of Physical Oceanography*, 2(3):218–224.

Leroy, A. and Wheeler, M. C. (2008). Statistical prediction of weekly tropical cyclone activity in the southern hemisphere. *Monthly Weather Review*, 136(10):3637–3654.

Lin, I. and Chan, J. C. (2015). Recent decrease in typhoon destructive potential and global warming implications. *Nature communications*, 6:7182.

Lin, I., Chou, M.-D., and Wu, C.-C. (2011). The Impact of a Warm Ocean Eddy on Typhoon Morakot (2009): A Preliminary Study from Satellite Observations and Numerical Modelling. *Terrestrial, Atmospheric & Oceanic Sciences*, 22(6).

Lin, I., Pun, I.-F., and Wu, C.-C. (2009a). Upper-ocean thermal structure and the western North Pacific category 5 typhoons. Part II: Dependence on translation speed. *Monthly Weather Review*, 137(11):3744–3757.

Lin, I., Wu, C.-C., Emanuel, K. A., Lee, I.-H., Wu, C.-R., and Pun, I.-F. (2005). The interaction of Supertyphoon Maemi (2003) with a warm ocean eddy. *Monthly Weather Review*, 133(9):2635–2649.

Lin, I., Wu, C.-C., Pun, I.-F., and Ko, D.-S. (2008). Upper-ocean thermal structure and the western North Pacific category 5 typhoons. Part I: Ocean features and the category 5 typhoons' intensification. *Monthly Weather Review*, 136(9):3288–3306.

Lin, I.-I. (2012). Typhoon-induced phytoplankton blooms and primary productivity increase in the western north pacific subtropical ocean. *Journal of Geophysical Research: Oceans*, 117(C3).

Lin, I.-I., Black, P., Price, J. F., Yang, C.-Y., Chen, S. S., Lien, C.-C., Harr, P., Chi, N.-H., Wu, C.-C., and D'Asaro, E. A. (2013a). An ocean coupling potential intensity index for tropical cyclones. *Geophysical Research Letters*, 40(9):1878–1882.

Lin, I.-I., Chen, C.-H., Pun, I.-F., Liu, W. T., and Wu, C.-C. (2009b). Warm ocean anomaly, air sea fluxes, and the rapid intensification of tropical cyclone Nargis (2008). *Geophysical Research Letters*, 36(3).

Lin, I.-I., Goni, G. J., Knaff, J. A., Forbes, C., and Ali, M. (2013b). Ocean heat content for tropical cyclone intensity forecasting and its impact on storm surge. *Natural hazards*, 66(3):1481–1500.

Lin, I.-I., Liu, W. T., Wu, C.-C., Chiang, J. C., and Sui, C.-H. (2003). Satellite observations of modulation of surface winds by typhoon-induced upper ocean cooling. *Geophysical research letters*, 30(3).

Lindesay, J. (1988). South african rainfall, the southern oscillation and a southern hemisphere semi-annual cycle. *International Journal of Climatology*, 8(1):17–30.

Liu, Z. and Alexander, M. (2007). Atmospheric bridge, oceanic tunnel, and global climatic teleconnections. *Reviews of Geophysics*, 45(2).

Lloyd, I. D. and Vecchi, G. A. (2011). Observational evidence for oceanic controls on hurricane intensity. *Journal of Climate*, 24(4):1138–1153.

Loveday, B. R., Durgadoo, J. V., Reason, C. J., Biastoch, A., and Penven, P. (2014). Decoupling of the agulhas leakage from the agulhas current. *Journal of Physical Oceanography*, 44(7):1776–1797.

Lutjeharms, J. (1981). Features of the southern agulhas current circulation from satellite remote sensing. *South African Journal of Science*, 77(5):231–236.

Lutjeharms, J. R. (2006). *The agulhas current*, volume 2. Springer.

Mainelli, M., DeMaria, M., Shay, L. K., and Goni, G. (2008). Application of oceanic heat content estimation to operational forecasting of recent Atlantic category 5 hurricanes. *Weather and Forecasting*, 23(1):3–16.

Malan, N., Reason, C., and Loveday, B. (2013). Variability in tropical cyclone heat potential over the southwest indian ocean. *Journal of Geophysical Research: Oceans*, 118(12):6734–6746.

Malauene, B., Shillington, F., Roberts, M., and Moloney, C. (2014). Cool, elevated chlorophyll-a waters off northern mozambique. *Deep Sea Research Part II: Topical Studies in Oceanography*, 100:68–78.

Malherbe, J., Engelbrecht, F. A., Landman, W. A., and Engelbrecht, C. J. (2012). Tropical systems from the southwest indian ocean making landfall over the limpopo river basin, southern africa: a historical perspective. *International Journal of Climatology*, 32(7):1018–1032.

Manatsa, D., Reason, C. J. C., and Mukwada, G. (2012). On the decoupling of the IODZM from southern Africa Summer rainfall variability. *International Journal of Climatology*, 32(5):727–746.

Manhique, A., Reason, C., Rydberg, L., and Fauchereau, N. (2011). Enso and indian ocean sea surface temperatures and their relationships with tropical temperate troughs over mozambique and the southwest indian ocean. *International Journal of Climatology*, 31(1):1–13.

Manhique, A., Reason, C., Silinto, B., Zucula, J., Raiva, I., Congolo, F., and Mavume, A. (2015). Extreme rainfall and floods in southern africa in january 2013 and associated circulation patterns. *Natural Hazards*, 77(2):679–691.

Manucharyan, G., Brierley, C., and Fedorov, A. (2011). Climate impacts of intermittent upper ocean mixing induced by tropical cyclones. *Journal of Geophysical Research: Oceans*, 116(C11).

Manyilizu, M., Dufois, F., Penven, P., and Reason, C. (2014). Interannual variability of sea surface temperature and circulation in the tropical western indian ocean. *African Journal of Marine Science*, 36(2):233–252.

Manyilizu, M., Penven, P., and Reason, C. (2016). Annual cycle of the upper-ocean circulation and properties in the tropical western indian ocean. *African journal of marine science*, 38(1):81–99.

Mason, S. (1995). Sea-surface temperature—south african rainfall associations, 1910–1989. *International Journal of Climatology*, 15(2):119–135.

Matyas, C. J. (2015). Tropical cyclone formation and motion in the mozambique channel. *International Journal of Climatology*, 35(3):375–390.

Mavume, A. F. (2008). *Tropical cyclones in the South-West Indian Ocean: Intensity changes, oceanic interaction and impacts*. PhD thesis, University of Cape Town.

Mavume, A. F., Rydberg, L., Rouault, M., and Lutjeharms, J. R. (2009). Climatology and landfall of tropical cyclones in the south-west indian ocean. *Western Indian Ocean Journal of Marine Science*, 8(1).

Mawren, D. and Reason, C. (2017). Variability of upper-ocean characteristics and tropical cyclones in the south west indian ocean. *Journal of Geophysical Research: Oceans*, 122(3):2012–2028.

McCreary Jr, J. P., Kundu, P. K., and Molinari, R. L. (1993). A numerical investigation of dynamics, thermodynamics and mixed-layer processes in the indian ocean. *Progress in Oceanography*, 31(3):181–244.

McPhaden, M. J., Foltz, G. R., Lee, T., Murty, V., Ravichandran, M., Vecchi, G. A., Vialard, J., Wiggert, J. D., and Yu, L. (2009). Ocean-atmosphere interactions during cyclone nargis. *Eos, Transactions American Geophysical Union*, 90(7):53–54.

Mendelsohn, R., Emanuel, K., Chonabayashi, S., and Bakkensen, L. (2012). The impact of climate change on global tropical cyclone damage. *Nature climate change*, 2(3):205.

Merrill, R. T. (1988). Characteristics of the upper-tropospheric environmental flow around hurricanes. *Journal of the atmospheric sciences*, 45(11):1665–1677.

Morales, R. A., Barton, E. D., and Heywood, K. J. (1996). Variability of water masses in the western indian ocean. *Journal of Geophysical Research: Oceans*, 101(C6):14027–14038.

Morrison, J. M. (1997). Inter-monsoonal changes in the t-s properties of the near-surface waters of the northern arabian sea. *Geophysical Research Letters*, 24(21):2553–2556.

Mulenga, H., Rouault, M., and Reason, C. (2003). Dry summers over northeastern south africa and associated circulation anomalies. *Climate Research*, 25(1):29–41.

Munk, W. and Wunsch, C. (1998). Abyssal recipes ii: Energetics of tidal and wind mixing. *Deep Sea Research Part I: Oceanographic Research Papers*, 45(12):1977–2010.

Munk, W. H. (1966). Abyssal recipes. In *Deep Sea Research and Oceanographic Abstracts*, volume 13, pages 707–730. Elsevier.

Murtugudde, R., McCreary, J. P., and Busalacchi, A. J. (2000). Oceanic processes associated with anomalous events in the indian ocean with relevance to 1997–1998. *Journal of Geophysical Research: Oceans*, 105(C2):3295–3306.

Naeraa, M. and Jury, M. (1998). Tropical cyclone composite structure and impacts over eastern madagascar during january–march 1994. *Meteorology and Atmospheric Physics*, 65(1-2):43–53.

Nauw, J., Van Aken, H., Webb, A., Lutjeharms, J., and De Ruijter, W. (2008). Observations of the southern east madagascar current and undercurrent and countercurrent system. *Journal of Geophysical Research: Oceans*, 113(C8).

Nehama, F. and Reason, C. (2015). Modelling the zambezi river plume. *African journal of marine science*, 37(4):593–604.

New, A., Alderson, S., Smeed, D., and Stansfield, K. (2007). On the circulation of water masses across the mascarene plateau in the south indian ocean. *Deep Sea Research Part I: Oceanographic Research Papers*, 54(1):42–74.

Pailler, K., Bourlès, B., and Gouriou, Y. (1999). Barrier layer in the western Tropical Atlantic Ocean. *Geophysical Research Letters*, 26(14):2069–2072.

Palastanga, V., Van Leeuwen, P., and De Ruijter, W. (2006). A link between low-frequency mesoscale eddy variability around madagascar and the large-scale indian ocean variability. *Journal of Geophysical Research: Oceans*, 111(C9).

Palmen, E. (1948). On the formation and structure of tropical hurricanes. *Geophysica*, 3(1):26–38.

Park, Y.-H., Gamberoni, L., and Charriaud, E. (1993). Frontal structure, water masses, and circulation in the crozet basin. *Journal of Geophysical Research: Oceans*, 98(C7):12361–12385.

Parker, B. and Jury, R. (1999). Synoptic environment of composite tropical cyclones in the south-west indian ocean. *African Journal of Marine Science*, 21.

Payet, R., Soogun, N., Ranaivoson, E., Payet, R., and Ali Abdallah, F. (2004). Indian ocean islands: Giwa regional assessment 45b. Technical report, United Nations Environment Programme (UNEP).

Peduzzi, P., Chatenoux, B., Dao, H., De Bono, A., Herold, C., Kossin, J., Mouton, F., and Nordbeck, O. (2012). Global trends in tropical cyclone risk. *Nature climate change*, 2(4):289.

Peeters, F. J., Acheson, R., Brummer, G.-J. A., De Ruijter, W. P., Schneider, R. R., Ganssen, G. M., Ufkes, E., and Kroon, D. (2004). Vigorous exchange between the indian and atlantic oceans at the end of the past five glacial periods. *Nature*, 430(7000):661.

Penven, P., Lutjeharms, J., and Florenchie, P. (2006). Madagascar: A pacemaker for the agulhas current system? *Geophysical Research Letters*, 33(17).

Pfeiffer, M., Timm, O., Dullo, W.-C., and Garbe-Schönberg, D. (2006). Paired coral sr/ca and δ18o records from the chagos archipelago: Late twentieth century warming affects rainfall variability in the tropical indian ocean. *Geology*, 34(12):1069–1072.

Pielke, R. A. (1990). *The Hurricane*. New York: Routledge, Chapman and Hall Inc.

Price, J. F. (1981). Upper ocean response to a hurricane. *Journal of Physical Oceanography*, 11(2):153–175.

Price, J. F. (2009). Metrics of hurricane-ocean interaction: vertically-integrated or vertically-averaged ocean temperature? *Ocean Science*.

Pugh, D. (1987). Tides, surges and mean sea-level: a handbook for engineers and scientists, 472 pp.

Pun, I., Chang, Y.-T., Lin, I.-I., Tang, T. Y., and Lien, R.-C. (2011). Typhoon-ocean interaction in the western North Pacific: Part 2. *Oceanography*.

Pun, I.-F., Lin, I.-I., Wu, C.-R., Ko, D.-S., and Liu, W. T. (2007). Validation and application of altimetry-derived upper ocean thermal structure in the western North Pacific Ocean for typhoon-intensity forecast. *Geoscience and Remote Sensing, IEEE Transactions on*, 45(6):1616–1630.

Qian, W., Hu, H., Deng, Y., and Tian, J. (2002). Signals of interannual and interdecadal variability of air-sea interaction in the basin-wide indian ocean. *Atmosphere-Ocean*, 40(3):293–311.

Quadfasel, D., Frische, A., and Cresswell, G. (1996). The circulation in the source area of the south equatorial current in the eastern indian ocean. *Journal of Geophysical Research: Oceans*, 101(C5):12483–12488.

Quartly, G. and Srokosz, M. (2004). Eddies in the southern mozambique channel. *Deep Sea Research Part II: Topical Studies in Oceanography*, 51(1-3):69–83.

Quetelard, H., Bessemoulin, P., Cerveny, R. S., Peterson, T. C., Burton, A., and Boodhoo, Y. (2009). Extreme weather: world-record rainfalls during tropical cyclone gamede. *Bulletin of the American Meteorological Society*, 90(5):603–608.

Rajeevan, M., Srinivasan, J., Niranjan Kumar, K., Gnanaseelan, C., and Ali, M. (2013). On the epochal variation of intensity of tropical cyclones in the Arabian Sea. *Atmospheric Science Letters*, 14(4):249–255.

Ramage, C. S. (1971). Monsoon meteorology. Technical report.

Rao, L. G. and Ram, P. S. (2005). Upper ocean physical processes in the tropical indian ocean.

Rao, R. and Sivakumar, R. (2000). Seasonal variability of near-surface thermal structure and heat budget of the mixed layer of the tropical indian ocean from a new global ocean temperature climatology. *Journal of Geophysical Research: Oceans*, 105(C1):995–1015.

Rao, V. B., Ferreira, C. C., Franchito, S., and Ramakrishna, S. (2008). In a changing climate weakening tropical easterly jet induces more violent tropical storms over the north indian ocean. *Geophysical research letters*, 35(15).

Rappaport, E. N. (2000). Loss of life in the united states associated with recent atlantic tropical cyclones. *Bulletin of the American Meteorological Society*, 81(9):2065–2073.

Reason, C. (2000). Multidecadal climate variability in the subtropics/mid-latitudes of the southern hemisphere oceans. *Tellus A*, 52(2):203–223.

Reason, C. (2001). Subtropical indian ocean sst dipole events and southern african rainfall. *Geophysical Research Letters*, 28(11):2225–2227.

Reason, C. (2007). Tropical cyclone dera, the unusual 2000/01 tropical cyclone season in the south west indian ocean and associated rainfall anomalies over southern africa. *Meteorology and Atmospheric Physics*, 97(1-4):181–188.

Reason, C. and Keibel, A. (2004). Tropical cyclone eline and its unusual penetration and impacts over the southern african mainland. *Weather and forecasting*, 19(5):789–805.

Reason, C. and Rouault, M. (2005). Links between the antarctic oscillation and winter rainfall over western south africa. *Geophysical research letters*, 32(7).

Reason, C. and Rouault, M. (2006). Sea surface temperature variability in the tropical southeast atlantic ocean and west african rainfall. *Geophysical research letters*, 33(21).

Reason, C. J. C. (2002). Sensitivity of the southern African circulation to dipole sea-surface temperature patterns in the south Indian Ocean. *International Journal of Climatology*, 22(4):377–393.

Reason, C. J. C., Allan, R., Lindesay, J., and Ansell, T. (2000). ENSO and climatic signals across the Indian Ocean basin in the global context: Part I, Interannual composite patterns. *International Journal of Climatology*, 20(11):1285–1327.

Reason, C. J. C. and Mulenga, H. (1999). Relationships between South African rainfall and SST anomalies in the southwest Indian Ocean. *International Journal of Climatology*, 19(15):1651–1673.

Ridderinkhof, H. and De Ruijter, W. (2003). Moored current observations in the mozambique channel. *Deep Sea Research Part II: Topical Studies in Oceanography*, 50(12-13):1933–1955.

Ridderinkhof, H., Van der Werf, P., Ullgren, J., Van Aken, H., Van Leeuwen, P., and De Ruijter, W. (2010). Seasonal and interannual variability in the mozambique channel from moored current observations. *Journal of Geophysical Research: Oceans*, 115(C6).

Robinson, C., Gibbes, B., and Li, L. (2006). Driving mechanisms for groundwater flow and salt transport in a subterranean estuary. *Geophysical Research Letters*, 33(3).

Roman, R. and Lutjeharms, J. (2009). Red sea intermediate water in the source regions of the agulhas current. *Deep Sea Research Part I: Oceanographic Research Papers*, 56(6):939–962.

Rouault, M., Florenchie, P., Fauchereau, N., and Reason, C. J. (2003). South east tropical atlantic warm events and southern african rainfall. *Geophysical Research Letters*, 30(5).

Roux, F., Chane-Ming, F., Lasserre-Bigorry, A., and Nuissier, O. (2004). Structure and evolution of intense tropical cyclone dina near la réunion on 22 january 2002: Gb-evtd analysis of single doppler radar observations. *Journal of Atmospheric and Oceanic Technology*, 21(10):1501–1518.

Ruijter, W. d., Biastoch, A., Drijfhout, S., Lutjeharms, J., Matano, R., Pichevin, T., Leeuwen, P. v., and Weijer, W. (1999). Indian-atlantic interocean exchange: Dynamics, estimation and impact. *Journal of Geophysical Research: Oceans*, 104(C9):20885–20910.

Sætre, R. (1985). Surface currents in the mozambique channel. *Deep Sea Research Part A. Oceanographic Research Papers*, 32(12):1457–1467.

Saetre, R. and Da Silva, A. J. (1982). Water masses and circulation of the mozambique channel. *Revista de Investigação Pesqueira*, 3:1–83.

Saha, S., Moorthi, S., Pan, H.-L., Wu, X., Wang, J., Nadiga, S., Tripp, P., Kistler, R., Woollen, J., Behringer, D., et al. (2010). The ncep climate forecast system reanalysis. *Bulletin of the American Meteorological Society*, 91(8):1015–1058.

Saji, N., Goswami, B., Vinayachandran, P., and Yamagata, T. (1999). A dipole mode in the tropical Indian Ocean. *Nature*, 401(6751):360–363.

Sanford, T. B., Price, J. F., and Girton, J. B. (2011). Upper-ocean response to hurricane frances (2004) observed by profiling em-apex floats. *Journal of Physical Oceanography*, 41(6):1041–1056.

Scharroo, R., Smith, W. H., and Lillibridge, J. L. (2005). Satellite altimetry and the intensification of Hurricane Katrina. *Eos, Transactions American Geophysical Union*, 86(40):366–366.

Schott, F., Fieux, M., Kindle, J., Swallow, J., and Zantopp, R. (1988). The boundary currents east and north of madagascar: 2. direct measurements and model comparisons. *Journal of Geophysical Research: Oceans*, 93(C5):4963–4974.

Schott, F. A. and Fischer, J. (2000). Winter monsoon circulation of the northern arabian sea and somali current. *Journal of Geophysical Research: Oceans*, 105(C3):6359–6376.

Schott, F. A. and McCreary Jr, J. P. (2001). The monsoon circulation of the indian ocean. *Progress in Oceanography*, 51(1):1–123.

Schott, F. A., Xie, S.-P., and McCreary, J. P. (2009). Indian Ocean circulation and climate variability. *Reviews of Geophysics*, 47(1).

Schouten, M. W., de Ruijter, W. P., Van Leeuwen, P. J., and Ridderinkhof, H. (2003). Eddies and variability in the mozambique channel. *Deep Sea Research Part II: Topical Studies in Oceanography*, 50(12-13):1987–2003.

Schumann, E. H. (1998). The coastal ocean off southeast africa, including madagascar. *The Sea*, 11:557–582.

Sengupta, D., Goddalehundi, B. R., and Anitha, D. (2008). Cyclone-induced mixing does not cool SST in the post-monsoon North Bay of Bengal. *Atmospheric Science Letters*, 9(1):1–6.

Seo, H. and Xie, S.-P. (2013). Impact of ocean warm layer thickness on the intensity of hurricane katrina in a regional coupled model. *Meteorology and Atmospheric Physics*, 122(1-2):19–32.

Shapiro, G. and Meschanov, S. (1991). Distribution and spreading of red sea water and salt lens formation in the northwest indian ocean. *Deep Sea Research Part A. Oceanographic Research Papers*, 38(1):21–34.

Shay, L. K., Goni, G. J., and Black, P. G. (2000). Effects of a warm oceanic feature on Hurricane Opal. *Monthly Weather Review*, 128(5):1366–1383.

Shchepetkin, A. F. and McWilliams, J. C. (2003). A method for computing horizontal pressure-gradient force in an oceanic model with a nonaligned vertical coordinate. *Journal of Geophysical Research: Oceans*, 108(C3).

Shchepetkin, A. F. and McWilliams, J. C. (2005). The regional oceanic modeling system (roms): a split-explicit, free-surface, topography-following-coordinate oceanic model. *Ocean modelling*, 9(4):347–404.

Shchepetkin, A. F. and McWilliams, J. C. (2009). Computational kernel algorithms for fine-scale, multiprocess, longtime oceanic simulations. In *Handbook of Numerical Analysis*, volume 14, pages 121–183. Elsevier.

Sheets, R. C. (1990). The national hurricane center—past, present, and future. *Weather and Forecasting*, 5(2):185–232.

Siedler, G., Rouault, M., Biastoch, A., Backeberg, B., Reason, C. J., and Lutjeharms, J. R. (2009). Modes of the southern extension of the east madagascar current. *Journal of Geophysical Research: Oceans*, 114(C1).

Sikka, D. and Gadgil, S. (1980). On the maximum cloud zone and the itcz over indian, longitudes during the southwest monsoon. *Monthly Weather Review*, 108(11):1840–1853.

Simpson, J. H. and Sharples, J. (2012). *Introduction to the physical and biological oceanography of shelf seas*. Cambridge University Press.

Slingo, J., Spencer, H., Hoskins, B., Berrisford, P., and Black, E. (2005). The meteorology of the western indian ocean, and the influence of the east african highlands. *Philosophical Transactions of the Royal Society of London A: Mathematical, Physical and Engineering Sciences*, 363(1826):25–42.

Song, Q., Gordon, A. L., and Visbeck, M. (2004). Spreading of the indonesian throughflow in the indian ocean. *Journal of Physical Oceanography*, 34(4):772–792.

Song, Y. and Haidvogel, D. (1994). A semi-implicit ocean circulation model using a generalized topography-following coordinate system. *Journal of Computational Physics*, 115(1):228–244.

Sprintall, J. and Tomczak, M. (1992). Evidence of the barrier layer in the surface layer of the tropics. *Journal of Geophysical Research: Oceans*, 97(C5):7305–7316.

Steinberg, C. (2007). Impacts of climate change on the physical oceanography of the great barrier reef. *The Great Barrier Reef Marine Park Authority*.

Stommel, H. M. (1958). *The Gulf Stream: a physical and dynamical description*. Univ of California Press.

Stramma, L. and Lutjeharms, J. R. (1997). The flow field of the subtropical gyre of the south indian ocean. *Journal of Geophysical Research: Oceans*, 102(C3):5513–5530.

Subrahmanyam, B., Murty, V., Sharp, R. J., and O'Brien, J. J. (2005). Air-sea coupling during the tropical cyclones in the indian ocean: A case study using satellite observations. *pure and applied geophysics*, 162(8-9):1643–1672.

Subrahmanyam, B., Robinson, I., Blundell, J., and Challenor, P. (2001). Indian Ocean Rossby waves observed in TOPEX/POSEIDON altimeter data and in model simulations. *International Journal of Remote Sensing*, 22(1):141–167.

Sutyrin, G. and Khain, A. (1979). Interaction between the ocean and the atmosphere in the region of a migratory tropical cyclone. *DOKLADY AKADEMII NAUK SSSR*, 249(2):467–470.

Suzuki, R., Behera, S. K., Iizuka, S., and Yamagata, T. (2004). Indian ocean subtropical dipole simulated using a coupled general circulation model. *Journal of Geophysical Research: Oceans*, 109(C9).

Swallow, J., Fieux, M., and Schott, F. (1988). The boundary currents east and north of madagascar: 1. geostrophic currents and transports. *Journal of Geophysical Research: Oceans*, 93(C5):4951–4962.

Swallow, J. C., Molinari, R. L., Bruce, J. G., Brown, O. B., and Evans, R. H. (1983). Development of near-surface flow pattern and water mass distribution in the somali basin in response to the southwest monsoon of 1979. *Journal of Physical Oceanography*, 13(8):1398–1415.

Taljaard, J. J. and Phil, D. (1994). *Atmospheric circulation systems, synoptic climatology and weather phenomena of South Africa*. Government Printer, South Africa.

Ternon, J.-F., Roberts, M., Morris, T., Hancke, L., and Backeberg, B. (2014). In situ measured current structures of the eddy field in the mozambique channel. *Deep Sea Research Part II: Topical Studies in Oceanography*, 100:10–26.

Toffoli, A., McConochie, J., Ghantous, M., Loffredo, L., and Babanin, A. V. (2012). The effect of wave-induced turbulence on the ocean mixed layer during tropical cyclones: Field observations on the australian north-west shelf. *Journal of Geophysical Research: Oceans*, 117(C11).

Tomczak, M. and Godfrey, J. S. (2003). *Regional Oceanography: An Introduction*, volume 2nd improved ed., 390 pp. Daya Publ. House, Delhi, India.

Toole, J. M. and Warren, B. A. (1993). A hydrographic section across the subtropical south indian ocean. *Deep Sea Research Part I: Oceanographic Research Papers*, 40(10):1973–2019.

Tozuka, T. and Cronin, M. F. (2014). Role of mixed layer depth in surface frontogenesis: The agulhas return current front. *Geophysical Research Letters*, 41(7):2447–2453.

van Aken, H. M., Ridderinkhof, H., and de Ruijter, W. P. (2004). North atlantic deep water in the south-western indian ocean. *Deep Sea Research Part I: Oceanographic Research Papers*, 51(6):755–776.

Van der Werf, P., Schouten, M., Van Leeuwen, P., Ridderinkhof, H., and De Ruijter, W. (2009). Observation and origin of an interannual salinity anomaly in the mozambique channel. *Journal of Geophysical Research: Oceans*, 114(C3).

van Heerden, J. and Taljaard, J. (1998). Africa and surrounding waters. In *Meteorology of the Southern Hemisphere*, pages 141–174. Springer.

Venzke, S., Latif, M., and Villwock, A. (2000). The coupled gcm echo-2. part ii: Indian ocean response to enso. *Journal of Climate*, 13(8):1371–1383.

Vialard, J., Duvel, J.-P., Mcphaden, M. J., Bouruet-Aubertot, P., Ward, B., Key, E., Bourras, D., Weller, R., Minnett, P., Weill, A., et al. (2009). Cirene: air–sea interactions in the seychelles–chagos thermocline ridge region. *Bulletin of the American Meteorological Society*, 90(1):45–61.

Vianna, M., Menezes, V., Pezza, A., and Simmonds, I. (2010). Interactions between hurricane catarina (2004) and warm core rings in the south atlantic ocean. *Journal of Geophysical Research: Oceans*, 115(C7).

Vinayachandran, P., Chauhan, P., Mohan, M., and Nayak, S. (2004). Biological response of the sea around sri lanka to summer monsoon. *Geophysical Research Letters*, 31(1).

Vinayachandran, P. and Nanjundiah, R. S. (2009). Indian ocean sea surface salinity variations in a coupled model. *Climate dynamics*, 33(2-3):245–263.

Vincent, E. M., Emanuel, K. A., Lengaigne, M., Vialard, J., and Madec, G. (2014). Influence of upper ocean stratification interannual variability on tropical cyclones. *Journal of Advances in Modeling Earth Systems*, 6(3):680–699.

Vincent, E. M., Lengaigne, M., Vialard, J., Madec, G., Jourdain, N. C., and Masson, S. (2012). Assessing the oceanic control on the amplitude of sea surface cooling induced by tropical cyclones. *Journal of Geophysical Research: Oceans*, 117(C5).

Vissa, N. K., Satyanarayana, A., and Kumar, B. P. (2013). Intensity of tropical cyclones during pre-and post-monsoon seasons in relation to accumulated tropical cyclone heat potential over Bay of Bengal. *Natural hazards*, 68(2):351–371.

Vitart, F., Anderson, D., and Stockdale, T. (2003). Seasonal forecasting of tropical cyclone landfall over mozambique. *Journal of Climate*, 16(23):3932–3945.

Vitart, F., Leroy, A., and Wheeler, M. C. (2010). A comparison of dynamical and statistical predictions of weekly tropical cyclone activity in the southern hemisphere. *Monthly Weather Review*, 138(9):3671–3682.

Wada, A. and Usui, N. (2010). Impacts of oceanic preexisting conditions on predictions of Typhoon Hai-Tang in 2005. *Advances in Meteorology*, 2010.

Wada, A., Usui, N., and Sato, K. (2012). Relationship of maximum tropical cyclone intensity to sea surface temperature and tropical cyclone heat potential in the north pacific ocean. *Journal of Geophysical Research: Atmospheres*, 117(D11).

Wallace, J. and Hobbs, P. (1977). Atmosphere science-an introductory survey. *Atmospheric Science*.

Wallcraft, A., Metzger, E., and Carroll, S. (2009). Software Design Description for the HYbrid Coordinate Ocean Model (HYCOM), Version 2.2. Technical report, DTIC Document.

Wang, B., Xu, S., and Wu, L. (2012). Intensified arabian sea tropical storms. *Nature*, 489(7416):E1–E2.

Wang, X., Han, G., Qi, Y., and Li, W. (2011). Impact of barrier layer on typhoon-induced sea surface cooling. *Dynamics of Atmospheres and Oceans*, 52(3):367–385.

Warren, B., Stommel, H., and Swallow, J. (1976). Water masses and patterns of flow in the somali basin during the southwest monsoon of 1964. In *Deep Sea Research and Oceanographic Abstracts*, volume 13, pages 825–860. Elsevier.

Washington, R. and Preston, A. (2006). Extreme wet years over southern africa: Role of indian ocean sea surface temperatures. *Journal of Geophysical Research: Atmospheres*, 111(D15).

Weatherford, C. L. (1989). The structural evolution of typhoons. *Atmospheric science paper; no. 446*.

Webster, P. J., Moore, A. M., Loschnigg, J. P., and Leben, R. R. (1999). Coupled ocean–atmosphere dynamics in the indian ocean during 1997–98. *Nature*, 401(6751):356–360.

Weijer, W., de Ruijter, W. P., Dijkstra, H. A., and Van Leeuwen, P. J. (1999). Impact of interbasin exchange on the atlantic overturning circulation. *Journal of Physical Oceanography*, 29(9):2266–2284.

Woodberry, K. E., Luther, M. E., and O'Brien, J. J. (1989). The wind-driven seasonal circulation in the southern tropical indian ocean. *Journal of Geophysical Research: Oceans*, 94(C12):17985–18002.

Wu, C.-C., Lee, C.-Y., and Lin, I. (2007). The effect of the ocean eddy on tropical cyclone intensity. *Journal of the Atmospheric Sciences*, 64(10):3562–3578.

Wyrtki, K. (1971). *Oceanographic atlas of the international Indian Ocean expedition*. National Science Foundation.

Wyrtki, K. (1973). Physical oceanography of the indian ocean. In *The biology of the Indian Ocean*, pages 18–36. Springer.

Xie, S.-P., Annamalai, H., Schott, F. A., and McCreary Jr, J. P. (2002). Structure and mechanisms of south indian ocean climate variability*. *Journal of Climate*, 15(8):864–878.

Yamagata, T., Behera, S. K., Luo, J.-J., Masson, S., Jury, M. R., and Rao, S. A. (2004). Coupled ocean-atmosphere variability in the tropical indian ocean. *Earth's Climate*, pages 189–211.

You, Y. (2000). Implications of the deep circulation and ventilation of the indian ocean on the renewal mechanism of north atlantic deep water. *Journal of Geophysical Research: Oceans*, 105(C10):23895–23926.

You, Y. and Tomczak, M. (1993). Thermocline circulation and ventilation in the indian ocean derived from water mass analysis. *Deep Sea Research Part I: Oceanographic Research Papers*, 40(1):13–56.

Yu, L. and McPhaden, M. J. (2011). Ocean preconditioning of cyclone nargis in the bay of bengal: Interaction between rossby waves, surface fresh waters, and sea surface temperatures. *Journal of Physical Oceanography*, 41(9):1741–1755.

Appendix A

Model Validation

In this section, ROMs model simulations forced with tides (***Tide***) and without tides (***NoTide***) are compared with observational and satellite data in order to establish whether the salient features of the Mozambique Channel, as described in Chapter 3 and Chapter 5, are realistically simulated. The ROMS simulation will be validated for the domain 30 ^{o}E - 50 ^{o}E and 5 ^{o}S – 28 ^{o}S based on the seasonal mean states of, among other parameters, sea surface temperature (SST), sea surface salinity and velocity fields. Both ROMS simulations are forced with interannual data and will likely simulate anomalous climate events and display interannual variability.

Sea surface temperature

The seasonal mean sea surface temperatures of ***Tide*** and ***NoTide*** are evaluated using satellite derived seasonal mean surface temperatures. Since this study is focused on tropical cyclones in the South Indian Ocean, normally generated between October and April, the evaluation of the model will therefore exclude winter months, i.e. May-August. Both models adequately represent the seasonal variability of SSTs in the Mozambique Channel (Figure A.1) with a positive bias in both simulation not exceeding 1 ^{o}C between March-April and September-October and a negative bias less than -1.5 ^{o}C between November through to February. However, the SSTs in ***Tide*** are, in general, about 0.2 ^{o}C cooler along the southern coast of Mozambique and southwestern coast of Madagascar and 0.2 ^{o}C warmer along the main currents SEC, NEMC SEMC (Discussed in Chapter 5) compared to ***NoTide***.

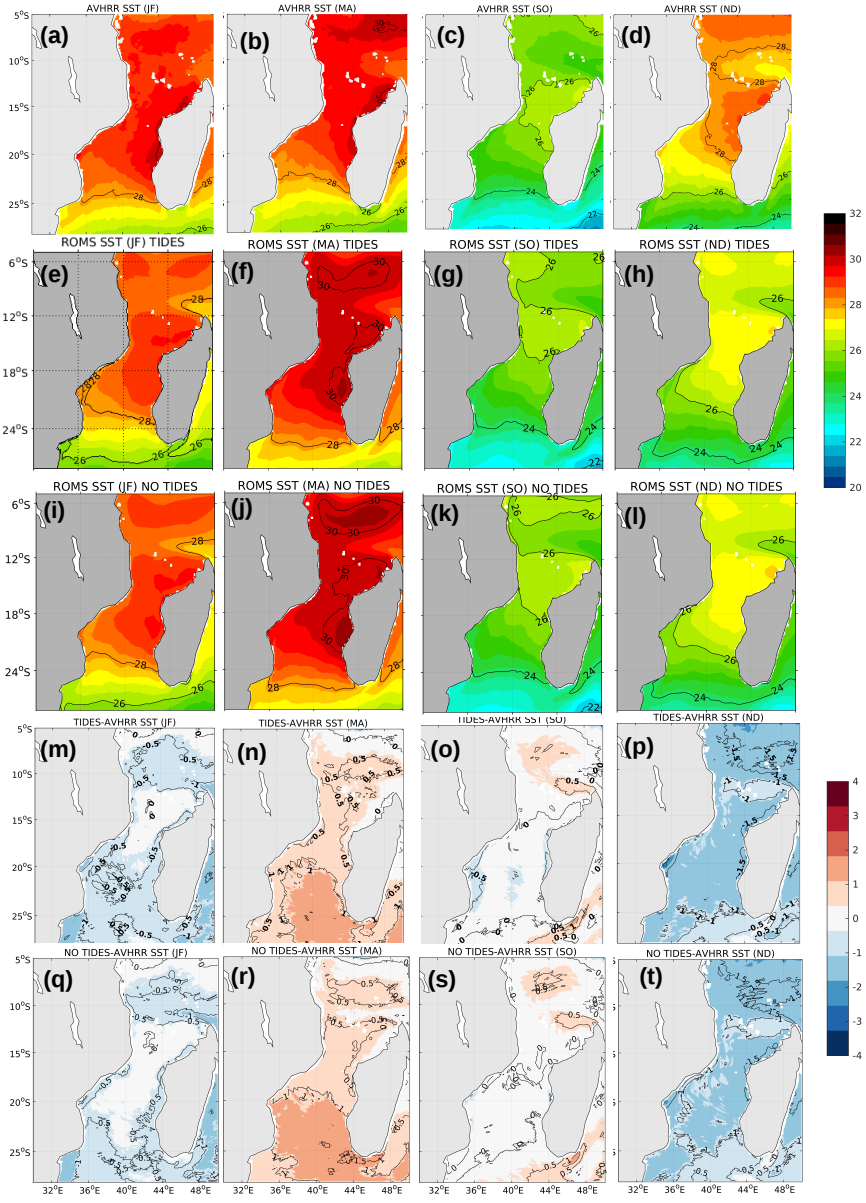

Fig. A.1 The seasonal mean SSTs (^{o}C) for AVHRR (a-d), ***Tide*** (e-h), ***NoTide*** (i-l), the difference between ***Tide*** and AVHRR (m-p) and the difference between ***NoTide*** and AVHRR (q-t) for Jan-Feb, Mar-Apr, Sep-Oct and Nov-Dec (TC season only). Positive (negative) values in the 2 last rows indicate an over-estimation (under-estimation) of SSTs by the model.

Sea surface salinity

Maps of surface salinity distribution (Figure A.2), show features that stands out in terms of similarities between model and observations in the Mozambique Channel. The distinct salinity tongue is observed at the northeastern part of Madagascar which is relatively fresher,

about 35 psu. Its lower salinity has been associated to the excess of precipitation over evaporation in the tropics (Wyrtki, 1971). Another similar pattern is the southward spreading of high salinity water with 35.25, towards the Mozambique Channel, along the african coast, and also the southward spreading of the isohaline of 35 along the east coast of Madagascar. Compared to WOA, salinity values are underestimated in the two model simulations. The differences between WOA and ROMS simulations show that there is an over-estimation of about 0.2 psu along the west coast of Madagascar and across Sofala bank. An under-estimation of about 0.4 psu is observed along the east coast of Madagscar, probaly related to boundary problems. However, the salinity bias is lower in ***Tide*** compared to ***NoTide***.

Tropical cyclone Heat Potential (TCHP)

Figure A.3 shows the distribution of seasonal mean TCHP during the tropical cyclone season in the Mozambique Channel. The two model simulations seem to reproduce similar TCHP patterns throughout the seasons with maximum TCHP values exceeding 40 KJ/cm^2 at 8-10 S; 40 E during March-April. However, an over-estimation is observed in the models in summer, particularly between January and April, but this may be due to the coarser resolution of WOA. The differences between the two simulations show in general, cooler values in the ***Tide*** model, reducing the bias when compared to observations.

Sub surface temperature

Similar to TCHP above, the subsurface temperature averaged in the upper 100 m also show some similarities between the model simulations and observations in terms of the spatial distribution. A higher subsurface temperature is observed between March and April particularly around in the northern part of the Mozambique Channel (12 S; 42 E). However, as observed in the differences between the model simulations and observations, an overestimation is observed along the coast of Mozambique and Madagascar, which is probably due to the limitation of satellites to sample close to the coast or due to the lower resolution of observational data. The comparison between ***Tide*** and ***NoTide*** with CARS indicate a lower bias in the simulation with tide, which shows the importance of tidal forcing in coastal modelling.

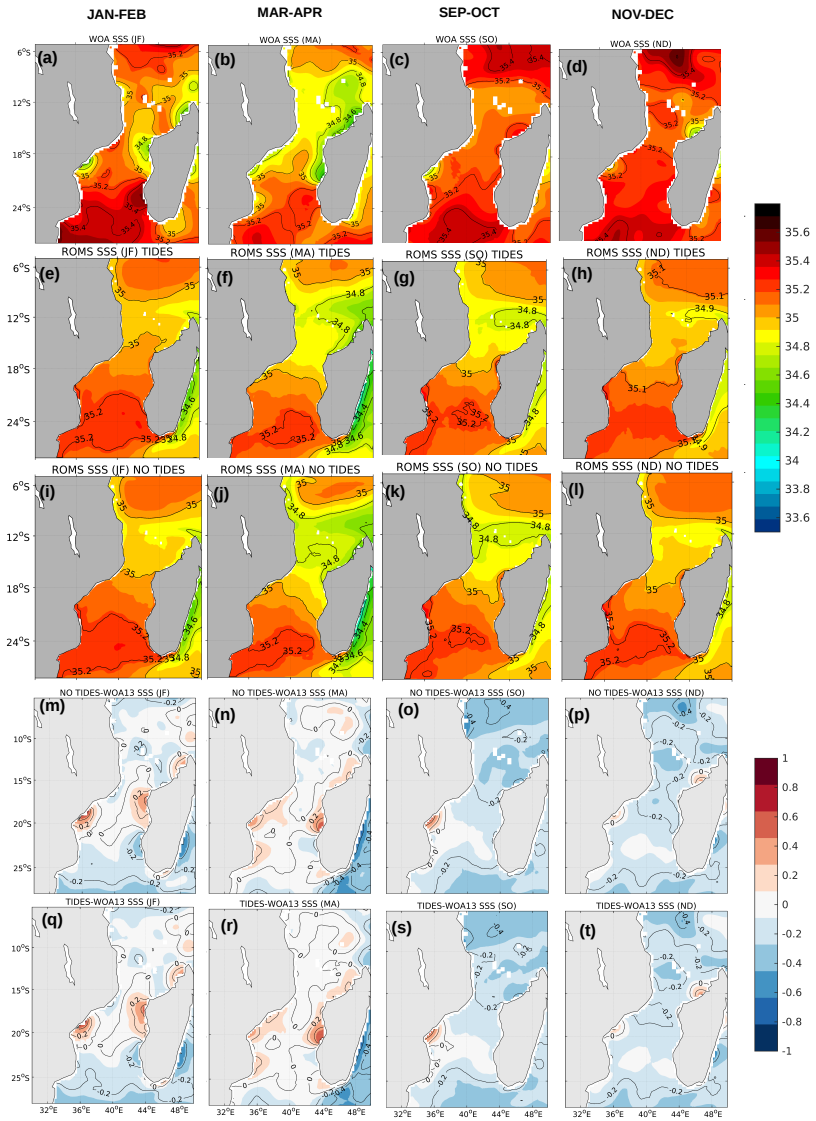

Fig. A.2 The seasonal mean SSSs (psu) for WOA (a-d), ***Tide*** (e-h), ***NoTide*** (i-l), the difference between ***NoTide*** and WOA (m-p) and the difference between ***Tide*** and WOA (q-t) for Jan-Feb, Mar-Apr, Sep-Oct and Nov-Dec (TC season only). Positive (negative) values in the 2 last rows indicate an over-estimation (under-estimation) of SSSs by the model.

Surface currents

The seasonal mean surface velocity fields of ***Tide*** and ***NoTide*** are compared with satellite derived mean surface geostrophic velocities for the period 1996-2008 (Figure A.5). The geographic location of the main oceanographic features evident in the altimeter surface geostrophic velocities are well represented in both simulation. In agreement with the altimeter

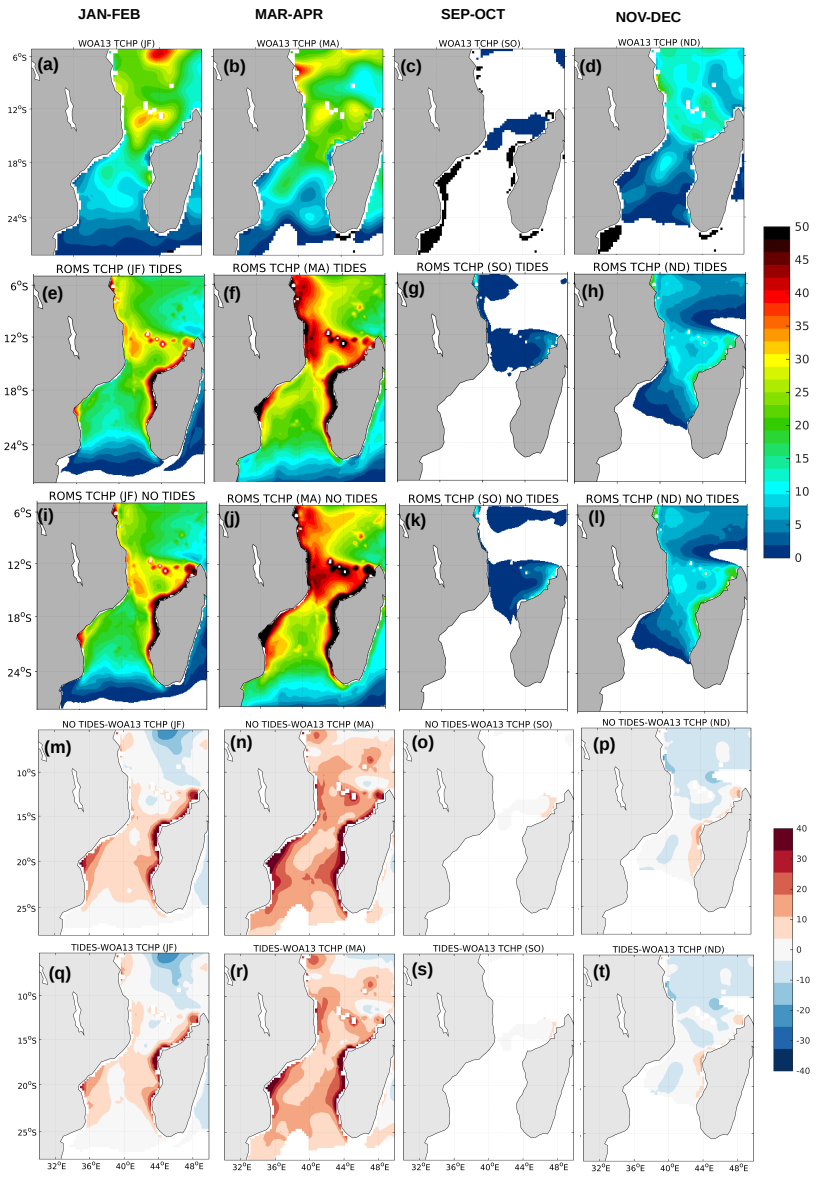

Fig. A.3 The seasonal mean TCHP (KJ/cm^2) for WOA (a-d), ***Tide*** (e-h), ***NoTide*** (i-l), the difference between ***Tide*** and WOA (m-p) and the difference between ***Tide*** and WOA (q-t) for Jan-Feb, Mar-Apr, Sep-Oct and Nov-Dec (TC season only). Positive (negative) values in the 2 last rows indicate an over-estimation (under-estimation) of TCHP by the model.

data and previous literature (lutjeharms et al.,2000), the SEC in both models bifurcates into the equatorward NEMC and poleward SEMC. The bifurcation at the coast of Madagascar displays no seasonality neither simulation nor altimeter data and shows a stronger velocity in the model compared to AVISO.

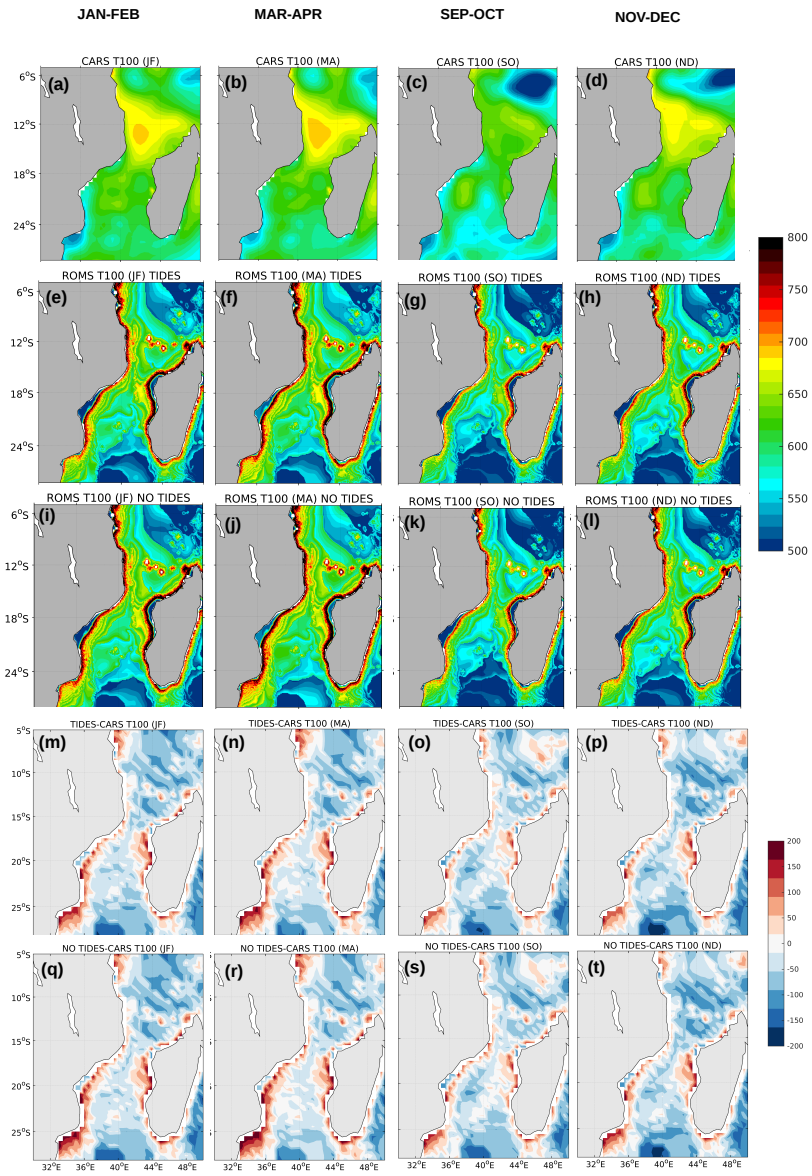

Fig. A.4 The seasonal mean of the sub surface temperature averaged over the upper 100m (kg/m3) for CARS (a-d), ***Tide*** (e-h), ***NoTide*** (i-l), the difference between ***NoTide*** and CARS (m-p) and the difference between ***Tide*** and CARS (q-t) for Jan-Feb, Mar-Apr, Sep-Oct and Nov-Dec (TC season only). Positive (negative) values in the 2 last rows indicate an over-estimation (under-estimation) of TCHP by the model.

The NEMC transports about 31+/-10Sv and 33+/-10Sv past the northern tip of Madagascar in the ***Tide*** and ***NoTide*** simulation respectively, indicating a stronger current in the

simulation without tide. The transport estimates of the two simulations are in good agreement with the transports of 30 Sv calculated from hydrographic data (Swallow et al., 1988).

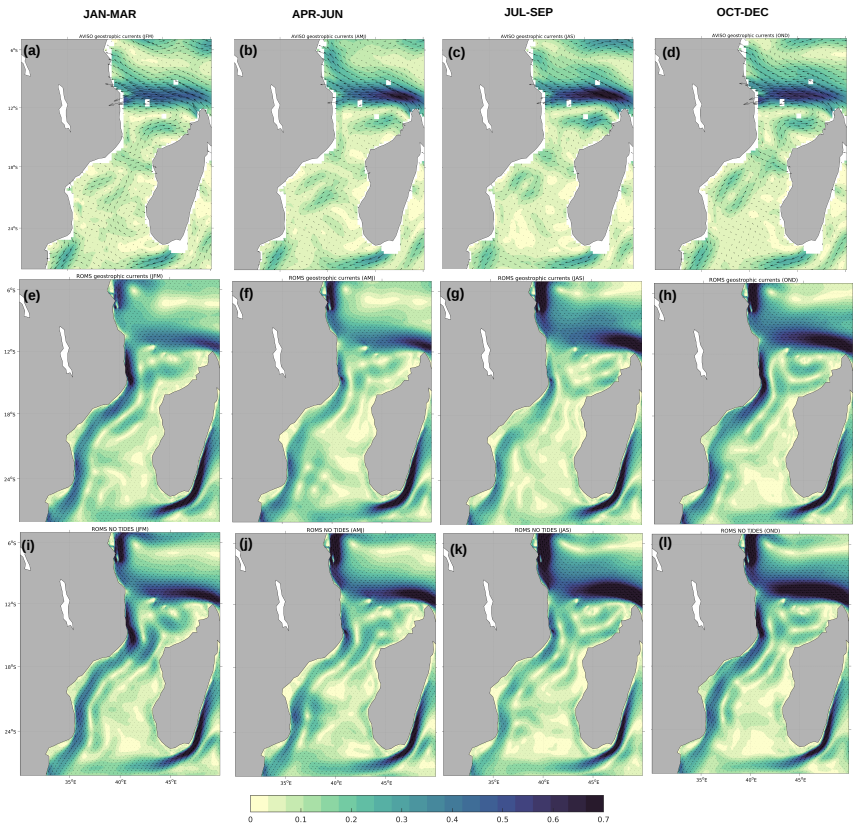

Fig. A.5 The seasonal mean geostrophic velocities from AVISO (a-d), surface velocities from ***Tide*** (e-h) and ***NoTide*** (i-l).

CFSR winds

Figure A.6 shows the daily evolution of tropical cyclone Japhet from CFSR data formed on the 25th of February 2003 until it made landfall and dissipated on the 4th of March 2003. The results clearly show that the tropical cyclone is existent in the atmospheric data used to force the model in Chapter 5. CFSR data is described in more details in Chapter 3.

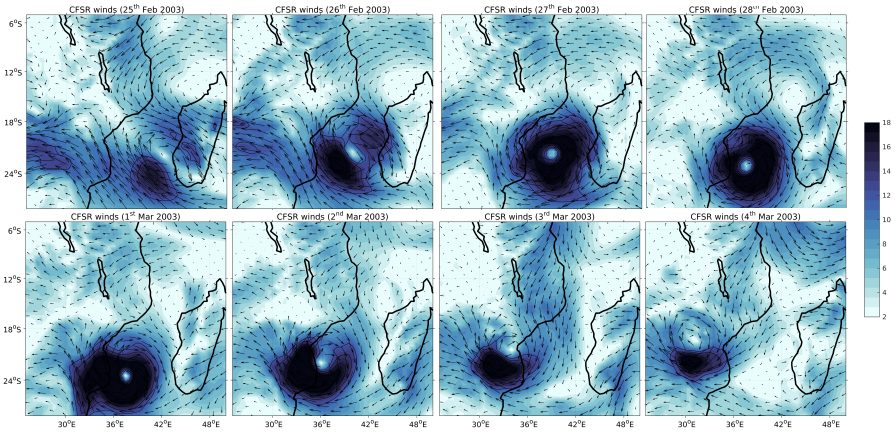

Fig. A.6 Daily snapshots of 850 hPa winds from CFSR during tropical cyclone Japhet 25th Feb 2003 to 4th March 2003.